QM
for
Ψ AMOP

Chapter 25

Tensor Operators and
Wigner-Eckart Matrices

W. G. Harter

The Wigner-Eckart representations of tensor operators are an important part of the development of Clebsch-Gordan-Wigner angular momentum calculus. Hamilton-Pauli spinor representations of spin-1/2 operators of U(2) are generalized to tensor operator matrix representations of spin-j operators of U(2j+1). By noting that spinor operator matrices are $1/2 \otimes 1/2$ Wigner coefficients, it is straightforward to generalize spin-j tensor operator matrices to $j \otimes j$ or $j \otimes k$ Wigner coefficients. Generalization to states of 2, 3, …,n particles is done two

ways. First, 2-particle operators are evaluated using Racah recoupling coefficients. Second, unitary and permutational symmetry is introduced for treating n-particle orbitals and compared to Racah analysis of n=2. Finally, the spectra of tensor operators are considered and applied to crystal field splitting. Techniques for analyzing high-J tensor spectra are introduced and applied to high resolution laser molecular spectroscopy.

25.1 TENSOR OPERATORS AND THE WIGNER-ECKART THEOREM

The theory and application of R_3 tensor operators will be introduced in this section. The development takes off from a CGC-construction of scalar, vector, and tensor products in Section 24.2 and uses CGC-products of ket-bras to make general tensor operators. This leads to the Wigner-Eckart theorem and its application to atomic perturbations and transitions between N-particle orbital states of Section 24.4. Two-particle matrix theory introduces Racah-Wigner 6j-coefficients and continues the comparison between the standard tensor algebra and the more modern unitary $U(m) \times S_N$ algebra introduced at the end of Ch. 24.

a. Construction of R₃ tensor operators

For each set of irrep bases $\left| {}^{j}_{m} \right\rangle : \left\{ \left| {}^{j}_{j} \right\rangle, \left| {}^{j}_{j-1} \right\rangle, \ldots, \left| {}^{j}_{-j} \right\rangle \right\}$ of $2j + 1$ ket vectors, an equal number of bra vectors

$$(-1)^{j-m} \left\langle {}^{\;j}_{-m} \right| : \quad \left\{ \left\langle {}^{\;j}_{-j} \right|, -\left\langle {}^{\quad j}_{-j+1} \right|, \ldots, (-1)^{2j} \left\langle {}^{j}_{j} \right| \right\},$$

belong to the same irrep D^j. (Recall 24.2.20.) By combining the two using coupling coefficients, one may construct the *irreducible tensorial operators* or *Fano-Racah tensorial sets*.

$$T(jj)^k_q = \sum_{m,m'} C^{j\;j\;k}_{m\;m'\;q} \left| {}^{j}_{m} \right\rangle \left\langle {}^{\quad j}_{-m'} \right| (-1)^{j-m'}, \tag{25.1.1a}$$

Set members transform among themselves much as states do using irrep $D^k (2j \geq k \geq 0)$ as follows.

$$R(a\beta y) T(jj)^k_q R^\dagger(a\beta y) = \sum_{q'} D^k_{q'q}(a\beta y) T(jj)^k_{q'}. \tag{25.1.1b}$$

This is similar to the scalar, vector, and tensor ket-ket products introduced in Section 24.2a. However, now we must account for the slightly different transformation behavior of the bra vectors.

If two or more sets $\left\{ \left| {}^{j_1}_{j_1} \right\rangle, \ldots, \left| {}^{j_1}_{m_1} \right\rangle, \ldots, \left| {}^{j_2}_{j_2} \right\rangle, \ldots, \left| {}^{j_2}_{m_2} \right\rangle, \ldots, \right\}, \ldots$ of angular-momentum states need to be considered, then one may make hetrogeneous tensorial combinations

$$T(j_1 j_2)^k_q = \sum_{m_1, m_2} C^{j_1\;j_2\;k}_{m_1\;m_2\;q} \left| {}^{j_1}_{m_1} \right\rangle \left\langle {}^{\quad j_2}_{-m_2} \right| (-1)^{j_2-m_2}, \tag{25.1.2a}$$

where:
$$j_1 + j_2 \geq k \geq |j_1 - j_2|. \tag{25.1.2b}$$

All combinations are needed to make a complete set of irreducible tensor operators acting on any basis. The first few examples treated in the following will be based on a single set $\left\{ \left| {}^{j}_{m} \right\rangle \right\}$ of angular-momentum states, and so there will be one combination $T^k_q(jj) = T^k_q$ for each $k = 0, 1, \ldots, 2j$, and q. $(k \geq q \geq -k)$.

Tensor operators for spin-$\frac{1}{2}$ states: Hamilton-Pauli-spinors

From the spin-$\frac{1}{2}$ states $\left\{ \left| \begin{smallmatrix} 1/2 \\ 1/2 \end{smallmatrix} \right\rangle, \left| \begin{smallmatrix} 1/2 \\ -1/2 \end{smallmatrix} \right\rangle \right\}$ one may construct the tensor operators

$$T_q^k = \sum_{m_1} C_{m_1 \ m_2 \ q}^{1/2 \ 1/2 \ k} \left| \begin{smallmatrix} 1/2 \\ m_1 \end{smallmatrix} \right\rangle \left\langle \begin{smallmatrix} 1/2 \\ -m_2 \end{smallmatrix} \right| (-1)^{\frac{1}{2} - m_2} \qquad (25.1.3a)$$

Using $\frac{1}{2} \otimes \frac{1}{2}$ coupling coefficients (24.1.7). The results are given in the following with their representations in the spin-$\frac{1}{2}$ basis:

$$T_{-1}^1 = \begin{pmatrix} 0 & 0 \\ -1 & 0 \end{pmatrix} \qquad\qquad T_0^1 = \frac{1}{\sqrt{2}} \begin{pmatrix} -1 & 0 \\ 0 & 1 \end{pmatrix} \qquad\qquad T_1^1 = \begin{pmatrix} 0 & 1 \\ 0 & 0 \end{pmatrix}$$

$$= -\left| \begin{smallmatrix} 1/2 \\ -1/2 \end{smallmatrix} \right\rangle \left\langle \begin{smallmatrix} 1/2 \\ 1/2 \end{smallmatrix} \right|, \quad = -\frac{1}{\sqrt{2}} \left[\left| \begin{smallmatrix} 1/2 \\ 1/2 \end{smallmatrix} \right\rangle \left\langle \begin{smallmatrix} 1/2 \\ 1/2 \end{smallmatrix} \right| - \left| \begin{smallmatrix} 1/2 \\ -1/2 \end{smallmatrix} \right\rangle \left\langle \begin{smallmatrix} 1/2 \\ -1/2 \end{smallmatrix} \right| \right], \quad = \left| \begin{smallmatrix} 1/2 \\ 1/2 \end{smallmatrix} \right\rangle \left\langle \begin{smallmatrix} 1/2 \\ -1/2 \end{smallmatrix} \right|,$$

$$(25.1.3b)$$

$$T_0^0 = -\frac{1}{\sqrt{2}} \begin{pmatrix} 1 & 0 \\ 0 & 1 \end{pmatrix}$$

$$= -\frac{1}{\sqrt{2}} \left[\left| \begin{smallmatrix} 1/2 \\ 1/2 \end{smallmatrix} \right\rangle \left\langle \begin{smallmatrix} 1/2 \\ 1/2 \end{smallmatrix} \right| + \left| \begin{smallmatrix} 1/2 \\ -1/2 \end{smallmatrix} \right\rangle \left\langle \begin{smallmatrix} 1/2 \\ -1/2 \end{smallmatrix} \right| \right].$$

The first three operators form a vector set. Consider the following Cartesian combinations:

$$T_x \equiv -\frac{T_{-1}^1 - T_1^1}{\sqrt{2}} \qquad\qquad T_y \equiv -i\frac{T_{-1}^1 + T_1^1}{\sqrt{2}} \qquad\qquad T_z \equiv -T_0^1$$

$$= \frac{1}{\sqrt{2}} \begin{pmatrix} 0 & 1 \\ 1 & 0 \end{pmatrix} \qquad\qquad = \frac{1}{\sqrt{2}} \begin{pmatrix} 0 & -i \\ i & 0 \end{pmatrix} \qquad\qquad = \frac{1}{\sqrt{2}} \begin{pmatrix} 1 & 0 \\ 0 & 1 \end{pmatrix}$$

$$\equiv \frac{1}{\sqrt{2}} \sigma_x \qquad\qquad \equiv \frac{1}{\sqrt{2}} \sigma_y \qquad\qquad \equiv \frac{1}{\sqrt{2}} \sigma_z \qquad (25.1.4)$$

$$\equiv \sqrt{2} J_x \qquad\qquad \equiv \sqrt{2} J_y \qquad\qquad \equiv \sqrt{2} J_z$$

Except for an overall minus phase, these relations correspond to circular-to-linear polarization definitions (24.2.3). The resulting Cartesian tensors are proportional to the Pauli spinor operators:

$$\sigma_x \to \begin{pmatrix} 0 & 1 \\ 1 & 0 \end{pmatrix}, \qquad \sigma_y \to \begin{pmatrix} 0 & -i \\ i & 0 \end{pmatrix}, \qquad \sigma_z \to \begin{pmatrix} 1 & 0 \\ 0 & -1 \end{pmatrix}, \qquad (25.1.5)$$

The spin-$\frac{1}{2}$ angular-momentum operators recall the original ABC-definitions in Eq. (10.5.10).

$$J_x = \frac{\sigma_x}{2}, \qquad J_y = \frac{\sigma_y}{2}, \qquad J_z = \frac{\sigma_z}{2}, \qquad (25.1.6)$$

An explicit example of tensorial set transformation behavior in (25.1.1b) is represented in the following:

$$
\underset{\downarrow}{R(0\beta0)} \qquad \underset{\downarrow}{T_0^1} \qquad \underset{\downarrow}{R^\dagger(0\beta0)} \qquad \underset{\downarrow}{=} \qquad \underset{\downarrow}{T_0'}
$$

$$
\begin{pmatrix} \cos\dfrac{\beta}{2} & -\sin\dfrac{\beta}{2} \\ \sin\dfrac{\beta}{2} & \cos\dfrac{\beta}{2} \end{pmatrix} \begin{pmatrix} -1/\sqrt{2} & 0 \\ 0 & 1/\sqrt{2} \end{pmatrix} \begin{pmatrix} \cos\dfrac{\beta}{2} & \sin\dfrac{\beta}{2} \\ -\sin\dfrac{\beta}{2} & \cos\dfrac{\beta}{2} \end{pmatrix} = -\dfrac{1}{\sqrt{2}}\begin{pmatrix} \cos\beta & \sin\beta \\ \sin\beta & -\cos\beta \end{pmatrix} \qquad (25.1.7)
$$

$$
= \underset{\downarrow}{D_{10}^1(0\beta0)T_1^1} \qquad +\underset{\downarrow}{D_{00}^1(0\beta0)T_0^1} \qquad +\underset{\downarrow}{D_{-10}^1(0\beta0)T_{-1}^1}
$$

$$
= \dfrac{-\sin\beta}{\sqrt{2}}\begin{pmatrix} 0 & 1 \\ 0 & 0 \end{pmatrix} \quad +\cos\beta\begin{pmatrix} -1/\sqrt{2} & 0 \\ 0 & 1/\sqrt{2} \end{pmatrix} \quad +\dfrac{\sin\beta}{\sqrt{2}}\begin{pmatrix} 0 & 0 \\ -1 & 0 \end{pmatrix}
$$

The Cartesian form of this equation is simpler. Multiplying the angular-momentum form by $-1/\sqrt{2}$ and using (25.1.4) yields

$$
J_z(\beta\text{-}rotated) \equiv R(0\beta0)J_z R^\dagger(0\beta0) = \sin\beta J_x + \cos\beta J_z. \qquad (25.1.8)
$$

It should be clear that products of spinor bases form operator quantities that behave like ordinary vectors in 3-space. In this sense spinors are "square roots" of vectors. In order to appreciate the physical meaning of (25.1.8) one may take its expectation value in an arbitrary state $|\psi\rangle$:

$$
\langle\psi|J_z(\beta\text{-}rotated)|\psi\rangle = \sin\beta\langle\psi|J_x|\psi\rangle + \cos\beta\langle\psi|J_z|\psi\rangle. \qquad (25.1.9)
$$

Fig. 25.1.1 shows how the average or expectation value of the component of J on the (z-rotated) axis is given by (25.1.9) by vector geometry.
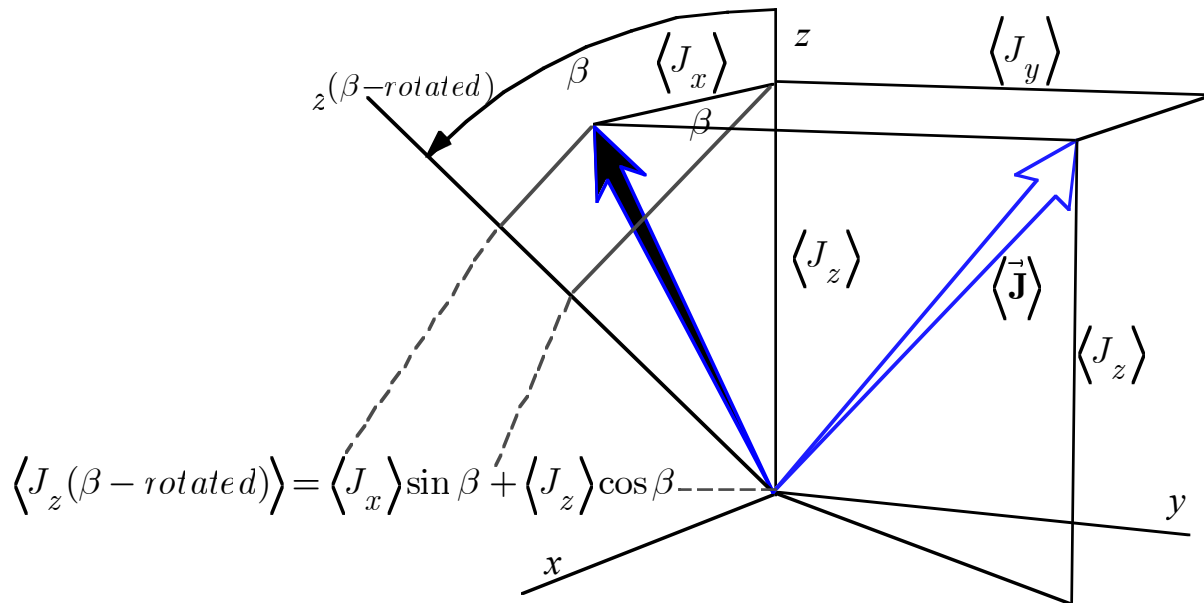

Fig. 25.1.1 Geometry of angular momentum expectation values (25.1.9)

However, the *actual* values for the component in a Stern-Gerlach spin-$\frac{1}{2}$ analyzer will be $\pm\hbar/2$ for each click. (Recall discussions at the beginning of Chapter 1 and in Section 23.2.) By expanding the expectation matrix, one obtains the result in terms of probabilities $\left|\langle\psi|R|_m^{1/2}\rangle\right|^2$ $(\hbar=1)$.

$$\langle\psi|R(a\beta y)J_zR^\dagger(a\beta y)|\psi\rangle = \sum_m\sum_{m'}\langle\psi|R\left|\begin{matrix}1/2\\m\end{matrix}\right\rangle\left\langle\begin{matrix}1/2\\m\end{matrix}\right|j_z\left|\begin{matrix}1/2\\m'\end{matrix}\right\rangle\left\langle\begin{matrix}1/2\\m'\end{matrix}\right|R^\dagger|\psi\rangle = \sum_m\left|\langle\psi|R\left|\begin{matrix}1/2\\m\end{matrix}\right\rangle\right|^2 m$$

$$= \frac{1}{2}\left|\langle\psi|R\left|\begin{matrix}1/2\\1/2\end{matrix}\right\rangle\right|^2 - \frac{1}{2}\left|\langle\psi|R\left|\begin{matrix}1/2\\-1/2\end{matrix}\right\rangle\right|^2 .$$

(25.1.10a)

Each amplitude $\left|\langle\psi|R\left|\begin{matrix}1/2\\m\end{matrix}\right\rangle\right|^2$ depends on initial unrotated amplitudes $\psi_{m'}=\left\langle\psi\left|\begin{matrix}1/2\\m'\end{matrix}\right.\right\rangle$ and rotation matrices:

$$\langle\psi|R(a\beta y)\left|\begin{matrix}1/2\\m\end{matrix}\right\rangle = \sum_{m'}\psi_{m'}D^{1/2}_{m'm}(a\beta y).$$

(25.1.10b)

The well-known classical behavior of the angular-momentum vector emerges after many spin-$\frac{1}{2}$ states have passed the analyzer. The "expectation vector" for $|\psi\rangle$ states has components

$$\langle J_x\rangle = \langle\psi|J_x|\psi\rangle, \qquad \langle J_y\rangle = \langle\psi|J_y|\psi\rangle, \qquad \langle J_z\rangle = \langle\psi|J_z|\psi\rangle. \quad (25.1.11)$$

as indicated in Fig. 25.1.1. This vector provides a useful picture of the properties of particles in a given pure spin-$\frac{1}{2}$ state. The vector picture is the basis of all *ABCD 2*-level dynamics due to time independent spinor Hamiltonians in Ch.10 and resonance due to time dependent Hamiltonians in Ch. 19.

b. Tensor operators for higher spin states (j=1, 3/2, 2, 5/2, 3, 4)

The $1\otimes1$ coupling coefficients (24.1.19) are used to construct a complete set of nine tensor operators for the $j=1$ basis. The tensor operators and their representations are given by (25.1.12) on the next page.

The lower four operators are the scalar ($k=0$) and vector ($k=1$) operators. T^0_0 is proportional to the identity (**1**), and T^1_{-1}, T^1_0 and T^1_1 are proportional to the angular-momentum operators $J_-, J_z,$ and $J_+,$ respectively as seen by comparing to the $D^{j=1}$ or vector representations in (23.1.2b) and (23.1.2).

$$T^1_{-1}=J_-/2=\left(J_x-iJ_y\right)/\sqrt{2}, \qquad T^1_0=J_z/\sqrt{2}, \qquad T^1_{-1}=J_+/2=\left(J_x+iJ_y\right)/2. \quad (25.1.13)$$

The three rank-1-tensor or vector operators $\left(T^1_{-1},T^1_0,T^1_1\right)$ or $\left(J_x,J_y,J_z\right)$ have the same symmetry properties as vector operators constructed in the spin-$\frac{1}{2}$ basis. Of course, the scalar operator T^0_0 is invariant.

Beyond the scalar and vector operators in Eq. (25.1.12) there are five more ($k=2$) operators $\left(T^2_{-2},T^2_{-1},T^2_0,T^2_1,T^2_2\right)$ known as *unit quadrupole* operators. These are the tensor operators that deserve this old-fashioned "tensor" name. To label a ($j=1$)-state completely, one needs a set of quadrupole tensor expectation values T^2_q as well as the T^1_q or J_a vector expectation values. These are components of multipole density matrices just as spin expectation values are density operator components in Sec. 10.5.

$$T_{-2}^2 = \left|\begin{smallmatrix}1\\-1\end{smallmatrix}\right\rangle\left\langle\begin{smallmatrix}1\\1\end{smallmatrix}\right|, \quad T_{-1}^2 = \frac{\left|\begin{smallmatrix}1\\0\end{smallmatrix}\right\rangle\left\langle\begin{smallmatrix}1\\1\end{smallmatrix}\right| - \left|\begin{smallmatrix}1\\-1\end{smallmatrix}\right\rangle\left\langle\begin{smallmatrix}1\\0\end{smallmatrix}\right|}{\sqrt{2}}, \quad T_0^2 = \frac{\left|\begin{smallmatrix}1\\1\end{smallmatrix}\right\rangle\left\langle\begin{smallmatrix}1\\1\end{smallmatrix}\right| - 2\left|\begin{smallmatrix}1\\0\end{smallmatrix}\right\rangle\left\langle\begin{smallmatrix}1\\0\end{smallmatrix}\right| + \left|\begin{smallmatrix}1\\-1\end{smallmatrix}\right\rangle}{\sqrt{6}}, \quad T_1^2 = \frac{-\left|\begin{smallmatrix}1\\1\end{smallmatrix}\right\rangle\left\langle\begin{smallmatrix}1\\0\end{smallmatrix}\right| + \left|\begin{smallmatrix}1\\0\end{smallmatrix}\right\rangle\left\langle\begin{smallmatrix}1\\-1\end{smallmatrix}\right|}{\sqrt{2}}, \quad T_2^2 = \left|\begin{smallmatrix}1\\1\end{smallmatrix}\right\rangle\left\langle\begin{smallmatrix}1\\-1\end{smallmatrix}\right|$$

$$\rightarrow \begin{pmatrix} 0 & 0 & 0 \\ 0 & 0 & 0 \\ 1 & 0 & 0 \end{pmatrix} \quad \rightarrow \begin{pmatrix} 0 & 0 & 0 \\ 1/\sqrt{2} & 0 & 0 \\ 0 & -1/\sqrt{2} & 0 \end{pmatrix} \quad \rightarrow \begin{pmatrix} 1/\sqrt{6} & 0 & 0 \\ 0 & -2/\sqrt{6} & 0 \\ 0 & 0 & 1/\sqrt{6} \end{pmatrix} \quad \rightarrow \begin{pmatrix} 0 & -1/\sqrt{2} & 0 \\ 0 & 0 & 1/\sqrt{2} \\ 0 & 0 & 0 \end{pmatrix} \quad \rightarrow \begin{pmatrix} 0 & 0 & 1 \\ 0 & 0 & 0 \\ 0 & 0 & 0 \end{pmatrix}$$

$$T_{-1}^1 = \frac{\left|\begin{smallmatrix}1\\0\end{smallmatrix}\right\rangle\left\langle\begin{smallmatrix}1\\1\end{smallmatrix}\right| + \left|\begin{smallmatrix}1\\-1\end{smallmatrix}\right\rangle\left\langle\begin{smallmatrix}1\\0\end{smallmatrix}\right|}{\sqrt{2}}, \quad T_0^1 = \frac{\left|\begin{smallmatrix}1\\1\end{smallmatrix}\right\rangle\left\langle\begin{smallmatrix}1\\1\end{smallmatrix}\right| - \left|\begin{smallmatrix}1\\-1\end{smallmatrix}\right\rangle\left\langle\begin{smallmatrix}1\\-1\end{smallmatrix}\right|}{\sqrt{2}}, \quad T_1^1 = \frac{-\left|\begin{smallmatrix}1\\1\end{smallmatrix}\right\rangle\left\langle\begin{smallmatrix}1\\0\end{smallmatrix}\right| - \left|\begin{smallmatrix}1\\0\end{smallmatrix}\right\rangle\left\langle\begin{smallmatrix}1\\-1\end{smallmatrix}\right|}{\sqrt{2}}$$

$$\rightarrow \begin{pmatrix} 0 & 0 & 0 \\ 1/\sqrt{2} & 0 & 0 \\ 0 & 1/\sqrt{2} & 0 \end{pmatrix} \quad \rightarrow \begin{pmatrix} 1/\sqrt{2} & 0 & 0 \\ 0 & 0 & 0 \\ 0 & 0 & -1/\sqrt{2} \end{pmatrix} \quad \rightarrow \begin{pmatrix} 0 & -1/\sqrt{2} & 0 \\ 0 & 0 & -1/\sqrt{2} \\ 0 & 0 & 0 \end{pmatrix}$$

(25.1.12)

$$T_0^0 = \frac{\left|\begin{smallmatrix}1\\1\end{smallmatrix}\right\rangle\left\langle\begin{smallmatrix}1\\1\end{smallmatrix}\right| + \left|\begin{smallmatrix}1\\0\end{smallmatrix}\right\rangle\left\langle\begin{smallmatrix}1\\0\end{smallmatrix}\right| + \left|\begin{smallmatrix}1\\-1\end{smallmatrix}\right\rangle\left\langle\begin{smallmatrix}1\\-1\end{smallmatrix}\right|}{\sqrt{2}}$$

$$\rightarrow \begin{pmatrix} 1/\sqrt{3} & 0 & 0 \\ 0 & 1/\sqrt{3} & 0 \\ 0 & 0 & 1/\sqrt{3} \end{pmatrix}$$

Similarly, the quantum mechanics of higher j-states will require in general a complete set of $(2j+1)^2$ tensor operators. We define new tensor operators that differ by an overall phase factor $(-1)^{2j}$:

$$\mathbf{v}_q^k = \sum_{m,m'} C_{m-m'\ q}^{j\ j\ k} (-1)^{j-m'} \left|\begin{smallmatrix}j\\m\end{smallmatrix}\right\rangle\left\langle\begin{smallmatrix}j\\m'\end{smallmatrix}\right| = (-1)^{2j} T_q^k . \qquad (25.1.14a)$$

The 3–j definition (24.2.30a) and symmetry relations (24.2.31) and (24.2.32) yield the following:

$$\mathbf{v}_q^k = \sum_{m,m'} (-1)^{j-m} \sqrt{2k+1} \begin{pmatrix} k & j & j \\ q & m' & -m \end{pmatrix} \left|\begin{smallmatrix}j\\m\end{smallmatrix}\right\rangle\left\langle\begin{smallmatrix}j\\m'\end{smallmatrix}\right| \qquad (25.1.14b)$$

The phase eliminates the annoying minus sign that occurs in T^k for half-integral j. [Recall Eqs. (25.1.3)$_x$.] The $\mathbf{v}_q^k$ representations are recorded in Tables 25.1-3 in a condensed form. To understand the condensed form, compare the ($j = 1$) tensor derived in Eq. (25.1.12) with the $j=l=1$ tables in Table 25.2(p). Note that each T_q^k has nonzero entries only in particular super- or sub-diagonals of the matrix. Each super-diagonal is labeled by a number $q = 1$, ..., k in the tables. The main or center diagonal belongs to $q=0$ and the sub-diagonals belong to $q = -1, -2, \ldots, -k$. At the end of each super-diagonal is a factored-out denominator. These act as norms of the super-diagonal vectors described below.

Note that each qth super-diagonal in a set of $\mathbf{v}_q^q, \mathbf{v}_q^{q+1}, \ldots$ matrices gives a set of orthonormal vectors. For example, with $j = 2$ the $q = 2$ super-diagonals of Table 25.2[d] are as follows.

$$\left|\begin{array}{ccc} \dfrac{\sqrt{3}}{\sqrt{14}} & \cdot & \cdot \\ \cdot & -\dfrac{\sqrt{8}}{\sqrt{14}} & \cdot \\ \cdot & \cdot & \dfrac{\sqrt{3}}{\sqrt{14}} \end{array}\right| \quad \left|\begin{array}{ccc} \dfrac{1}{\sqrt{2}} & \cdot & \cdot \\ \cdot & 0 & \cdot \\ \cdot & \cdot & -\dfrac{1}{\sqrt{2}} \end{array}\right| \quad \left|\begin{array}{ccc} \dfrac{\sqrt{2}}{\sqrt{7}} & \cdot & \cdot \\ \cdot & \dfrac{\sqrt{3}}{\sqrt{7}} & \cdot \\ \cdot & \cdot & \dfrac{\sqrt{2}}{\sqrt{7}} \end{array}\right|$$

$$\left(\text{for } k = 4\right) \qquad \left(\text{for } k = 3\right) \qquad \left(\text{for } k = 2\right).$$

Because of orthonormality of coupling coefficients, these diagonals are orthonormal vectors. This makes it easy to express any $(2j + 1)$ by $(2j +1)$ matrix in terms of the v_q^k. For example, using the second numbers from the $q = 2$ super-diagonals we easily find the following elementary matrix or operator:

$$\begin{pmatrix} 0 & 0 & 0 & 0 & 0 \\ 0 & 0 & 0 & 1 & 0 \\ 0 & 0 & 0 & 0 & 0 \\ 0 & 0 & 0 & 0 & 0 \\ 0 & 0 & 0 & 0 & 0 \end{pmatrix} \rightarrow -\frac{\sqrt{8}}{\sqrt{14}} v_2^4 + 0 v_2^3 + \frac{\sqrt{3}}{\sqrt{7}} v_2^2 = E_{24}. \qquad (25.1.15)$$

Linear relations between the irreducible tensor operators v_q^k and the elementary unitary operators $\mathrm{E}_{m,m+q}$ will be used in later chapters. A simple example of such a relation involves the $q = 0$ operators for $(j = 1)$. From Eq. (25.1.12) (or the diagonals of Table 25.2[p]) one may write

$$\begin{aligned} v_0^2 &= \left(E_{11} - 2E_{22} + E_{33}\right)\big/\sqrt{6}, \\ v_0^1 &= \left(E_{11} - E_{33}\right)\big/\sqrt{2}, \qquad (25.1.16) \\ v_0^0 &= \left(E_{11} + E_{22} + E_{33}\right)\big/\sqrt{3}. \end{aligned}$$

Here the row-column indices of the elementary operators E_{kk} are simply numbers (1, 2, and 3) rather than angular-momentum quanta ($m = 1$, 0, and -1).] These operators are proportional to the diagonal U_3 operators or number operators $a_k^\dagger a_k$.

The $(2j + 1)^2$ tensor operators $v_q^k(jj)$ are a complete set of generators of the group U_{2j+1}, and so are the elementary operators $E_{m,n}$. Every operator that acts on a $(2j + 1)$-dimensional angular-momentum basis $\left\{ \left|{}^j_j\right\rangle, \left|{}^j_{j-1}\right\rangle, \ldots, \left|{}^j_{-j}\right\rangle \right\}$ is a linear combination of elementary operators $E_{m,n}$, and hence a combination of v_q^k 's.

$q = 0 \quad 1 \quad 2 \quad 3 \quad 4 \quad 5 \quad 6$

$$
v_q^6 = \begin{array}{ccccccc}
1 & -\sqrt{2} & 1 & -\sqrt{2} & \sqrt{5} & -1 & 1 \\
\sqrt{2} & -6 & \sqrt{30} & -\sqrt{8} & 3 & -\sqrt{12} & 1 \\
1 & -\sqrt{30} & 15 & -10 & \sqrt{15} & -3 & \sqrt{5} \\
\sqrt{2} & -\sqrt{8} & 10 & -20 & 10 & -\sqrt{8} & \sqrt{2} \\
\sqrt{5} & -3 & \sqrt{15} & -10 & 15 & -\sqrt{30} & 1 \\
1 & -\sqrt{12} & 3 & -\sqrt{8} & \sqrt{30} & -6 & \sqrt{2} \\
1 & -1 & \sqrt{5} & -\sqrt{2} & 1 & -\sqrt{2} & 1
\end{array}
\quad
\begin{array}{c}
1 \\ \sqrt{2} \\ \sqrt{22} \\ \sqrt{22} \\ \sqrt{33} \\ \sqrt{264} \\ \sqrt{924}
\end{array}
$$

(first row label -1)

$$
v_q^5 = \begin{array}{ccccccc}
1 & -\sqrt{5} & 1 & -\sqrt{2} & 1 & -1 & \\
\sqrt{5} & -4 & \sqrt{27} & -\sqrt{2} & 1 & 0 & -1 \\
1 & -\sqrt{27} & 5 & -\sqrt{10} & 0 & 1 & -1 \\
\sqrt{2} & -\sqrt{2} & \sqrt{10} & 0 & -\sqrt{10} & \sqrt{2} & \sqrt{2} \\
1 & -1 & 0 & \sqrt{10} & -5 & \sqrt{27} & -1 \\
1 & 0 & -1 & \sqrt{2} & -\sqrt{27} & 4 & -\sqrt{5} \\
\cdot & 1 & -1 & \sqrt{2} & -1 & \sqrt{5} & -1
\end{array}
\quad
\begin{array}{c}
\sqrt{2} \\ \sqrt{2} \\ \sqrt{6} \\ \sqrt{6} \\ \sqrt{84} \\ \sqrt{84}
\end{array}
$$

$$
v_q^4 = \begin{array}{ccccccc}
3 & -\sqrt{30} & \sqrt{54} & -3 & \sqrt{3} & \cdot & \cdot \\
\sqrt{30} & -7 & \sqrt{32} & -\sqrt{3} & -\sqrt{2} & \sqrt{5} & \cdot \\
\sqrt{54} & -\sqrt{32} & 1 & \sqrt{15} & -\sqrt{40} & \sqrt{2} & \sqrt{3} \\
3 & -\sqrt{3} & -\sqrt{15} & 6 & -\sqrt{15} & -\sqrt{3} & 3 \\
\sqrt{3} & \sqrt{2} & -\sqrt{40} & \sqrt{15} & 1 & -\sqrt{32} & \sqrt{54} \\
\cdot & \sqrt{5} & -\sqrt{2} & -\sqrt{3} & \sqrt{32} & -7 & \sqrt{30} \\
\cdot & \cdot & \sqrt{3} & -3 & \sqrt{54} & -\sqrt{30} & 3
\end{array}
\quad
\begin{array}{c}
\sqrt{11} \\ \sqrt{22} \\ \sqrt{154} \\ \sqrt{154} \\ \sqrt{154} \\ \sqrt{154}
\end{array}
$$

$$
v_q^3 = \begin{array}{ccccccc}
1 & -\sqrt{2} & \sqrt{2} & -1 & \cdot & \cdot & \cdot \\
\sqrt{2} & -1 & 0 & 1 & -\sqrt{2} & \cdot & \cdot \\
\sqrt{2} & 0 & -1 & 1 & 0 & -\sqrt{2} & \cdot \\
1 & 1 & -1 & 0 & 1 & -1 & -1 \\
\cdot & \sqrt{2} & 0 & -1 & 1 & 0 & -\sqrt{2} \\
\cdot & \cdot & \sqrt{2} & -1 & 0 & 1 & -\sqrt{2} \\
\cdot & \cdot & \cdot & 1 & -\sqrt{2} & \sqrt{2} & -1
\end{array}
\quad
\begin{array}{c}
\sqrt{6} \\ \sqrt{6} \\ \sqrt{6} \\ \sqrt{6}
\end{array}
$$

$$
v_q^2 = \begin{array}{ccccccc}
5 & -5 & \sqrt{5} & \cdot & \cdot & \cdot & \cdot \\
5 & 0 & -\sqrt{15} & \sqrt{10} & \cdot & \cdot & \cdot \\
\sqrt{5} & \sqrt{15} & -3 & -\sqrt{2} & \sqrt{12} & \cdot & \cdot \\
\cdot & \sqrt{10} & \sqrt{2} & -4 & \sqrt{2} & \sqrt{10} & \cdot \\
\cdot & \cdot & \sqrt{12} & -\sqrt{2} & -3 & \sqrt{15} & \sqrt{5} \\
\cdot & \cdot & \cdot & \sqrt{10} & -\sqrt{15} & 0 & 5 \\
\cdot & \cdot & \cdot & \cdot & \sqrt{5} & -5 & 5
\end{array}
\quad
\begin{array}{c}
\sqrt{42} \\ \sqrt{84} \\ \sqrt{84}
\end{array}
$$

$$
v_q^1 = \begin{array}{ccccccc}
3 & -\sqrt{3} & \cdot & \cdot & \cdot & \cdot & \cdot \\
\sqrt{3} & 2 & -\sqrt{5} & \cdot & \cdot & \cdot & \cdot \\
\cdot & \sqrt{5} & 1 & -\sqrt{6} & \cdot & \cdot & \cdot \\
\cdot & \cdot & \sqrt{6} & 0 & -\sqrt{6} & \cdot & \cdot \\
\cdot & \cdot & \cdot & \sqrt{6} & -1 & -\sqrt{5} & \cdot \\
\cdot & \cdot & \cdot & \cdot & \sqrt{5} & -2 & -\sqrt{3} \\
\cdot & \cdot & \cdot & \cdot & \cdot & \sqrt{3} & -3
\end{array}
\quad
\begin{array}{c}
\sqrt{28} \\ \sqrt{28}
\end{array}
$$

(f) $l = 3$

$q = 0 \quad 1 \quad 2 \quad 3 \quad 4$

$$
\begin{array}{ccccc}
1 & -1 & \sqrt{3} & -1 & 1 \\
1 & -4 & \sqrt{6} & -\sqrt{8} & 1 \\
\sqrt{3} & -\sqrt{6} & 6 & -\sqrt{6} & \sqrt{3} \\
1 & -\sqrt{8} & \sqrt{6} & -4 & 1 \\
1 & -1 & \sqrt{3} & -1 & 1
\end{array}
\quad
\begin{array}{c}
1 \\ \sqrt{2} \\ \sqrt{14} \\ \sqrt{14} \\ \sqrt{70}
\end{array}
$$

$$
\begin{array}{ccccc}
1 & -\sqrt{3} & 1 & -1 & \cdot \\
\sqrt{3} & -2 & \sqrt{2} & 0 & -1 \\
1 & -\sqrt{2} & 0 & \sqrt{2} & -1 \\
1 & 0 & -\sqrt{2} & 2 & -\sqrt{3} \\
\cdot & 1 & -1 & \sqrt{3} & -1
\end{array}
\quad
\begin{array}{c}
\sqrt{2} \\ \sqrt{2} \\ \sqrt{10} \\ \sqrt{10}
\end{array}
$$

$$
\begin{array}{ccccc}
2 & -\sqrt{6} & \sqrt{2} & \cdot & \cdot \\
\sqrt{6} & -1 & -1 & \sqrt{3} & \cdot \\
\sqrt{2} & 1 & -2 & 1 & \sqrt{2} \\
\cdot & \sqrt{3} & -1 & -1 & \sqrt{6} \\
\cdot & \cdot & \sqrt{2} & -\sqrt{6} & 2
\end{array}
\quad
\begin{array}{c}
\sqrt{7} \\ \sqrt{14} \\ \sqrt{14}
\end{array}
$$

$q = 0 \quad 1 \quad 2$

$$
\begin{array}{ccc}
1 & -1 & 1 \\
1 & -2 & 1 \\
1 & -1 & -1
\end{array}
$$

$$
\begin{array}{ccccc}
2 & -\sqrt{2} & \cdot & \cdot & \cdot \\
\sqrt{2} & 1 & -\sqrt{3} & \cdot & \cdot \\
\cdot & \sqrt{3} & 0 & -\sqrt{3} & \cdot \\
\cdot & \cdot & \sqrt{3} & -1 & -\sqrt{2} \\
\cdot & \cdot & \cdot & \sqrt{2} & -2
\end{array}
\quad
\begin{array}{c}
\sqrt{10} \\ \sqrt{10}
\end{array}
$$

$$
\begin{array}{ccc}
1 & -1 & \cdot \\
1 & 0 & -1 \\
\cdot & 1 & -1
\end{array}
$$

(d) $l = 2$ **(p) $l = 1$**

Tables 25.2 Orbital (integer momentum) tensor matrices [p] l=1, [d] l=2, [f] l=3, and [g] l=4.

$q = 0 \quad 1 \quad 2 \quad 3 \quad 4 \quad 5 \quad 6 \quad 7 \quad 8$

$$V_q^8 = \begin{bmatrix}
1 & -1 & 1 & -1 & \sqrt{5} & -1 & \sqrt{7} & -1 & 1 \\
1 & -8 & \sqrt{28} & -4 & \sqrt{10} & -\sqrt{32} & 2 & -4 & 1 \\
1 & -\sqrt{28} & 28 & -14 & \sqrt{70} & -\sqrt{28} & \sqrt{56} & -2 & \sqrt{7} \\
1 & -4 & 14 & -56 & \sqrt{490} & -\sqrt{112} & \sqrt{28} & -\sqrt{32} & 1 \\
\sqrt{5} & -\sqrt{10} & \sqrt{70} & -\sqrt{490} & 70 & -\sqrt{490} & \sqrt{70} & -\sqrt{10} & \sqrt{5} \\
1 & -\sqrt{32} & \sqrt{28} & -\sqrt{112} & \sqrt{490} & -56 & 14 & -4 & 1 \\
\sqrt{7} & -2 & \sqrt{56} & -\sqrt{28} & \sqrt{70} & -14 & 28 & -\sqrt{28} & 1 \\
1 & -4 & 2 & -\sqrt{32} & \sqrt{10} & -4 & \sqrt{28} & -8 & 1 \\
1 & -1 & \sqrt{7} & -1 & \sqrt{5} & -1 & 1 & -1 & 1
\end{bmatrix}$$

Row normalizations (right column): $1,\ \sqrt{2},\ \sqrt{30},\ \sqrt{10},\ \sqrt{130},\ \sqrt{78},\ \sqrt{286},\ \sqrt{1430},\ \sqrt{12870}$

$$V_q^7 = \begin{bmatrix}
1 & -\sqrt{7} & 3 & -5 & \sqrt{5} & -3 & 1 & -1 & \cdot \\
\sqrt{7} & -6 & 10 & -8 & \sqrt{90} & -\sqrt{8} & 2 & 0 & -1 \\
3 & -10 & 14 & -\sqrt{252} & \sqrt{70} & -\sqrt{28} & 0 & 2 & -1 \\
5 & -8 & \sqrt{252} & -14 & \sqrt{70} & 0 & -\sqrt{28} & \sqrt{8} & -3 \\
\sqrt{5} & -\sqrt{90} & \sqrt{70} & -\sqrt{70} & 0 & \sqrt{70} & -\sqrt{70} & \sqrt{90} & -\sqrt{5} \\
3 & -\sqrt{8} & \sqrt{28} & 0 & -\sqrt{70} & 14 & -\sqrt{252} & 8 & -5 \\
1 & -2 & 0 & \sqrt{28} & -\sqrt{70} & \sqrt{252} & -14 & 10 & -3 \\
1 & 0 & -2 & \sqrt{8} & -\sqrt{90} & 8 & -10 & 6 & -\sqrt{7} \\
\cdot & 1 & -1 & 3 & -\sqrt{5} & 5 & -3 & \sqrt{7} & -1
\end{bmatrix}$$

Row normalizations (right column): $\sqrt{2},\ \sqrt{2},\ \sqrt{26},\ \sqrt{26},\ \sqrt{286},\ \sqrt{286},\ \sqrt{858},\ \sqrt{858}$

$$V_q^6 = \begin{bmatrix}
4 & -\sqrt{28} & 2 & -4 & \sqrt{40} & -2 & 2 & \cdot & \cdot \\
\sqrt{28} & -17 & 13 & -3 & \sqrt{10} & -1 & -1 & \sqrt{7} & \cdot \\
2 & -13 & 22 & -\sqrt{63} & 0 & \sqrt{7} & -\sqrt{28} & 1 & 2 \\
4 & -3 & \sqrt{63} & 1 & -\sqrt{70} & \sqrt{7} & -\sqrt{7} & -1 & 2 \\
\sqrt{40} & -\sqrt{10} & 0 & \sqrt{70} & -20 & \sqrt{70} & 0 & -\sqrt{10} & \sqrt{40} \\
2 & -1 & -\sqrt{7} & \sqrt{7} & -\sqrt{70} & 1 & \sqrt{63} & -3 & 4 \\
2 & 1 & -\sqrt{28} & \sqrt{7} & 0 & -\sqrt{63} & 22 & -13 & 2 \\
\cdot & \sqrt{7} & -1 & -1 & \sqrt{10} & -3 & 13 & -17 & \sqrt{28} \\
\cdot & \cdot & 2 & -2 & \sqrt{40} & -4 & 2 & -\sqrt{28} & 4
\end{bmatrix}$$

Row normalizations (right column): $\sqrt{15},\ \sqrt{10},\ \sqrt{110},\ \sqrt{66},\ \sqrt{33},\ \sqrt{660},\ \sqrt{1980}$

$$V_q^5 = \begin{bmatrix}
4 & -\sqrt{20} & \sqrt{20} & -\sqrt{80} & \sqrt{8} & -2 & \cdot & \cdot & \cdot \\
\sqrt{20} & -11 & \sqrt{35} & -\sqrt{5} & -\sqrt{2} & \sqrt{5} & -3 & \cdot & \cdot \\
\sqrt{20} & -\sqrt{35} & 4 & \sqrt{5} & -\sqrt{14} & \sqrt{35} & 0 & -3 & \cdot \\
\sqrt{80} & -\sqrt{5} & -\sqrt{5} & 9 & -\sqrt{18} & 0 & \sqrt{35} & -\sqrt{5} & -2 \\
\sqrt{8} & \sqrt{2} & -\sqrt{14} & \sqrt{18} & 0 & -\sqrt{18} & \sqrt{14} & -\sqrt{2} & -\sqrt{8} \\
2 & \sqrt{5} & -\sqrt{35} & 0 & \sqrt{18} & -9 & \sqrt{5} & \sqrt{5} & -\sqrt{80} \\
\cdot & 3 & 0 & -\sqrt{35} & \sqrt{14} & -\sqrt{5} & -4 & \sqrt{35} & -\sqrt{20} \\
\cdot & \cdot & 3 & -\sqrt{5} & \sqrt{2} & \sqrt{5} & -\sqrt{35} & 11 & -\sqrt{20} \\
\cdot & \cdot & \cdot & 2 & -\sqrt{8} & \sqrt{80} & -\sqrt{20} & \sqrt{20} & -4
\end{bmatrix}$$

Row normalizations (right column): $\sqrt{26},\ \sqrt{26},\ \sqrt{234},\ \sqrt{78},\ \sqrt{156},\ \sqrt{468}$

Tables 25.2 Orbital (integer momentum) tensor matrices *(continued)* [g] l=4.

$q = 0 \quad 1 \quad 2 \quad 3 \quad 4 \quad 5 \quad 6 \quad 7 \quad 8$

$$
V_q^4 = \begin{bmatrix}
14 & -\sqrt{490} & \sqrt{630} & -\sqrt{70} & \sqrt{14} & \cdot & \cdot & \cdot & \cdot \\
\sqrt{490} & -21 & \sqrt{70} & \sqrt{70} & -\sqrt{63} & \sqrt{35} & \cdot & \cdot & \cdot \\
\sqrt{630} & -\sqrt{70} & -11 & \sqrt{360} & -11 & -\sqrt{10} & \sqrt{45} & \cdot & \cdot \\
\sqrt{70} & \sqrt{70} & -\sqrt{360} & 9 & 9 & -\sqrt{360} & \sqrt{10} & \sqrt{35} & \cdot \\
\sqrt{14} & \sqrt{63} & -11 & -9 & 18 & -9 & -11 & \sqrt{63} & \sqrt{14} \\
\cdot & \sqrt{35} & \sqrt{10} & -\sqrt{360} & 9 & 9 & -\sqrt{360} & \sqrt{70} & \sqrt{70} \\
\cdot & \cdot & \sqrt{45} & -\sqrt{10} & -11 & \sqrt{360} & -11 & -\sqrt{70} & \sqrt{630} \\
\cdot & \cdot & \cdot & \sqrt{35} & -\sqrt{63} & \sqrt{70} & \sqrt{70} & -21 & \sqrt{490} \\
\cdot & \cdot & \cdot & \cdot & \sqrt{14} & -\sqrt{70} & \sqrt{630} & -\sqrt{490} & 14 \\
\end{bmatrix}
\begin{matrix}
\\ \\ \\ \\ \\
\sqrt{143} \\ \sqrt{286} \\ \sqrt{2002} \\ \sqrt{2002} \\ \sqrt{2002}
\end{matrix}
$$

$$
V_q^3 = \begin{bmatrix}
14 & -\sqrt{98} & \sqrt{14} & -\sqrt{14} & \cdot & \cdot & \cdot & \cdot & \cdot \\
\sqrt{98} & -7 & -\sqrt{14} & \sqrt{14} & -\sqrt{35} & \cdot & \cdot & \cdot & \cdot \\
\sqrt{14} & \sqrt{14} & -13 & \sqrt{8} & \sqrt{5} & -\sqrt{50} & \cdot & \cdot & \cdot \\
\sqrt{14} & \sqrt{14} & -\sqrt{8} & -9 & \sqrt{45} & 0 & -\sqrt{50} & \cdot & \cdot \\
\cdot & \sqrt{35} & \sqrt{5} & -\sqrt{45} & 0 & \sqrt{45} & -\sqrt{5} & -\sqrt{35} & \cdot \\
\cdot & \cdot & \sqrt{50} & 0 & -\sqrt{45} & 9 & \sqrt{8} & -\sqrt{14} & -\sqrt{14} \\
\cdot & \cdot & \cdot & \sqrt{50} & -\sqrt{5} & -\sqrt{8} & 13 & -\sqrt{14} & -\sqrt{14} \\
\cdot & \cdot & \cdot & \cdot & \sqrt{35} & -\sqrt{14} & \sqrt{14} & 7 & -\sqrt{98} \\
\cdot & \cdot & \cdot & \cdot & \cdot & \sqrt{14} & -\sqrt{14} & \sqrt{98} & -14 \\
\end{bmatrix}
\begin{matrix}
\\ \\ \\ \\ \\ \\
\sqrt{198} \\ \sqrt{66} \\ \sqrt{330} \\ \sqrt{990}
\end{matrix}
$$

$$
V_q^2 = \begin{bmatrix}
28 & -14 & \sqrt{28} & \cdot & \cdot & \cdot & \cdot & \cdot & \cdot \\
14 & 7 & -\sqrt{175} & \sqrt{63} & \cdot & \cdot & \cdot & \cdot & \cdot \\
\sqrt{28} & \sqrt{175} & -8 & -9 & \sqrt{90} & \cdot & \cdot & \cdot & \cdot \\
\cdot & \sqrt{63} & 9 & -17 & -\sqrt{10} & 10 & \cdot & \cdot & \cdot \\
\cdot & \cdot & \sqrt{90} & \sqrt{10} & -20 & \sqrt{10} & \sqrt{90} & \cdot & \cdot \\
\cdot & \cdot & \cdot & 10 & -\sqrt{10} & -17 & 9 & \sqrt{63} & \cdot \\
\cdot & \cdot & \cdot & \cdot & \sqrt{90} & -9 & -8 & \sqrt{175} & \sqrt{28} \\
\cdot & \cdot & \cdot & \cdot & \cdot & \sqrt{63} & -\sqrt{175} & 7 & 14 \\
\cdot & \cdot & \cdot & \cdot & \cdot & \cdot & \sqrt{28} & -14 & 28 \\
\end{bmatrix}
\begin{matrix}
\\ \\ \\ \\ \\ \\ \\
\sqrt{462} \\ \sqrt{924} \\ \sqrt{2772}
\end{matrix}
$$

$$
V_q^1 = \begin{bmatrix}
4 & -2 & \cdot & \cdot & \cdot & \cdot & \cdot & \cdot & \cdot \\
2 & 3 & -\sqrt{7} & \cdot & \cdot & \cdot & \cdot & \cdot & \cdot \\
\cdot & \sqrt{7} & 2 & -3 & \cdot & \cdot & \cdot & \cdot & \cdot \\
\cdot & \cdot & 3 & 1 & -\sqrt{10} & \cdot & \cdot & \cdot & \cdot \\
\cdot & \cdot & \cdot & \sqrt{10} & 0 & -\sqrt{10} & \cdot & \cdot & \cdot \\
\cdot & \cdot & \cdot & \cdot & \sqrt{10} & -1 & -3 & \cdot & \cdot \\
\cdot & \cdot & \cdot & \cdot & \cdot & 3 & -2 & -\sqrt{7} & \cdot \\
\cdot & \cdot & \cdot & \cdot & \cdot & \cdot & \sqrt{7} & -3 & -2 \\
\cdot & \cdot & \cdot & \cdot & \cdot & \cdot & \cdot & 2 & -4 \\
\end{bmatrix}
\begin{matrix}
\\ \\ \\ \\ \\ \\ \\ \\
\sqrt{60} \\ \sqrt{60}
\end{matrix}
$$

Tables 25.2 [g] l=4. *(continued)*

(a) $j = \frac{1}{2}$ (b) $j = \frac{3}{2}$ (c) $j = \frac{5}{2}$

$q = 0 \quad 1$

$$v_q^1 = \begin{bmatrix} 1 & -1 \\ 1 & -1 \end{bmatrix} \begin{matrix} 1 \\ \ \end{matrix} \quad \frac{}{\sqrt{2}}$$

$q = 0 \quad 1 \quad 2 \quad 3$

$$v_q^1 = \begin{bmatrix} 3 & -\sqrt{3} & \cdot & \cdot \\ \sqrt{3} & 1 & -2 & \cdot \\ \cdot & 2 & -1 & -\sqrt{3} \\ \cdot & \cdot & \sqrt{3} & -3 \end{bmatrix} \begin{matrix} \sqrt{10} \\ \\ \sqrt{20} \end{matrix}$$

$$v_q^2 = \begin{bmatrix} 1 & -1 & 1 & \cdot \\ 1 & -1 & 0 & 1 \\ 1 & 0 & -1 & 1 \\ \cdot & 1 & -1 & 1 \end{bmatrix} \begin{matrix} \sqrt{2} \\ \sqrt{2} \\ \sqrt{4} \end{matrix}$$

$$v_q^3 = \begin{bmatrix} 1 & -1 & 1 & -1 \\ 1 & -3 & \sqrt{3} & -1 \\ 1 & -\sqrt{3} & 3 & -1 \\ 1 & -1 & 1 & -1 \end{bmatrix} \begin{matrix} 1 \\ \sqrt{2} \\ \sqrt{5} \\ \sqrt{20} \end{matrix}$$

$q = 0 \quad 1 \quad 2 \quad 3 \quad 4 \quad 5$

$$v_q^1 = \begin{bmatrix} 5 & -\sqrt{5} & \cdot & \cdot & \cdot & \cdot \\ \sqrt{5} & 3 & -\sqrt{8} & \cdot & \cdot & \cdot \\ \cdot & \sqrt{8} & 1 & -3 & \cdot & \cdot \\ \cdot & \cdot & 3 & -1 & -\sqrt{8} & \cdot \\ \cdot & \cdot & \cdot & \sqrt{8} & -3 & -\sqrt{5} \\ \cdot & \cdot & \cdot & \cdot & \sqrt{5} & -5 \end{bmatrix} \begin{matrix} \\ \\ \\ \\ \sqrt{35} \\ \sqrt{70} \end{matrix}$$

$$v_q^2 = \begin{bmatrix} 5 & -\sqrt{5} & \sqrt{5} & \cdot & \cdot & \cdot \\ \sqrt{5} & -1 & -\sqrt{2} & 3 & \cdot & \cdot \\ \sqrt{5} & \sqrt{2} & -4 & 0 & 3 & \cdot \\ \cdot & 3 & 0 & -4 & \sqrt{2} & \sqrt{5} \\ \cdot & \cdot & 3 & -\sqrt{2} & -1 & \sqrt{5} \\ \cdot & \cdot & \cdot & \sqrt{5} & -\sqrt{5} & 5 \end{bmatrix} \begin{matrix} \\ \\ \sqrt{28} \\ \sqrt{14} \\ \sqrt{84} \end{matrix}$$

$$v_q^3 = \begin{bmatrix} 5 & -\sqrt{10} & \sqrt{5} & -\sqrt{5} & \cdot & \cdot \\ \sqrt{10} & -7 & 1 & 1 & -\sqrt{8} & \cdot \\ \sqrt{5} & -1 & -4 & \sqrt{8} & -1 & -\sqrt{5} \\ \sqrt{5} & 1 & -\sqrt{8} & 4 & 1 & -\sqrt{5} \\ \cdot & \sqrt{8} & -1 & -1 & 7 & -\sqrt{10} \\ \cdot & \cdot & \sqrt{5} & -\sqrt{5} & \sqrt{10} & -5 \end{bmatrix} \begin{matrix} \\ \sqrt{18} \\ \sqrt{12} \\ \sqrt{30} \\ \sqrt{180} \end{matrix}$$

$$v_q^4 = \begin{bmatrix} 1 & -\sqrt{2} & 3 & -1 & 1 & \cdot \\ \sqrt{2} & -3 & \sqrt{5} & -\sqrt{5} & 0 & 1 \\ 3 & -\sqrt{5} & 2 & 0 & -\sqrt{5} & 1 \\ 1 & -\sqrt{5} & 0 & 2 & -\sqrt{5} & 3 \\ 1 & 0 & -\sqrt{5} & \sqrt{5} & -3 & \sqrt{2} \\ \cdot & 1 & -1 & 3 & -\sqrt{2} & 1 \end{bmatrix} \begin{matrix} \sqrt{2} \\ \sqrt{2} \\ \sqrt{28} \\ \sqrt{14} \\ \sqrt{28} \end{matrix}$$

$$v_q^5 = \begin{bmatrix} 1 & -1 & 1 & -\sqrt{2} & 1 & -1 \\ 1 & -5 & \sqrt{10} & -\sqrt{5} & \sqrt{5} & -1 \\ 1 & -\sqrt{10} & 10 & -\sqrt{20} & \sqrt{5} & -\sqrt{2} \\ \sqrt{2} & -\sqrt{5} & \sqrt{20} & -10 & \sqrt{10} & -1 \\ 1 & -\sqrt{5} & \sqrt{5} & -\sqrt{10} & 5 & -1 \\ 1 & -1 & \sqrt{2} & -1 & 1 & -1 \end{bmatrix} \begin{matrix} 1 \\ \sqrt{2} \\ \sqrt{9} \\ \sqrt{12} \\ \sqrt{42} \\ \sqrt{252} \end{matrix}$$

Tables 25.3 *Spinor (half-integer momentum) tensor matrices [a] j=1/2, [b] j=3/2, and [c] j=5/2.*

c. Mixed angular-momentum bases

Two or more sets

$$\left\{ \left| \begin{matrix} j_1 \\ j_1 \end{matrix} \right\rangle, \left| \begin{matrix} j_1 \\ j_1-1 \end{matrix} \right\rangle \right\}, \cdots \left\{ \left| \begin{matrix} j_2 \\ j_2 \end{matrix} \right\rangle, \cdots \right\}, \cdots$$

of the angular-momentum bases are connected by generalized tensor operators of the following form:

$$\mathbf{v}_q^k \left(j_1 j_2 \right) = \left(-1 \right)^{2j_1} \sum_{m_1 m_2} C_{m_1 \ -m_2 \ q}^{j_1 \ j_2 \ k} \left| \begin{matrix} j_1 \\ m_1 \end{matrix} \right\rangle \left\langle \begin{matrix} j_2 \\ m_2 \end{matrix} \right| \left(-1 \right)^{j_2+m_2} \qquad (25.1.17a)$$

$$= \sum_{m_1 m_2} \left(-1 \right)^{j_1-m_1} \sqrt{2k+1} \begin{pmatrix} k & j_2 & j_1 \\ q & m_2 & -m_1 \end{pmatrix} \left| \begin{matrix} j_1 \\ m_1 \end{matrix} \right\rangle \left\langle \begin{matrix} j_2 \\ m_2 \end{matrix} \right| \qquad (25.1.17b)$$

This differs only by a phase $\left(-1 \right)^{2j_1}$ from the T operator given in Eq. (25.1.2). For $j_1 = j_2$ it reduces to the definition of Eq. (25.1.14). For nonzero "shift" Δ, where

$$\Delta = j_1 - j_2, \qquad (25.1.18)$$

The matrix representations of the operators are rectangular. Some examples are shown in Table 25.4 for integral $j_1, j_2 = 1-3$. Two explicit examples are the following:

$$\sqrt{10} V_1^1 \left(pd \right) = \begin{bmatrix} \cdot & \cdot & 1 & \cdot & \cdot \\ \cdot & \cdot & \cdot & \sqrt{3} & \cdot \\ \cdot & \cdot & \cdot & \cdot & \sqrt{6} \end{bmatrix} \qquad \sqrt{10} V_{-2}^1 \left(dp \right) = \begin{bmatrix} \cdot & \cdot & \cdot \\ \cdot & \cdot & \cdot \\ 1 & \cdot & \cdot \\ \cdot & \sqrt{3} & \cdot \\ \cdot & \cdot & \sqrt{6} \end{bmatrix}$$

$$= E_{63} + \sqrt{3} E_{74} + \sqrt{6} E_{85} \qquad = E_{36} + \sqrt{3} E_{47} + \sqrt{6} E_{58}.$$

The numbering for E_{ij} reflects the choice of numbers 1 to 5 for d states $\left(\left| 1 \right\rangle = \left| \begin{matrix} 2 \\ 2 \end{matrix} \right\rangle, \left| 2 \right\rangle = \left| \begin{matrix} 2 \\ 1 \end{matrix} \right\rangle, \ldots, \left| 5 \right\rangle = \left| \begin{matrix} 2 \\ -2 \end{matrix} \right\rangle \right)$ and 6 to 8 for the p states $\left(\left| 6 \right\rangle = \left| \begin{matrix} 1 \\ 1 \end{matrix} \right\rangle, \left| 7 \right\rangle = \left| \begin{matrix} 1 \\ 0 \end{matrix} \right\rangle, \left| 8 \right\rangle = \left| \begin{matrix} 1 \\ -1 \end{matrix} \right\rangle \right)$. The tables exhibit the $\mathbf{v}_q^k \left(l_1 l_2 \right)$ matrices for $l_1 - l_2 \equiv \Delta > 0$, and the transpose is found using the symmetry relation

$$\mathbf{v}_a^k \left(l_2 l_1 \right) = \left(-1 \right)^{l+q} \tilde{\mathbf{v}}_{-a}^k \left(l_1 l_2 \right) \qquad (25.1.19)$$

(f) (d)

$$q = 1 \quad 2 \quad 3 \quad 4 \quad 5$$

$V_q^5 =$

q=0	1	−1	√2	−√2	1	1
	1	−√24	3	−√8	√3	√5
	√15	−√10	√90	−√15	√5	√15
	√5	−√80	√20	−√80	√5	√30
	√5	−√15	√90	−√10	√15	√210
	√3	−√8	3	−√24	1	√42
	1	−√2	√2	−1	1	

$V_q^4 =$

√6	−√27	3	−√3	·	
√2	−7	√48	−1	−√2	√5
√40	−√5	√15	√5	−√10	√20
√60	−√30	0	√30	−√60	√140
√10	−√5	−√15	√5	−√40	√140
√2	1	−√48	7	−√2	√14
·	√3	−3	√27	−√6	

$V_q^3 =$

√10	−√5	√5	·	·	
√10	−√15	0	√5	·	
√24	−1	−3	√3	√2	
2	√2	−√8	√2	2	√12
√2	√3	−3	−1	√24	√12
·	√5	0	−√15	√10	√60
·	·	√5	−√5	√10	√30

$V_q^2 =$

√5	−√5	·	·	·	
√5	0	−√5	·	·	
√3	√2	−√2	−√3	·	
1	2	0	−2	−1	
·	√3	√2	−√2	−√3	√14
·	·	√5	0	−√5	√14
·	·	·	√5	−√5	√14

$V_q^1 =$

√15	·	·	·	·	
√5	√10	·	·	·	
1	√8	√6	·	·	
·	√3	3	√3	·	
·	·	√6	√8	1	√35
·	·	·	√10	√5	√35
·	·	·	·	√15	

(f) (p)

$$q = 2 \quad 3 \quad 4$$

q=1	1	−1	1	
q=0	√3	−√12	√3	1
	√3	−√15	√15	2
	√10	−√8	√10	√28
	√15	−√15	√3	√28
	√3	−√12	√3	√14
	1	−1	1	

√3	−√3	·	
√5	−2	−1	2
1	−1	−√5	√12
√6	0	−√6	√12
√5	1	−1	√2
1	2	−√5	
·	√3	−√3	

√15	·	·	
√10	√5	·	
√2	√8	1	
√3	√3	√3	√21
1	√8	√2	√21
·	√5	√10	√7
·	·	√15	

(d) (p)

$$q = 1 \quad 2 \quad 3$$

q=0	1	−1	1	1
	1	−√8	√2	√3
	√6	−√3	√6	√15
	√2	−√8	1	√5
	1	−1	1	

√2	−√2	·	
1	−1	−1	√3
√3	0	−√3	√6
1	1	−1	√2
·	√2	−√2	

√6	·	·	
√3	√3	·	
1	2	1	√10
·	√3	√3	√10
·	·	√6	

Tables 25.4 *Mixed orbital tensor matrices [f+d] l=3 and 2, [f+p] l=3 and 1, and [d+p] l=2 and 1.*

d. Wigner-Eckart Theorem for R_3

The Wigner-Eckart theorem is related to the R_3-factorization lemmas (24.2.25) or (24.2.30).

$$\int d\left(\alpha\beta\gamma\right) D^{j_3^*}_{m_3 m_3'}\left(\alpha\beta\gamma\right) D^{k}_{q q'}\left(\alpha\beta\gamma\right) D^{j_2}_{m_2 m_2'}\left(\alpha\beta\gamma\right) = C^{k\ j_2\ j_3}_{q\ m_2\ m_3}\, C^{k\ j_2\ j_3}_{q'\ m_2'\ m_3'} / \left(2j_3+1\right) \qquad (24.2.25)_{repeated}$$

Operator $T^k_{q_{j_1}}$ in a tensorial set $\left(T^k_{-q},\dots,T^k_q\right)$ transforms according to R_3 rotation matrices as follows:

$$R\left(\alpha\beta\gamma\right) T^k_q R^\dagger\left(\alpha\beta\gamma\right) = \sum_{q'=-k}^{k} T^k_{q'} D^k_{q'q}\left(\alpha\beta\gamma\right),$$

Then matrix elements of T^k_q in angular-momentum basis are of the form

$$\left\langle \begin{matrix} j_3 \\ m_3 \end{matrix} \middle| T^k_q \middle| \begin{matrix} j_2 \\ m_2 \end{matrix} \right\rangle = C^{k\ j_2\ j_3}_{q\ m_2\ m_3}\left\langle j_3 \middle\| T^k \middle\| j_2 \right\rangle, \qquad (25.1.20a)$$

where the $C^{k\ j_2\ j_3}_{q\ m_2\ m_3}$ are coupling coefficients, and the constants called *reduced matrix elements*

$$\left\langle j_3 \middle\| T^k \middle\| j_2 \right\rangle \equiv \frac{1}{2j_3+1}\ \sum_{q'=-k}\sum_{m_2'=-j_2}\sum_{m_3'=-j_3} C^{k\ j_2\ j_3}_{q'\ m_2'\ m_3'}\left\langle \begin{matrix} j_3 \\ m_3' \end{matrix} \middle| T^k_{q'} \middle| \begin{matrix} j_2 \\ m_2' \end{matrix} \right\rangle \qquad (25.1.20b)$$

are independent of q, m_2, or m_3.

The theorem implies that the representations of different tensor operators that transform according to a given irrep D^k must be proportional to each other. The proportionality constants $\left\langle j_1 \middle\| T^k \middle\| j_2 \right\rangle$ are called *reduced matrix elements*.

A tensor operator T^k_q representation must be proportional to unit tensor $\mathbf{v}^k_q$ in (25.1.17):

$$\mathbf{v}^k_q = \left(-1\right)^{2j_1} \sum C^{j_1\ j_2\ k}_{m_1\ -m_2\ q}\left(-1\right)^{j_2+m_2}\middle| \begin{matrix} j_1 \\ m_1 \end{matrix} \right\rangle\left\langle \begin{matrix} j_2 \\ m_2 \end{matrix} \middle| = \sum\left(-1\right)^{j_1-m_1}\sqrt{2k+1}\left(\begin{matrix} k & j_2 & j_1 \\ q & m_2 & -m_1 \end{matrix}\right)\middle| \begin{matrix} j_1 \\ m_1 \end{matrix} \right\rangle\left\langle \begin{matrix} j_2 \\ m_2 \end{matrix} \middle|$$

The 3j definitions (7.2.30a) and symmetry relations (7.2.31) and (25.1.32) yield the following:

$$\left\langle \begin{matrix} j_1 \\ m_1 \end{matrix} \middle| \mathbf{v}^k_q \middle| \begin{matrix} j_2 \\ m_2 \end{matrix} \right\rangle = \left(-1\right)^{2j_1} C^{j_1\ j_2\ k}_{m_1\ -m_2\ q}\left(-1\right)^{j_2+m_2} = \sum\left(-1\right)^{j_1-m_1}\sqrt{2k+1}\left(\begin{matrix} k & j_2 & j_1 \\ q & m_2 & -m_1 \end{matrix}\right) \qquad (25.1.21)$$

$$= C^{k\ j_2\ j_1}_{q\ m_2\ m_1}\left(-1\right)^{k+j_1-j_2}\sqrt{\left(2k+1\right)/\left(2j_1+1\right)}$$

This has the Wigner-Eckart form (25.1.20a) with the following reduced matrix element:

$$\left\langle j_1 \middle\| \mathbf{v}^k_q \middle\| j_2 \right\rangle = \left(-1\right)^{k+j_1-j_2}\sqrt{\left(2k+1\right)/\left(2j_1+1\right)}. \qquad (25.1.22)$$

Therefore, a general tensor operators T^k_q is just $\mathbf{v}^k_q$ in tables (25.1 – 25.4) times a constant.

$$\left\langle \begin{matrix} j_1 \\ m_1 \end{matrix} \middle| T^k_q \middle| \begin{matrix} j_2 \\ m_2 \end{matrix} \right\rangle = \left\langle \begin{matrix} j_1 \\ m_1 \end{matrix} \middle| \mathbf{v}^k_q \middle| \begin{matrix} j_2 \\ m_2 \end{matrix} \right\rangle \frac{\left\langle j_1 \middle\| T^k_q \middle\| j_2 \right\rangle}{\left\langle j_1 \middle\| \mathbf{v}^k_q \middle\| j_2 \right\rangle} \qquad (25.1.23)$$

Each matrix of T^k_q between bases $\left| j_1 \right\rangle$ and $\left| j_2 \right\rangle$ equals a $\mathbf{v}^k_q$ matrix multiplied by the following factor:

$$\frac{\left\langle j_1 \middle\| T^k_q \middle\| j_2 \right\rangle}{\left\langle j_1 \middle\| \mathbf{v}^k_q \middle\| j_2 \right\rangle} = \left\langle j_1 \middle\| T^k \middle\| j_2 \right\rangle\left(-1\right)^{k+j_1-j_2}\sqrt{\frac{2j_1+1}{2k+1}}, \qquad (25.1.24)$$

and it is proportional to the reduced matrix element of T^k. We now apply the Wigner-Eckart theorem.

e. Evaluation of crystal field splitting

Let us consider an elementary octahedral potential having the form

$$V^{(4)} = D\left[x^4 + y^4 + z^4 - \tfrac{3}{4}r^4\right] = D\left[\frac{2}{\sqrt{70}}\left(X_4^4 + X_{-4}^4\right) + \tfrac{2}{5}X_0^4\right] \tag{25.1.25}$$

This form is derived using the multipole expansion (23.4.10). It also follows from the form of the elementary multipole functions (23.3.8) of fourth degree. The $V^{(4)}$ is the fourth-rank octahedral scalar $\left(A_{1g}\right)$ function since the combination $x^4 + y^4 + z^4$ clearly has cubic-octahedral symmetry.

Let us consider the effect of this potential on a d orbital, i.e., orbitals belonging to total angular momentum $j = 2$. Setting $j_1 = j_2 = 2$ in Eqs. (25.1.23) and (25.1.24) gives

$$\left\langle V^{(4)}\right\rangle_{j=2} = D\left\langle \frac{2}{\sqrt{70}}\left(v_4^4 + v_{-4}^4\right) + \tfrac{2}{5}v_0^4 \right\rangle_{j=2} \frac{\sqrt{5}}{3}\langle 2\|X^4\|2\rangle. \tag{25.1.26}$$

From the ($j = 2$) tables [Tables 25.2(d)] the following representation of the $V^{(4)}$ potential is derived:

$$\left\langle V^{(4)}\right\rangle_{j=2} = \frac{D}{\sqrt{70}}\begin{pmatrix} \tfrac{2}{5} & \cdot & \cdot & \cdot & 2 \\ \cdot & -\tfrac{8}{5} & \cdot & \cdot & \cdot \\ \cdot & \cdot & \tfrac{12}{5} & \cdot & \cdot \\ \cdot & \cdot & \cdot & -\tfrac{8}{5} & \cdot \\ 2 & \cdot & \cdot & \cdot & \tfrac{2}{5} \end{pmatrix} \frac{\sqrt{5}}{3}\langle 2\|X^4\|2\rangle. \tag{25.1.27}$$

The eigenvectors and eigenvalues of this matrix are easy to find. In fact, we derived the eigenvectors $\left\{\left|\begin{smallmatrix}T_2\\1\end{smallmatrix}\right\rangle, \left|\begin{smallmatrix}T_2\\2\end{smallmatrix}\right\rangle, \left|\begin{smallmatrix}T_2\\3\end{smallmatrix}\right\rangle\right\}$ and $\left\{\left|\begin{smallmatrix}E\\1\end{smallmatrix}\right\rangle, \left|\begin{smallmatrix}E\\2\end{smallmatrix}\right\rangle\right\}$ in Eqs. (23.4.20) by symmetry projection even before introducing the potential. Now the eigenvalues follow by multiplying $\left\langle V^{(4)}\right\rangle$ by $\left|\begin{smallmatrix}T_2\\j\end{smallmatrix}\right\rangle$ or $\left|\begin{smallmatrix}E\\j\end{smallmatrix}\right\rangle$. The triply degenerate T_2 eigenvalue is

$$\left\langle \begin{smallmatrix}T_2\\3\end{smallmatrix}\left|V^{(4)}\right|\begin{smallmatrix}T_2\\3\end{smallmatrix}\right\rangle = \tfrac{1}{2}\left(\left\langle\begin{smallmatrix}2\\-2\end{smallmatrix}\right| - \left\langle\begin{smallmatrix}2\\-2\end{smallmatrix}\right|\right)V^4\left(\left|\begin{smallmatrix}2\\2\end{smallmatrix}\right\rangle - \left|\begin{smallmatrix}2\\-2\end{smallmatrix}\right\rangle\right)$$

$$= -8D\langle 2\|X^4\|2\rangle/\left(15\sqrt{14}\right), \tag{25.1.28a}$$

And the double degenerate E eigenvalue is

$$\left\langle \begin{smallmatrix}E\\2\end{smallmatrix}\left|V^{(4)}\right|\begin{smallmatrix}E\\2\end{smallmatrix}\right\rangle = \tfrac{1}{2}\left(\left\langle\begin{smallmatrix}2\\2\end{smallmatrix}\right| + \left\langle\begin{smallmatrix}2\\-2\end{smallmatrix}\right|\right)V^4\left(\left|\begin{smallmatrix}2\\2\end{smallmatrix}\right\rangle + \left|\begin{smallmatrix}2\\2\end{smallmatrix}\right\rangle\right)$$

$$= 12D\langle 2\|X^4\|2\rangle/\left(15\sqrt{14}\right). \tag{25.1.28b}$$

Note the (-2:3) ratio of the eigenvalues. This preserves the "center of gravity" of the energy levels, since T_2 has three levels while E has only two. In fact, the scalar $\left(V^{(0)} = v_0^0\right)$ tensor operator is the only one with nonzero trace. No other tensor operator can shift the center of gravity.

Hence, the $j = 2$ example is a little too simple. The Wigner-Eckart results (25.1.28) do not predict anything interesting for the two levels E and T_2 unless one knows the value of the reduced matrix element $\langle 2 \| X^4 \| 2 \rangle$. Before we discuss formulas for the reduced matrix elements, let us treat examples of crystal field splitting of $j = 3$ levels. Setting $j_1=j_2=3$ in Eqs. (25.1.23) and (25.1.24) gives the following representation of $V^{(4)}$ after using Table 25.2(f):

$$\langle V^{(4)} \rangle_{j=3} = D \langle 2 (v_4^4 + v_{-4}^4)/\sqrt{70} + (2/5) v_0^4 \rangle (\sqrt{7/3}) \langle 3 \| X^4 \| 3 \rangle \qquad (25.1.29a)$$

$$= D \begin{pmatrix} 3 & \cdot & \cdot & \cdot & \sqrt{15} & \cdot & \cdot \\ \cdot & -7 & \cdot & \cdot & \cdot & 5 & \cdot \\ \cdot & \cdot & 1 & \cdot & \cdot & \cdot & \sqrt{15} \\ \cdot & \cdot & \cdot & 6 & \cdot & \cdot & \cdot \\ \sqrt{15} & \cdot & \cdot & \cdot & 1 & \cdot & \cdot \\ \cdot & 5 & \cdot & \cdot & \cdot & -7 & \cdot \\ \cdot & \cdot & \sqrt{15} & \cdot & \cdot & \cdot & 3 \end{pmatrix} (2\sqrt{7}/15\sqrt{154}) \langle 3 \| X^4 \| 3 \rangle . \qquad (25.1.29b)$$

The eigenvectors of this $\langle V^{(4)} \rangle$ matrix can be found by symmetry projection as in Section 23.4, by direct solution of the matrix eigenvalue problem, or by inspection of multipole functions. We will use the third method now, since it has not been discussed.

From the $O_3 \supset O_h$ correlation table of (23.4.18) it is found that $(j = 3)$ splits into $(A_{2u} \oplus T_{1u} \oplus T_{2u})$. From O_h and O_3 multipole functions, arise relations between polynomials of O_h and O_3. For A_{2u} one has

$$X^{A_{2u}} = xyz = -i(X_{-2}^3 - X_2^3)/\sqrt{30} . \qquad (25.1.30)$$

For the third component of T_{1u} one has

$$X_3^{T_{1u}} = (x^2 - y^2)z = i(X_2^3 + X_{-2}^3)/\sqrt{2} . \qquad (25.1.31)$$

Finally, for the third component of T_{2u} one has

$$X_3^{T_{2u}} = (x^2 + y^2)z = -X_0^3/10. \qquad (25.1.32)$$

From this we easily deduce three normalized eigenvectors

$$|A_{2u}\rangle = \left(\left| \begin{smallmatrix} 3 \\ 2 \end{smallmatrix} \right\rangle - \left| \begin{smallmatrix} 3 \\ -2 \end{smallmatrix} \right\rangle \right)/\sqrt{2}, \qquad \left| \begin{smallmatrix} T_{1u} \\ 3 \end{smallmatrix} \right\rangle = \left(\left| \begin{smallmatrix} 3 \\ 2 \end{smallmatrix} \right\rangle - \left| \begin{smallmatrix} 3 \\ -2 \end{smallmatrix} \right\rangle \right)/\sqrt{2}, \qquad \text{and} \quad \left| \begin{smallmatrix} T_{2u} \\ 3 \end{smallmatrix} \right\rangle = \left| \begin{smallmatrix} 3 \\ 0 \end{smallmatrix} \right\rangle . \qquad (25.1.33)$$

$$\langle A_{2u} | V^{(4)} | A_{2u} \rangle = -12\delta^{(4)}, \qquad \left\langle \begin{smallmatrix} T_{1u} \\ 3 \end{smallmatrix} \right| V^{(4)} \left| \begin{smallmatrix} T_{1u} \\ 3 \end{smallmatrix} \right\rangle = -2\delta^{(4)}, \qquad \left\langle \begin{smallmatrix} T_{2u} \\ 3 \end{smallmatrix} \right| V^{(4)} \left| \begin{smallmatrix} T_{2u} \\ 3 \end{smallmatrix} \right\rangle = 6\delta^{(4)}. \qquad (25.1.34a)$$

respectively, where the reduced factor is

$$\delta^{(4)} = D(2/15\sqrt{22}) \langle 3 \| X^4 \| 3 \rangle. \qquad (25.1.34b)$$

From this we predict a (12-2):(6+2) or 5:4 splitting ratio with A_{2u} and T_{2u} levels sandwiching T_{1u}. This is indicated in Fig. 25.1.2(a). The 4th rank octahedral crystal fields will split all ($j = 3$) levels into the order (A_2, T_1, T_2) with a 5:4 ratio. However, angular-momentum levels with $j = 3$ and higher may be effected by a *sixth*-rank tensor operator whose splitting ratios will be quite different.

$$V^{(6)} = E\left[\left(\sqrt{8}/8\right)X_0^y - \left(2\sqrt{7}/8\right)\left(X_4^6 + X_{-4}^6\right)\right].$$
(25.1.35)

This 6th rank operator is the next term in an octahedral multipole expansion (23.4.10). Its representation for ($j = 3$) follows from Table 25.2(f).

$$\left(V^{(6)}\right)_{j-3} = E\begin{pmatrix} 1 & \cdot & \cdot & \cdot & -7\sqrt{15} & \cdot & \cdot \\ \cdot & -6 & \cdot & \cdot & \cdot & 42 & \cdot \\ \cdot & \cdot & 15 & \cdot & \cdot & \cdot & -7\sqrt{15} \\ \cdot & \cdot & \cdot & -20 & \cdot & \cdot & \cdot \\ -7\sqrt{15} & \cdot & \cdot & \cdot & 15 & \cdot & \cdot \\ \cdot & 42 & \cdot & \cdot & \cdot & -6 & \cdot \\ \cdot & \cdot & -7\sqrt{15} & \cdot & \cdot & \cdot & 1 \end{pmatrix} \times \langle 3\|X^6\|3\rangle / \left(4\sqrt{462}\right).$$
(25.1.36)

This gives a different set of eigenvalues

$$\langle A_{2u}|V^{(6)}|A_{2u}\rangle = -12\delta^{(6)}, \qquad \left\langle \frac{T_{1u}}{3}\Big|V^{(6)}\Big|T_{1u}\right\rangle = -9\delta^{(6)}, \quad \text{and} \quad \left\langle \frac{T_{2u}}{3}\Big|V^{(6)}\Big|\frac{T_{2u}}{3}\right\rangle = -5\delta^{(6)},$$
(25.1.37a)

where
$$\delta^{(6)} = E\langle 3\|X^6\|3\rangle / \left(4\sqrt{462}\right).$$
(25.1.37b)

A pure $V^{(6)}$ makes the T_{1u} level move into the high position as shown in Fig. 25.1.2(b). A 1:2 splitting ratio results for the three levels (A_2, T_2, T_1).

An eighth-rank $V^{(8)}$ octahedral scalar operator exists but cannot have any effect on a ($j = 3$) level. (Its matrix must be zero, since $C_{q\ m\ n}^{3\ 8\ 3} = 0$.) However, another scalar operator is not needed. The fourth- and sixth-rank octahedral operators $V^{(4)}$ and $V^{(6)}$ are sufficient in combination to cause any ordering or splitting of the A_2, T_2, and T_1 sublevels of the $j = 3$ manifold. In fact, there are three O_h-scalar operators $V^{(6)}$, $V^{(4)}$, and $V^{(0)}$, but the $V^{(0)}$ only shifts the center of gravity. The number of independent scalar operators is exactly the number needed to determine all eigenvalues and eigenvectors subject to the constraints of symmetry. Constraints symmetry on C_6 eigensolutions were introduced in Ch. 8.

At this point it may be instructive to review the counting of multipole functions and operators introduced in Section 23.4. Also the treatment of $j = 4$, 5, and 6 octahedral levels should be examined. The analyses for $j = 5$ and 6 are complicated by the fact that octahedral species T_1 or T_2 are repeated. Then the T_1 or T_2 eigenvectors are not determined totally by symmetry constraints.

For high j the number of repeated species can be large. For $l = j = 50$ one predicts in Section 23.4 that 12 T_1 levels and 13 T levels will appear. Since high values of angular quanta are common in molecular spectra it is important to learn how to deal with them. In Section 25.4 we will discuss some efficient methods for deriving

tensor operator eigensolutions for high-j states. The methods are based upon the theory of level clusters and induced representation bases.

Related problems involve very high crystal potentials, which cause splitting that is comparable to or greater than the spacing between j levels. A large enough crystal potential could mix states of different angular momentum (j) strongly enough to make j a useless quantum number. This happens in the theory of ions tunneling in solids. The theory of level clusters may also be useful then, too.

(a) $T^{(4)}$ Splitting   (b) $T^{(6)}$ Splitting

T_{1u}

$9\ \delta^{(6)}$

T_{2u}

$6\ \delta^{(4)}$

$j=3$

$j=3$

T_{1u}

$-2\ \delta^{(4)}$

T_{2u}

$-5\ \delta^{(6)}$

A_{2u}

$-12\ \delta^{(4)}$

A_{2u}

$-12\ \delta^{(6)}$
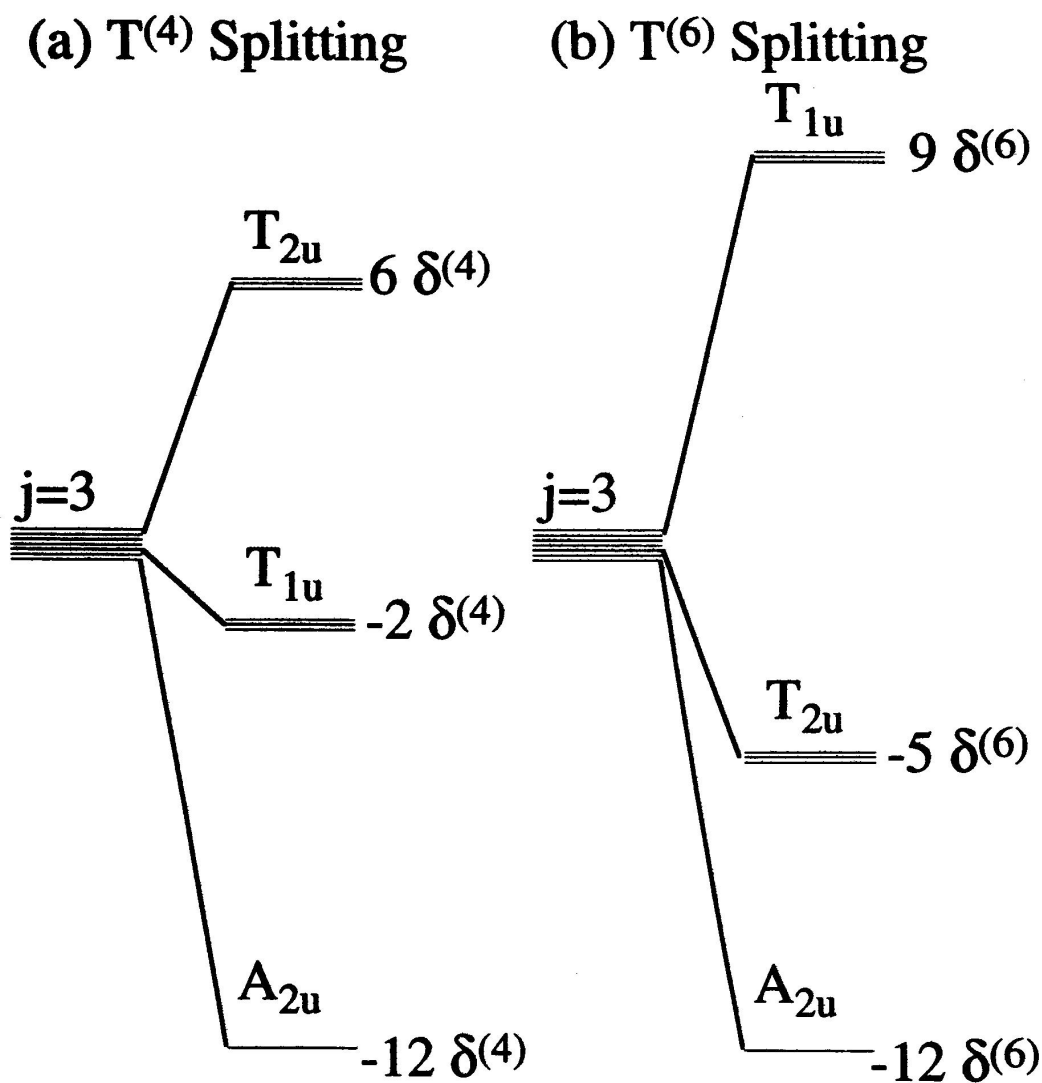
Fig. 25.1.2 Comparison of octahedral tensor splitting (a) Rank-4 (25.1.34) (b) Rank-6 (25.1.36)

25.2. Evaluation of Reduced Matrix Elements

So far we have used the Wigner-Eckart theorem while treating the reduced matrix elements as undetermined constants. Relative splitting does not require the values of these constants. Also, the constants can be fitted to experiment, and then the tensor analysis can be used to predict further results. Such approaches require that we know only the rotational symmetry properties of the system being studied.

However, in order to compute the numerical value of a reduced matrix element one must define the involved operators and states in more detail. So far we have not assumed much about anything except R(3) symmetry properties. It did not matter whether the *(j = 2)*-states treated in Eqs. (25.1.28) were *d*-orbitals of one electron in hydrogen or *D*-orbitals made of over 100 electrons in mendelevium. R(3) Wigner-Eckart results only care that *(j=2)*-states belong to symmetry irrep $D^{[2]}$ while $T^{[k]}$ operators belong to irreps $D^{[k]}$ and $D^{A_{1g}}$ of O_3 and O_h, respectively. We now compare the splitting of *(l = 2)*-orbitals for one electron with the splitting of *(L = 2)*-orbitals for two electrons, in the same cubic O_h symmetry perturbation.

a. Single-electron orbitals in potential fields

Let us assume a single-electron orbital state with a wave function of the form

$$\left\langle r\theta\phi \left| \begin{matrix} l \\ m \end{matrix} N \right. \right\rangle = R_{Nl}(r)Y_m^l(\phi\theta) \quad (25.2.1)$$

Here $R_l(r)$ is the radial wave function and Y_m^l is the angular wave. The radial wave is of the form discussed before in Sec. 21.3 for 3D oscillator or later in Sec. 26.1 for Coulomb H-orbital (26.1.26).

$$R_{N\ell}(r) = f_0 \frac{e^{-\rho/N}\rho^\ell}{a}\left[1 + \frac{(0-n)}{(2\ell+2)}\left(\frac{2\rho}{N}\right) + \frac{(0-n)(1-n)}{2!(2\ell+2)(2\ell+3)}\left(\frac{2\rho}{N}\right)^2 + \frac{(0-n)(1-n)(2-n)}{3!(2\ell+2)(2\ell+3)(2\ell+4)}\left(\frac{2\rho}{N}\right)^3\right] \quad (25.2.2)$$

The latter is a Laquerre polynomial of radius $r=a\rho$ scaled to Bohr length a. The angular wave is a spherical harmonic given by (23.1.16) in terms of the *R(3)* irrep matrix components $D^{[\ell]}$.

$$D_{m,n=0}^{\ell}{}^*(\phi\theta 0)\sqrt{2\ell+1/4\pi} = Y_m^\ell(\phi\theta) \quad (25.2.3)$$

Let us compute matrix elements of a general potential field multipole expansion (23.4.10).

$$V(r,\phi,\theta) = \sum_c \frac{q_c}{|\mathbf{r}-\mathbf{r}_c|} = \begin{cases} \displaystyle\sum_{k=0}^{k}\sum_{q=-\ell}^{k} \frac{Q_q^k(near)}{r^{k+1}}Y_q^k(\phi,\theta) & \text{for: } r>r_C \\ \displaystyle\sum_{k=0}^{k}\sum_{q=-k}^{k} Q_q^k(far)\,r^k\,Y_q^k(\phi,\theta) & \text{for: } r<r_C \end{cases} \quad (25.2.4)$$

Here we consider the far-charge case wherein the atomic orbital lies inside a cubic charge array.

$$V(r,\phi,\theta) = \sum_{k=0}^{k}\sum_{q=-k}^{k} Q_q^k\,r^k\,Y_q^k(\phi,\theta) = \sum_{k,q} A_q^k X_q^k \quad (25.2.5)$$

Y^k-potential terms relate to multipole X^k-functions by (23.3.8) and D^k-functions by (25.2.3).

$$X_q^k = \sqrt{\frac{4\pi}{2k+1}} r^k Y_q^k = r^k D_{q,0}^{k*} \tag{25.2.6}$$

This completes the 3D-polar-radial integral for the potential matrix.

$$\left\langle {}_{m'}^{l'\ N'} \left| V \right| {}_m^{l\ N} \right\rangle = \sum_{kq} A_q^k \left\langle {}_{m'}^{l'\ N'} \left| X_q^k \right| {}_m^{l\ N} \right\rangle$$

$$= \sum_{kq} A_q^k \int r^2\ dr\ R_{N'l'}^*(r) r^k R_{Nl}(r) \int d\phi \int d\theta \sin\theta Y_{m'}^{l'*}(\theta\phi) \sqrt{\frac{4\pi}{2k+1}}\ Y_q^k(\theta\phi) Y_m^l(\theta\phi). \tag{25.2.7}$$

This integral can be written as a product of angular and radial integrals.

$$\left\langle {}_{m'}^{l'\ N} \left| V \right| {}_m^{l\ N} \right\rangle = \sum_{kq} A_q^k \left\langle r^k \right\rangle \sqrt{\frac{4\pi}{2k+1}}\ \int d\theta \sin\theta\ \ Y_{m'}^{l'*}(\theta\phi) Y_q^k(\theta\phi) Y_m^l(\theta\phi) \tag{25.2.8a}$$

Here the diagonal case $(N' = N)$ for the radial integral is denoted by

$$\left\langle r^k \right\rangle = \int_0^\infty r^2 dr \left| R_{Nl}(r) \right|^2 r^k\ . \tag{25.2.8b}$$

We replace the spherical harmonics Y_m^j by irrep components D_{mo}^j using (25.2.3).

$$\sqrt{\frac{4\pi}{2k+1}} \int d\phi \int \sin\theta\ d\theta\ Y_{m'}^{l'*}(\theta\phi) Y_q^k(\theta\phi) Y_m^l(\theta\phi) = \frac{\sqrt{(2l'+1)(2l+1)}}{4\pi} \int d\phi \int \sin\theta\ d\theta\ D_{m'0}^{l'} D_{q0}^{k*} D_{m0}^l \tag{25.2.9}$$

To get the integral into the $\int D^* D\ D$ form (24.2.25) we add third Euler-angle integral $\frac{1}{2\pi}\int d\gamma$. This does nothing if all the body quantum numbers are zero. Then the $\int D^* D\ D = CC$ relation (24.2.25) is used.

$$\left\langle {}_{m'}^{l'\ N} \left| V \right| {}_m^{l\ N} \right\rangle = C_{q\ m\ m'}^{k\ l\ l'} \left(\sum_{k,q} A_q^k \sqrt{\frac{2l+1}{2l'+1}} C_{000}^{kl\ l'} \left\langle r^k \right\rangle \right) = C_{q\ m\ m'}^{k\ l\ l'} \left(\sum_{k,q} A_q^k \left\langle l' \| X^k \| l \right\rangle \right) \tag{25.2.10a}$$

The reduced matrix element in parentheses is the following CGC or 3jC using (24.2.30).

$$\left\langle l' \| X^k \| l \right\rangle = \sqrt{\frac{2l+1}{2l'+1}}\ C_{000}^{kl\ l'} \left\langle r^k \right\rangle = \sqrt{2l+1}(-1)^{k-l} \begin{pmatrix} k & l & l' \\ 0 & 0 & 0 \end{pmatrix} \left\langle r^k \right\rangle \tag{25.2.10b}$$

For the crystal splitting example in (25.1.28) we would need the reduced matrix element

$$\left\langle 2 \| X^4 \| 2 \right\rangle = \sqrt{\frac{2}{7}} \left\langle r^4 \right\rangle. \tag{25.2.10c}$$

For hydrogen the radial integral can be shown to be [see K. Bockaster, *Phys. Rev. A* 9, 1087 (1974)]

$$\left\langle r^4 \right\rangle = (a_0)^4 \frac{n^4}{8} \left\{ 63n^4 - n^2 \left[70l(l+1) - 105 \right] + 15(l-1)l(l+1)(l+2) - 20l(l+1) + 12 \right\}$$

$$= (a_0)^4 \frac{63n^4}{8}(n=1)(n-1)(n+2)(n-2) \quad (\text{for } l = 2).$$

The hydrogen values are often used for approximate theories of other atoms.

b. Two-electron orbitals in potential fields

We shall now compare the splitting due to a cubic crystal field of a two-electron $L = 2$ level (d^2 ^1D) with that of

the one-electron orbital (d^1 ^2D). This amounts to a comparison of two separate applications of the Wigner-Eckart

theorem and two different reduced matrix elements. For the two-d-electron case we need energy matrix elements

given below. (Note that (p^2 ^1D) atomic levels are *not* split by a 4th rank field.)

$$\left\langle \left[d^2 \right]_{M'}^2 \left| \overset{\text{total}}{X_q^4} \right| \left[d^2 \right]_M^2 \right\rangle = C_{q\ M\ M'}^{4\ 2\ 2} \left\langle \left[d^2 \right] 2 \left\| \overset{\text{total}}{X^4} \right\| \left[d^2 \right] 2 \right\rangle, \tag{25.2.11a}$$

Here the perturbation

$$\overset{\text{total}}{X_q^4} = \overset{\text{electron 1}}{x_q^4} + \overset{\text{electron 2}}{x_q^4} \tag{25.2.11b}$$

is a sum of individual electron operators. For one electron we have

$$\left\langle d^1 \overset{2}{}_{M'} \left| x_q^4 \right| d^1 \overset{2}{}_M \right\rangle = C_{q\ M\ M'}^{4\ 2\ 2} \left\langle 2 \| x^4 \| 2 \right\rangle, \tag{25.2.12}$$

that is the same as Eq. (25.2.11a) except for the reduced matrix elements that we now compare.

For the sake of generality, let us evaluate the matrix element of a general multipole operator X_q^k between

general mixed configuration $\| l_1 l_2 | L \rangle$ states instead of pure $| l^2 L \rangle$ configuration states.

$$\left\langle \left[l_1 l_2 \right]_M^L \left| \overset{\text{total}}{X_q^k} \right| \left[l'_l l'_2 \right]_{M'}^{L'} \right\rangle = \left\langle \left[l_1 l_2 \right]_M^L \left| \overset{\text{electron 1}}{x_q^k} \right| \left[l'_l l'_2 \right]_{M'}^{L'} \right\rangle + \left\langle \left[l_1 l_2 \right]_M^L \left| \overset{\text{electron 2}}{x_q^k} \right| \left[l'_l l'_2 \right]_{M'}^{L'} \right\rangle \tag{25.2.13}$$

Treating the first term by the Wigner-Eckart theorem gives

$$\left\langle \left[l_1 l_2 \right]_M^L \left| \overset{\text{electron 1}}{x_q^k} \right| \left[l'_l l'_2 \right]_{M'}^{L'} \right\rangle = C_{q\ M'\ M}^{k\ L'\ L} \left\langle \left[l_1 l_2 \right]_M^L L \right\| \overset{\text{electron 1}}{x^k} \left\| \left[l'_l l'_2 \right] L' \right\rangle. \tag{25.2.14}$$

Each two-electron state is a coupling of the form

$$\left| \left[l'_l l'_2 \right]_{M'}^{L'} \right\rangle = \sum_{m'_1 m'_2} C_{m'_1\ m'_2\ M'}^{l'_1\ l'_2\ L'} \left| \begin{matrix} l'_1 \\ m'_1 \end{matrix} \right\rangle \left| \begin{matrix} l'_2 \\ m'_2 \end{matrix} \right\rangle \tag{25.2.15}$$

of single-electron states. Inserting these on the left of (25.2.14) gives

$$\sum_{m_1 m_2} \sum_{m'_1 m'_2} C_{m_1\ m_2\ M}^{l_1\ l_2\ L} C_{m'_1\ m'_2\ M'}^{l'_1\ l'_2\ L'} \left\langle \begin{matrix} l'_1 \\ m'_1 \end{matrix} \right| \left\langle \begin{matrix} l_2 \\ m_2 \end{matrix} \right| \overset{\text{electron 1}}{x_q^k} \left| \begin{matrix} l'_1 \\ m'_1 \end{matrix} \right\rangle \left| \begin{matrix} l'_2 \\ m'_2 \end{matrix} \right\rangle = C_{q\ M'\ M}^{k\ L'\ L} \left\langle \left[l_1 l_2 \right] L \right\| \overset{\text{electron 1}}{x^k} \left\| \left[l'_1 l'_2 \right] L' \right\rangle. \tag{25.2.16}$$

Now $\overset{\text{electron 1}}{x_q^k}$ only acts upon the state vectors of electron-1. Its Wigner-Eckart theorem follows.

$$\left\langle \begin{matrix} l_1 \\ m_1 \end{matrix} \middle| \left\langle \begin{matrix} l_2 \\ m_2 \end{matrix} \middle| \begin{matrix} \text{electron 1} \\ x_q^k \end{matrix} \middle| \begin{matrix} l'_1 \\ m'_1 \end{matrix} \right\rangle \middle| \begin{matrix} l'_2 \\ m'_2 \end{matrix} \right\rangle = \left\langle \begin{matrix} l_1 \\ m_1 \end{matrix} \middle| \begin{matrix} \text{electron 1} \\ x_q^k \end{matrix} \middle| \begin{matrix} l'_1 \\ m'_1 \end{matrix} \right\rangle \left\langle \begin{matrix} l_2 \\ m_2 \end{matrix} \middle| \begin{matrix} l'_2 \\ m'_2 \end{matrix} \right\rangle = C_{q\ m'_1\ m_1}^{k\ l'_1\ l_1} \left\langle l_1 \middle\| x_q^k \middle\| l'_1 \right\rangle \delta_{l_2 l'_2} \delta_{m_2 m'_2}. \quad (25.2.17)$$

We put this in (25.2.16) and let CGC orthonormality (24.2.21) bring $C_{q\ M'\ M}^{k\ L'\ L}$ to the left-hand side.

$$\left(\sum_{m_1 m_2\ m'_1} \sum_{qM'} C_{q\ m'_1\ m_1}^{k\ l'_1\ l_1} C_{m_1\ m_2\ M}^{l_1\ l_2\ L} C_{q\ M'\ M}^{k\ L'\ L} C_{m'_1\ m_2\ M'}^{l'_1\ l_2\ L'} \right) \left\langle l_1 \middle\| x_q^k \middle\| l'_1 \right\rangle = \left\langle [l_1 l_2] L \middle\| \overset{\text{electron 1}}{X^k} \middle\| [l'_1 l'_2] L' \right\rangle \quad (25.2.18)$$

The expression for electron-2 is similar.

$$\left(\sum_{m_1 m_2\ m'_2} \sum_{qM'} C_{q\ m'_2\ m_2}^{k\ l'_2\ l_2} C_{m_1\ m_2\ M}^{l_1\ l_2\ L} C_{q\ M'\ M}^{k\ L'\ L} C_{m_1\ m'_2\ M'}^{l_1\ l'_2\ L'} \right) \left\langle l_2 \middle\| x_q^k \middle\| l'_2 \right\rangle = \left\langle [l_1 l_2] L \middle\| \overset{\text{electron 2}}{x^k} \middle\| [l'_1 l'_2] L' \right\rangle \quad (25.2.19)$$

The combinations of coupling coefficients in the parentheses appear often in angular-momentum calculations. They involve the *Racah 6j recoupling coefficient* defined as follows.

$$\sum_{\substack{m_1, m_2, m_3 \\ m_{12}, m_{23}}} C_{m_1\ m_2\ m_{12}}^{j_1\ j_2\ j_{12}} C_{m_{12}\ m_3\ M}^{j_{12}\ j_3\ J} C_{m_1\ m_{23}\ M}^{j_1\ j_{23}\ J} C_{m_2\ m_3\ m_{23}}^{j_2\ j_3\ j_{23}} = (-1)^{j_1+j_2+j_3+J} \sqrt{(2j_{12}+1)(2j_{23}+1)} \begin{Bmatrix} j_{12} & j_1 & j_2 \\ j_{23} & j_3 & J \end{Bmatrix} \quad (25.2.20\text{a})$$

Using (25.2.20a) and (25.2.18) gives the electron-1 reduced matrix element.

$$\left\langle [l_1 l_2] L \middle\| \overset{\text{electron 1}}{x^k} \middle\| [l'_1 l'_2] L' \right\rangle = (-1)^{k+l'_1+l_2+L} \sqrt{(2l_1+1)(2L'+1)} \begin{Bmatrix} l_1 & k & l'_1 \\ L' & l_2 & L \end{Bmatrix} \left\langle l_1 \middle\| x^k \middle\| l'_1 \right\rangle \quad (25.2.20\text{b})$$

Similarly (25.2.18) gives the electron-2 element.

$$\left\langle [l_1 l_2] L \middle\| \overset{\text{electron 2}}{x^k} \middle\| [l'_1 l'_2] L' \right\rangle = (-1)^{k+l'_2+l_1+L} \sqrt{(2l_2+1)(2L'+1)} \begin{Bmatrix} l_2 & k & l'_2 \\ L' & l_1 & L \end{Bmatrix} \left\langle l_2 \middle\| x^k \middle\| l'_2 \right\rangle \quad (25.2.20\text{c})$$

The numerical values of the *6j* coefficient are given by a simplified formula that is derived later.

Our example has the following 2-electron reduced element in terms of 1-electron elements.

$$\left\langle [22]2 \middle\| X^4 \middle\| [22]2 \right\rangle = 2\sqrt{5 \cdot 5} \begin{Bmatrix} 2 & 4 & 2 \\ 2 & 2 & 2 \end{Bmatrix} \left\langle 2 \middle\| X^4 \middle\| 2 \right\rangle$$

$$= \tfrac{4}{7} \left\langle 2 \middle\| X^4 \middle\| 2 \right\rangle = 0.57 \left\langle 2 \middle\| X^4 \middle\| 2 \right\rangle,$$

$$(25.2.20)_\text{x}$$

This shows that the crystal field effect on a two-*d*-particle $L = 2$ level is 57% that of a single-electron state with the same radial and angular numbers. Coupled electrons can thus somewhat "protect" themselves from the

external potential field by their mutual correlations. As more electrons become so correlated their mutual "protection" can become very significant.

The following Section 25.3 introduces ways to deal with 3,4,…, and more identical fermions and bosons in a way that uses their underlying symmetry.

25.3 Unitary and Permutation Symmetry of N-Particle States

General coupled *N*-particle spin-*1/2* states are bases of *U(2)* irreps that have definite spin angular momentum *S*. Using Clebsch-Gordan coefficients (CGC) would require many terms like (24.3.22) made of products of *N* kets and *N-1* coefficients. Also, permutation symmetry for three or more particles is broken by 1-particle-at-time CGC coupling. That is a serious problem for physics of electrons, nuclei and atoms for which identity symmetry plays a major role. CGC-coupling makes an *oligarchy* and not a democracy!

The solution is to admit permutation symmetry operations and substitution groups S_N introduced in Unit 1-Appendix B and use S_N irreducible representations (ireps) defined by Young tableaus as was introduced in Section 24.3. The S_3 symmetry of three identical electrons is the first example. Since S_3 is the same group as the dihedral D_3 group solved in Chapter 15, its ireps can be recycled with Young tableaus labels in a way that shows how S_N ireps work on *N*-particle states in general.

The S_N groups are subgroups of unitary groups $U(N)$. The mixing of *A*-type and *B*-type particles by the $U(2)^{BODY}$ transformation (24.3.9) includes an S_N bicycle operation *(ab)* that simply *permutes A* and *B*, the strongest "mixing" operation possible. So S_N is a sub-group of the unitary mixing group $U(2)^{BODY}$ and thus part of a general inside-and-out symmetry $U(N)^{LAB} \times U(N)^{BODY} \supset U(N)^{LAB} \times S_N$. Once again, it pays to exploit reflections and the duality between outside "lab" and inside "body" quantum mechanics.

a. Lab-versus-body and particle-versus-state operations

The lab-versus-body duality manifests itself in atomic physics by distinguishing between internal bookkeeping operations like *(ab)* that work on imagined labels *A* and *B* of each individual particle, and external operations like [12] that work on labels 1 and 2 of each state available to particles. These two views are sketched in FIg. 25.3.0.

Let us consider an elementary case in which three particles *a*, *b*, and *c* occupy multiple states $|1\rangle$, $|2\rangle$, $|3\rangle$, and up to $|m\rangle$. An ordered Dirac-ket-ket-ket product represents particles *a*, *b*, and *c*, as follows.

$$|1,2,3\rangle \equiv |1\rangle_{particle-a} |2\rangle_{particle-b} |3\rangle_{particle-c} \equiv |1\rangle_a |2\rangle_b |3\rangle_c \qquad (25.3.1)$$

Lab operation $\mathbf{r} = (abc)$ sends particle-*a* to replace particle-*b* who then replaces *c* who then replaces *a*.

$$
\begin{aligned}
(abc)|1\rangle_a |2\rangle_b |3\rangle_c &= |1\rangle_c |2\rangle_a |3\rangle_b \\
&= \mathbf{r}|\mathbf{1}\rangle = |2\rangle_a |3\rangle_b |1\rangle_c
\end{aligned}
\qquad (25.3.2a)
$$

$$
\begin{aligned}
(acb)|1\rangle_a |2\rangle_b |3\rangle_c &= |1\rangle_b |2\rangle_c |3\rangle_a \\
&= \mathbf{r}^{-1}|\mathbf{1}\rangle = |3\rangle_a |1\rangle_b |2\rangle_c
\end{aligned}
\qquad (25.3.2b)
$$

Body operation $\bar{\mathbf{r}} = [123]$ moves state-1 to replace state-2 who then replaces 3 who then replaces 1.

$$[123]|1\rangle_a|2\rangle_b|3\rangle_c$$
$$= \bar{r}|1\rangle = |3\rangle_a|1\rangle_b|2\rangle_c \quad (25.3.3a)$$

$$[132]|1\rangle_a|2\rangle_b|3\rangle_c$$
$$= \bar{r}^{-1}|1\rangle = |2\rangle_a|3\rangle_b|1\rangle_c \quad (25.3.3b)$$

Lab and body operations share a group table since they differ only in notation: 1 for *a*, 2 for *b*, and 3 for *c*, but a

lab $\mathbf{r} = (abc)$ commutes with any body $\bar{\mathbf{r}} = [123]$ since each acts on distinct independent symbols.

Only *relative* positions of lab and body matter. So, effects (25.3.3) of lab operations $\mathbf{r} = (abc)$ or $\mathbf{i}_1 = (bc)$ on identity

state $|1\rangle \equiv |1\rangle_a|2\rangle_b|3\rangle_c$ are inverse to effects (25.3.2) of their body operations $\bar{\mathbf{r}} = [123]$ or $\bar{\mathbf{i}} = [23]$.

$$\mathbf{p}|1\rangle_a|2\rangle_b|3\rangle_c = |p\rangle = \bar{\mathbf{p}}^{-1}|1\rangle_a|2\rangle_b|3\rangle_c$$
$$\mathbf{p}|1\rangle = |p\rangle = \bar{\mathbf{p}}^{-1}|1\rangle \quad (25.3.3c)$$

$$\mathbf{q} \cdot \bar{\mathbf{p}} = \bar{\mathbf{p}} \cdot \mathbf{q}$$
$$\bar{\mathbf{q}} \cdot \mathbf{p} = \mathbf{p} \cdot \bar{\mathbf{q}} \quad (25.3.3d)$$

But, $\mathbf{p}$ and $\bar{\mathbf{q}}$ commute as do $\mathbf{q}$ and $\bar{\mathbf{p}}$ even if no commutation exists between $\mathbf{p}$ and $\mathbf{q}$ or between $\bar{\mathbf{p}}$ and $\bar{\mathbf{q}}$.

Three-particle symmetry projection

D_3-matrices (15.1.12) apply to lab $S_3 = \{(1),(abc),(acb),(bc),(ac),(ab)\}$ and $D_3 = \{\mathbf{1},\mathbf{r},\mathbf{r}^2,\mathbf{i}_1,\mathbf{i}_2,\mathbf{i}_3\}$ and body

$S_3 = \{[1],[123],[132],[23],[13],[12]\}$ and $\bar{D}_3 = \{\bar{\mathbf{1}},\bar{\mathbf{r}},\bar{\mathbf{r}}^2,\bar{\mathbf{i}}_1,\bar{\mathbf{i}}_2,\bar{\mathbf{i}}_3\}$ operations that are related in Fig. 25.3.1.
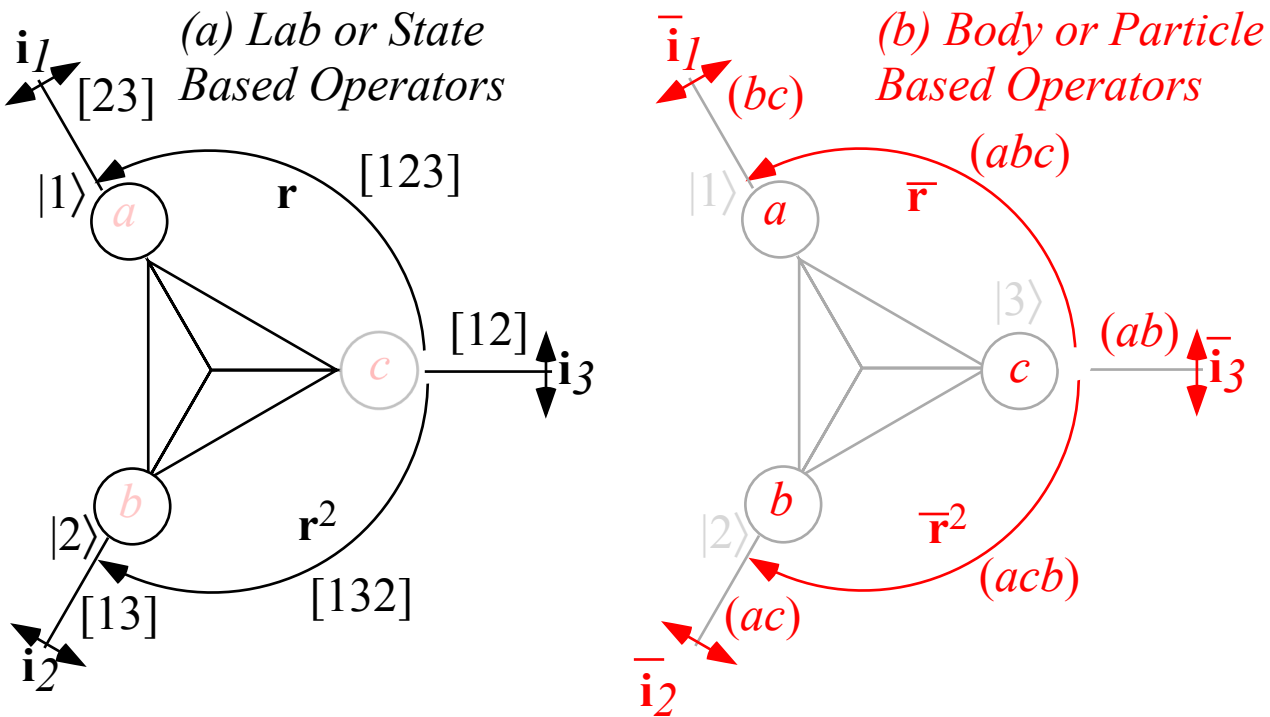
Fig. 25.3.0 Comparison of (a) Lab or State based operators with (b) Body or particle based operators

(a) Original state
$|1\rangle=|1_a,2_b,3_c\rangle$

*(b) Lab-fixed particle-3-cycle (120°rotation **r**)*
$|\mathbf{r}\rangle=\mathbf{r}|1\rangle$
$=(abc)|1_a,2_b,3_c\rangle$
$=|1_c,2_a,3_b\rangle=|2_a,3_b,1_c\rangle$
$=\bar{\mathbf{r}}^2|1\rangle=[132]|1_a,2_b,3_c\rangle$

(c) Particle-fixed lab-120°rotation $\bar{\mathbf{r}}$
$|\bar{\mathbf{r}}\rangle=\bar{\mathbf{r}}|1\rangle$
$=[123]|1_a,2_b,3_c\rangle$
$=|3_a,1_b,2_c\rangle$
$=\mathbf{r}^2|1\rangle$
$=(acb)|1_a,2_b,3_c\rangle$
$=|1_b,2_c,3_a\rangle$

(d) Apply to (b) particle-2-cycle
$\mathbf{i}_3=(ab)$
$\mathbf{i}_3\mathbf{r}^2=(ab)(abc)$
$=(ac)=\mathbf{i}_2$

(e) Apply to (b) lab-2-cycle
$\bar{\mathbf{i}}_3=[12]$
$\bar{\mathbf{i}}_3\bar{\mathbf{r}}=[12][132]$
$=[23]=\bar{\mathbf{i}}_1$

(f) Apply to (c) particle-2-cycle
$\mathbf{i}_3=(ab)$
$\mathbf{i}_3\mathbf{r}^2=(ab)(acb)$
$=(bc)=\mathbf{i}_1$

(g) Apply to (c) lab-2-cycle
$\bar{\mathbf{i}}_3=[12]$
$\bar{\mathbf{i}}_3\bar{\mathbf{r}}=[12][123]$
$=[13]=\bar{\mathbf{i}}_2$

Fig. 25.3.1 Relating D_3 *and* S_3 *permutation operations (a) Original state. (b-g) Transformed states.*

Both the group table and the irreducible representations of D_3 need to be adjusted in order to perform permutation symmetry analysis. Cycle products like those in Fig. 25.3.1 give the following tables. State group differs only in notation: 1 for *a*, 2 for *b*, and 3 for *c*,

(1)	(acb)	(abc)	(bc)	(ac)	(ab)
(abc)	(1)	(acb)	(ac)	(ab)	(bc)
(acb)	(abc)	(1)	(ab)	(bc)	(ac)
(bc)	(ac)	(ab)	(1)	(acb)	(abc)
(ac)	(ab)	(bc)	(abc)	(1)	(acb)
(ab)	(bc)	(ac)	(acb)	(abc)	(1)

(25.3.4a)

1	r^2	r	i_1	i_2	i_3
r	1	r^2	i_2	i_3	i_1
r^2	r	1	i_3	i_1	i_2
i_1	i_2	i_3	1	r^2	r
i_2	i_3	i_1	r	1	r^2
i_3	i_1	i_2	r^2	r	1

(25.3.4b)

S_3 products in Fig. 25.3.1 relate to D_3 operation products in Fig. 15.1.2. The bicycle subgroup $S_2 = \{(1),(ab)\}$ is the 180° *x*-axial subgroup $C_2 = \{\mathbf{1},\mathbf{i}_3\}$ that is made diagonal in an *E*-representation (15.1.12).

Tableau notation is used to show this. Eigenvalues *+1* and *-1* of $\mathbf{i}_3$ or *(ab)* have sub-tableaus ⊞ and ⊟ that label

their respective symmetry by a single row and anti-symmetry by a single column.

$$D^E[12] = \begin{array}{c} \boxed{1\,2} \\ \boxed{3} \\ \boxed{1\,3} \\ \boxed{2} \end{array} \begin{vmatrix} +1 & 0 \\ & \\ 0 & -1 \end{vmatrix} \qquad (25.3.5a) \qquad D^E(ab) = \begin{array}{c} \boxed{a\,b} \\ \boxed{c} \\ \boxed{a\,c} \\ \boxed{b} \end{array} \begin{vmatrix} +1 & 0 \\ & \\ 0 & -1 \end{vmatrix} \qquad (25.3.5d)$$

The lab state-labeled ireps are the same except for the symbol change: 1 is *a*, 2 is *b*, and 3 is *c*. The next is a big

step that uses the *Yamanouchi formula* for the irrep of a bicycle operation *[n,n-1]* such as [23].

$$D^E[23] = \begin{array}{c} \boxed{1\,2} \\ \boxed{3} \\ \boxed{1\,3} \\ \boxed{2} \end{array} \begin{vmatrix} \dfrac{-1}{2} & \dfrac{\sqrt{3}}{2} \\ \dfrac{\sqrt{3}}{2} & \dfrac{+1}{2} \end{vmatrix} \qquad (25.3.5a) \qquad D^E(bc) = \begin{array}{c} \boxed{a\,b} \\ \boxed{c} \\ \boxed{a\,c} \\ \boxed{b} \end{array} \begin{vmatrix} \dfrac{-1}{2} & \dfrac{\sqrt{3}}{2} \\ \dfrac{\sqrt{3}}{2} & \dfrac{+1}{2} \end{vmatrix} \qquad (25.3.5b)$$

The *E*-irrep uses tableau set $\{2,1\} = \left\{ \begin{array}{cc} \boxed{1\,2} & \boxed{1\,3} \\ \boxed{3} & \boxed{2} \end{array} \right\}$ having *both* [12]-symmetry (⊞) *and* anti-symmetry (⊟). But the

[23]-symmetry is neither, quite. The first tableau is nearly *2-over-3* so it is closer to anti-symmetry than the other

one which is closer to *2-besides-3* symmetry. (Neither *3-over-2* nor *3-besides-2* are allowed for reasons that will

be clear later.) The diagonal matrix elements are $\pm(1/d)$ where *d=2* here is the *tableau hook-length* between

blocks-*2*-and-*3*, that is, the number of streets you cross walking between blocks.

The off-diagonal matrix elements are both equal to $\sqrt{(d+1)(d-1)}/d$. This does not apply to totally

symmetric A_1-irrep labeled by a single row $\{3,0\} = $ ⊞⊞⊞ or the totally anti-symmetric A_2 –irrep labeled by single

column $\{1^3\} = \{1,1,1\} = \begin{array}{c}\boxed{1}\\\boxed{2}\\\boxed{3}\end{array}$. Both these are 1-by-1 matrices $D^{A_1}(p) = 1$ and $D^{A_2}(p) = -1$ for odd-*p*.

Together this defines a complete set of $S_3 \supset S_2$ permutation irreducible representations and projectors. The

S_3 projection operators are applied to a general 3-particle state $|1,2,3\rangle = |1\rangle_a |2\rangle_b |3\rangle_c$.

$g =$	$1 = (a)(b)(c)$	$r = (abc)$	$r^2 = (acb)$	$i_1 = (bc)$	$i_2 = (ac)$	$i_3 = (ab)$
$D^{A_1}(g) =$	1	1	1	1	1	1
$D^{A_2}(g) =$	1	1	1	-1	-1	-1
$D^{E_1}_{x_2 y_2}(g) =$	$\begin{pmatrix} 1 & 0 \\ 0 & 1 \end{pmatrix}$	$\begin{pmatrix} -1/2 & -\sqrt{3}/2 \\ \sqrt{3}/2 & -1/2 \end{pmatrix}$	$\begin{pmatrix} -1/2 & \sqrt{3}/2 \\ -\sqrt{3}/2 & -1/2 \end{pmatrix}$	$\begin{pmatrix} -1/2 & \sqrt{3}/2 \\ \sqrt{3}/2 & 1/2 \end{pmatrix}$	$\begin{pmatrix} -1/2 & -\sqrt{3}/2 \\ -\sqrt{3}/2 & 1/2 \end{pmatrix}$	$\begin{pmatrix} 1 & 0 \\ 0 & -1 \end{pmatrix}$

$$\mathbf{P}^{[\mu]}_{j,k} \; |1\rangle\,\mathrm{norm} = \sqrt{\frac{\ell^{[\mu]}}{{}^\circ G}} \left(D^{[\mu]}_{j,k}(1)|1\rangle + D(r)|r\rangle + D(r^2)\big|r^2\big\rangle + D(i_1)\big|\,i_1\big\rangle + D(i_2)\big|i_2\big\rangle + D(i_3)\big|i_3\big\rangle \right)$$

$$\left| \begin{smallmatrix}\square\square\square\\ \boxed{1}\boxed{2}\boxed{3}\end{smallmatrix} \right\rangle = \mathbf{P}^{\square\square\square}_{\boxed{a}\boxed{b}\boxed{c}\;\boxed{1}\boxed{2}\boxed{3}} |1,2,3\rangle \sqrt{6} = \left(\frac{|1,2,3\rangle + \; |2,3,1\rangle + \quad |3,1,2\rangle + \;|1,3,2\rangle + \;|3,2,1\rangle + \quad |2,1,3\rangle}{\sqrt{6}} \right)$$

$$\left| \begin{smallmatrix}\square\\\boxed{1}\\\boxed{2}\\\boxed{3}\end{smallmatrix} \right\rangle = \mathbf{P}^{\square}_{\begin{smallmatrix}\boxed{a}\;\boxed{1}\\\boxed{b}\;\boxed{2}\\\boxed{c}\;\boxed{3}\end{smallmatrix}} |1,2,3\rangle \sqrt{6} = \left(\frac{|1,2,3\rangle + \;|2,3,1\rangle + \quad |3,1,2\rangle + (-1)|1,3,2\rangle + (-1)|3,2,1\rangle + (-1)|2,1,3\rangle}{\sqrt{6}} \right)$$

$$\left| \begin{smallmatrix}\square\square\\\square\\\boxed{a}\boxed{b}\;\boxed{1}\boxed{2}\\\boxed{c}\;\boxed{3}\end{smallmatrix} \right\rangle = \mathbf{P}^{\square\square}_{\begin{smallmatrix}\boxed{a}\boxed{b}\;\boxed{a}\boxed{b}\\\boxed{c}\;\boxed{c}\end{smallmatrix}} |1,2,3\rangle \sqrt{3} = \left(\frac{2|1,2,3\rangle + (-1)|2,3,1\rangle + (-1)|3,1,2\rangle + (-1)|1,3,2\rangle + (-1)|3,2,1\rangle + 2|2,1,3\rangle}{2\sqrt{3}} \right)$$

$$\left| \begin{smallmatrix}\square\square\\\square\\\boxed{a}\boxed{c}\;\boxed{1}\boxed{2}\\\boxed{b}\;\boxed{3}\end{smallmatrix} \right\rangle = \mathbf{P}^{\square\square}_{\begin{smallmatrix}\boxed{a}\boxed{c}\;\boxed{a}\boxed{b}\\\boxed{b}\;\boxed{c}\end{smallmatrix}} |1,2,3\rangle \sqrt{3} = \left(\frac{0|1,2,3\rangle + (+1)|2,3,1\rangle + (-1)|3,1,2\rangle + (+1)|1,3,2\rangle + (-1)|3,2,1\rangle + 0|2,1,3\rangle}{2} \right) \quad (25.3.5e)$$

$$\left| \begin{smallmatrix}\square\square\\\square\\\boxed{a}\boxed{b}\;\boxed{1}\boxed{3}\\\boxed{c}\;\boxed{2}\end{smallmatrix} \right\rangle = \mathbf{P}^{\square\square}_{\begin{smallmatrix}\boxed{a}\boxed{b}\;\boxed{a}\boxed{c}\\\boxed{c}\;\boxed{b}\end{smallmatrix}} |1,2,3\rangle \sqrt{3} = \left(\frac{0|1,2,3\rangle + (-1)|2,3,1\rangle + (+1)|3,1,2\rangle + (+1)|1,3,2\rangle + (-1)|3,2,1\rangle + 0|2,1,3\rangle}{2} \right)$$

$$\left| \begin{smallmatrix}\square\square\\\square\\\boxed{a}\boxed{c}\;\boxed{1}\boxed{3}\\\boxed{b}\;\boxed{2}\end{smallmatrix} \right\rangle = \mathbf{P}^{\square\square}_{\begin{smallmatrix}\boxed{a}\boxed{c}\;\boxed{a}\boxed{c}\\\boxed{b}\;\boxed{b}\end{smallmatrix}} |1,2,3\rangle \sqrt{3} = \left(\frac{2|1,2,3\rangle + (-1)|2,3,1\rangle + (-1)|3,1,2\rangle + (+1)|1,3,2\rangle + (+1)|3,2,1\rangle - 2|2,1,3\rangle}{2} \right)$$

Tableau *particle* (abc) labels [j] of projectors $\mathbf{P}_{[j](k)}$ face left, and *state* (*123*) labels [k] face the state $|1,2,3\rangle$ on the right. State operators commute through to act on the right index-(k) of $\mathbf{P}_{[j](k)}$ while particle operators work on the left index-[j]. Later (abc) labels sum with those of matching spin states to make Fermi-Dirac-Pauli antisymmetry, and (abc)'s disappear leaving only orbital state [123] and spin ($\uparrow\uparrow\downarrow$) labels. Electron particle-labels must disappear since Nature cannot permanently label or distinguish a single electron! Spin states only temporarily "mark" otherwise indistinguishable particles.

To include spin, the projectors are applied to 3-electron spin states of which there are eight *($2^3=8$)*. Spin-up ($\uparrow$) or spin-down($\downarrow$) replace 1,2, and 3 states in (25.3.5e). The first is a single symmetric A_1 projection $\mathbf{P}^{A_1} = \mathbf{P}^{\square\square\square}$

of state $|\uparrow\uparrow\uparrow\rangle$. (Note that $\mathbf{P}^{E_1} = \mathbf{P}^{\begin{smallmatrix}\square\square\\\square\end{smallmatrix}}$ acting on $|\uparrow\uparrow\uparrow\rangle$ gives zero.)

$$\left| \begin{smallmatrix}\square\square\square\;\;3/2\\\boxed{\uparrow}\boxed{\uparrow}\boxed{\uparrow}\;\;3/2\end{smallmatrix} \right\rangle = \mathbf{P}^{\square\square\square}_{\boxed{a}\boxed{b}\boxed{c}\;\boxed{\uparrow}\boxed{\uparrow}\boxed{\uparrow}} |\uparrow,\uparrow,\uparrow\rangle = |\uparrow,\uparrow,\uparrow\rangle \qquad\qquad (25.3.6a)$$

Anti symmetric A_2 projection fails on *all* spin-1/2 states since 2-dimensions can't fill a triple column.

$$\left|\begin{array}{c}\\\uparrow\\\uparrow\\\uparrow\end{array}\right\rangle = \mathbf{P}_{\substack{a\\b\\c}\;\uparrow\atop\uparrow\atop\uparrow}\left\|\uparrow,\uparrow,\uparrow\right\rangle\right\rangle = 0 \;\; (Does\;not\;exist), \left|\begin{array}{c}\\\uparrow\\\uparrow\\\downarrow\end{array}\right\rangle = \mathbf{P}_{\substack{a\\b\\c}\;\uparrow\atop\uparrow\atop\downarrow}\left\|\uparrow,\uparrow,\downarrow\right\rangle\right\rangle = 0 \;\; (Does\;not\;exist),...etc. \quad (25.3.6b)$$

Symmetric $\mathbf{P}^{A_1} = \mathbf{P}^{\square\square\square}$ or para-symmetric $\mathbf{P}^{E_1} = \mathbf{P}^{\square\square}_{\square}$ projection of $\left|\uparrow\uparrow\downarrow\right\rangle$ and $\left|\uparrow\downarrow\downarrow\right\rangle$ give $\left|{}^{S=3/2}_{M=\pm1/2}\right\rangle$ or $\left|{}^{S=1/2}_{M=\pm1/2}\right\rangle$.

$$\left|{}^{\square\square\square}_{\uparrow\uparrow\downarrow}\;{}^{3/2}_{1/2}\right\rangle = \mathbf{P}^{\square\square\square}_{\boxed{abc}\;\boxed{abc}}\left|\uparrow,\uparrow,\downarrow\right\rangle\sqrt{3} = \left(\frac{\left|\uparrow,\uparrow,\downarrow\right\rangle + \left|\uparrow,\downarrow,\uparrow\right\rangle + \left|\downarrow,\uparrow,\uparrow\right\rangle + \left|\uparrow,\downarrow,\uparrow\right\rangle + \left|\downarrow,\uparrow,\uparrow\right\rangle + \left|\uparrow,\uparrow,\downarrow\right\rangle}{\sqrt{6}}\right)$$

$$= \left(\frac{\left|\uparrow,\uparrow,\downarrow\right\rangle + \left|\uparrow,\downarrow,\uparrow\right\rangle + \left|\downarrow,\uparrow,\uparrow\right\rangle}{\sqrt{3}}\right)$$

$$\left|{}^{\square\square}_{\square}\;{}^{1/2}_{1/2}\right\rangle = \mathbf{P}^{\square\square}_{\substack{\boxed{ab}\\\boxed{c}}\;\substack{\boxed{ab}\\\boxed{c}}}\left|\uparrow,\uparrow,\downarrow\right\rangle\sqrt{\frac{3}{2}} = \left(\frac{2\left|\uparrow,\uparrow,\downarrow\right\rangle+(-1)\left|\uparrow,\downarrow,\uparrow\right\rangle+(-1)\left|\downarrow,\uparrow,\uparrow\right\rangle+(-1)\left|\uparrow,\downarrow,\uparrow\right\rangle+(-1)\left|\downarrow,\uparrow,\uparrow\right\rangle+2\left|\uparrow,\uparrow,\downarrow\right\rangle}{2\sqrt{6}}\right)$$

$$= \left(\frac{2\left|\uparrow,\uparrow,\downarrow\right\rangle+(-1)\left|\uparrow,\downarrow,\uparrow\right\rangle+(-1)\left|\downarrow,\uparrow,\uparrow\right\rangle}{\sqrt{6}}\right)$$

$$\left|{}^{\square\square}_{\square}\;{}^{1/2}_{1/2}\right\rangle = \mathbf{P}^{\square\square}_{\substack{\boxed{ac}\\\boxed{b}}\;\substack{\boxed{ab}\\\boxed{c}}}\left|\uparrow,\uparrow,\downarrow\right\rangle\sqrt{\frac{3}{2}} = \left(\frac{0\left|\uparrow,\uparrow,\downarrow\right\rangle+(+1)\left|\uparrow,\downarrow,\uparrow\right\rangle+(-1)\left|\downarrow,\uparrow,\uparrow\right\rangle+(+1)\left|\uparrow,\downarrow,\uparrow\right\rangle+(-1)\left|\downarrow,\uparrow,\uparrow\right\rangle+0\left|\uparrow,\uparrow,\downarrow\right\rangle}{2\sqrt{2}}\right)$$

$$= \left(\frac{(+1)\left|\uparrow,\downarrow,\uparrow\right\rangle+(-1)\left|\downarrow,\uparrow,\uparrow\right\rangle}{\sqrt{2}}\right)$$

$$(25.3.6c)$$

The latter are a permutation doublet noted in (24.3.21). Two spin-$S=1/2$ states $\left|{}^{S=1/2}_{M=\pm1/2}\right\rangle$ but only one spin-$S=3/2$ state $\left|{}^{S=3/2}_{M=\pm1/2}\right\rangle$ have z-component $M=+1/2$. All three states are projections of $\left|\uparrow\uparrow\downarrow\right\rangle$ but the left $_{[j]}$-labels of the latter two make a particle permutation doublet $\left\{\substack{\boxed{ab}\\\boxed{c}} \quad \substack{\boxed{ac}\\\boxed{b}}\right\}$.

There are also two right hand $_{[k]=}\left\{\substack{\boxed{ab}\\\boxed{c}} \quad \substack{\boxed{ac}\\\boxed{b}}\right\}$ labels. But symmetry of state $\left|\uparrow\uparrow\downarrow\right\rangle$ makes $\substack{\boxed{ac}\\\boxed{b}}$ projection zero.

$$\mathbf{P}^{\square\square}_{\substack{\boxed{ab}\\\boxed{c}}\;\substack{\boxed{ac}\\\boxed{b}}}\left|\uparrow,\uparrow,\downarrow\right\rangle = 0 = \left(\frac{0\left|\uparrow,\uparrow,\downarrow\right\rangle+(-1)\left|\uparrow,\downarrow,\uparrow\right\rangle+(+1)\left|\downarrow,\uparrow,\uparrow\right\rangle+(+1)\left|\uparrow,\downarrow,\uparrow\right\rangle+(-1)\left|\downarrow,\uparrow,\uparrow\right\rangle+0\left|\uparrow,\uparrow,\downarrow\right\rangle}{2/\sqrt{3}}\right)$$

$$\mathbf{P}^{\square\square}_{\substack{\boxed{ac}\\\boxed{b}}\;\substack{\boxed{ac}\\\boxed{b}}}\left|\uparrow,\uparrow,\downarrow\right\rangle = 0 = \left(\frac{2\left|\uparrow,\uparrow,\downarrow\right\rangle+(-1)\left|\uparrow,\downarrow,\uparrow\right\rangle+(-1)\left|\downarrow,\uparrow,\uparrow\right\rangle+(+1)\left|\uparrow,\downarrow,\uparrow\right\rangle+(+1)\left|\downarrow,\uparrow,\uparrow\right\rangle-2\left|\uparrow,\uparrow,\downarrow\right\rangle}{2}\right)$$

$$(25.3.7a)$$

State $\left|\uparrow\uparrow\downarrow\right\rangle = \mathbf{P}^{\square\square}\left|\uparrow\uparrow\downarrow\right\rangle$ is invariant to symmetric subgroup projector $\mathbf{P}^{\square\square} = [1+(ab)]/2$ but $\mathbf{P}^{\square\square}$ zeros $\substack{\boxed{ac}\\\boxed{b}}$.

$$\left.\begin{array}{c}(ab)\left|\uparrow,\uparrow,\downarrow\right\rangle = \left|\uparrow,\uparrow,\downarrow\right\rangle\\[6pt]\mathbf{P}^{\square\square}_{\substack{\boxed{ab}\\\boxed{c}}\;\substack{\boxed{ac}\\\boxed{b}}}(ab) = -\mathbf{P}^{\square\square}_{\substack{\boxed{ab}\\\boxed{c}}\;\substack{\boxed{ac}\\\boxed{b}}}\end{array}\right\} implies: \mathbf{P}^{\square\square}_{\substack{\boxed{ab}\\\boxed{c}}\;\substack{\boxed{ac}\\\boxed{b}}}\left|\uparrow,\uparrow,\downarrow\right\rangle = -\mathbf{P}^{\square\square}_{\substack{\boxed{ab}\\\boxed{c}}\;\substack{\boxed{ac}\\\boxed{b}}}\left|\uparrow,\uparrow,\downarrow\right\rangle = 0 \qquad (25.3.7b)$$

Similarly, projections of $|\uparrow\downarrow\downarrow\rangle$ give three *M=-1/2* states.

$$\left|\begin{smallmatrix}\square\square\square\\\uparrow\uparrow\uparrow\end{smallmatrix}\,{}^{3/2}_{1/2}\right\rangle = \mathbf{P}^{\square\square\square}_{\boxed{a}\boxed{b}\boxed{c}\,\boxed{a}\boxed{b}\boxed{c}}|\uparrow,\downarrow,\downarrow\rangle\sqrt{3} = \left(\frac{|\uparrow,\downarrow,\downarrow\rangle+\;|\downarrow,\downarrow,\uparrow\rangle+\;|\downarrow,\uparrow,\downarrow\rangle+\;|\uparrow,\downarrow,\downarrow\rangle+\;|\downarrow,\downarrow,\uparrow\rangle+\;|\downarrow,\uparrow,\downarrow\rangle}{2\sqrt{3}}\right)$$

$$= \left(\frac{|\uparrow,\downarrow,\downarrow\rangle+\;|\downarrow,\uparrow,\downarrow\rangle+\;|\uparrow,\downarrow,\downarrow\rangle}{\sqrt{3}}\right)$$

$$\left|\begin{smallmatrix}\square\square\\\boxed{a}\boxed{b}\\c\end{smallmatrix}\begin{smallmatrix}\square\square\\\uparrow\downarrow\\\downarrow\end{smallmatrix}\,{}^{1/2}_{-1/2}\right\rangle = \mathbf{P}^{\square\square}_{\substack{\boxed{a}\boxed{b}\\c}\,\substack{\boxed{a}\boxed{b}\\c}}|\uparrow,\downarrow,\downarrow\rangle\sqrt{6} = \left(\frac{2|\uparrow,\downarrow,\downarrow\rangle+(-1)|\downarrow,\downarrow,\uparrow\rangle+(-1)|\downarrow,\uparrow,\downarrow\rangle+(-1)|\uparrow,\downarrow,\downarrow\rangle+(-1)|\downarrow,\downarrow,\uparrow\rangle+2|\downarrow,\uparrow,\downarrow\rangle}{\sqrt{6}}\right)$$

$$= \left(\frac{1|\uparrow,\downarrow,\downarrow\rangle+(+1)|\downarrow,\uparrow,\downarrow\rangle+(-2)|\downarrow,\downarrow,\uparrow\rangle}{\sqrt{6}}\right)$$

$$\left|\begin{smallmatrix}\square\square\\\boxed{a}\boxed{c}\\b\end{smallmatrix}\begin{smallmatrix}\square\square\\\uparrow\downarrow\\\downarrow\end{smallmatrix}\,{}^{1/2}_{-1/2}\right\rangle = \mathbf{P}^{\square\square}_{\substack{\boxed{a}\boxed{c}\\b}\,\substack{\boxed{a}\boxed{b}\\c}}|\uparrow,\downarrow,\downarrow\rangle\sqrt{6} = \left(\frac{0|\uparrow,\downarrow,\downarrow\rangle+(+1)|\downarrow,\downarrow,\uparrow\rangle+(-1)|\downarrow,\uparrow,\downarrow\rangle+(+1)|\uparrow,\downarrow,\downarrow\rangle+(-1)|\downarrow,\downarrow,\uparrow\rangle+0|\downarrow,\uparrow,\downarrow\rangle}{\sqrt{2}}\right)$$

$$= \left(\frac{(+1)|\uparrow,\downarrow,\downarrow\rangle+(-1)|\downarrow,\uparrow,\downarrow\rangle}{\sqrt{2}}\right)$$

$$\text{(25.3.8a)}$$

Finally, the fourth state of the spin-*S=3/2* quartet is the following.

$$\left|\begin{smallmatrix}\square\square\square\\\downarrow\downarrow\downarrow\end{smallmatrix}\,{}^{3/2}_{-3/2}\right\rangle = \mathbf{P}^{\square\square\square}_{\boxed{a}\boxed{b}\boxed{c}\,\downarrow\downarrow\downarrow}|\downarrow,\downarrow,\downarrow\rangle = |\downarrow,\downarrow,\downarrow\rangle \qquad\qquad \text{(25.3.8b)}$$

Are these a complete set of states?

Do a permutation-pair of spin-doublets and a spin-quartet account for all $2^3=8$ states in $(1/2)^3$?

Notice that projections (25.3.8) of $|\uparrow\downarrow\downarrow\rangle$ give the same as those of a *(ab)*-switched state $|\downarrow\uparrow\downarrow\rangle = (ab)|\uparrow\downarrow\downarrow\rangle$. But, an

(ac)-switched state $|\downarrow\downarrow\uparrow\rangle = (ac)|\uparrow\downarrow\downarrow\rangle$ projects to *(-2)* times the results in (25.3.8a) as seen below.

$$\mathbf{P}^{\square\square}_{\substack{\boxed{a}\boxed{b}\\c}\,\substack{\boxed{a}\boxed{b}\\c}}|\downarrow,\downarrow,\uparrow\rangle\sqrt{6} = \left(\frac{2|\downarrow,\downarrow,\uparrow\rangle+(-1)|\downarrow,\uparrow,\downarrow\rangle+(-1)|\uparrow,\downarrow,\downarrow\rangle+(-1)|\downarrow,\uparrow,\downarrow\rangle+(-1)|\uparrow,\downarrow,\downarrow\rangle+2|\downarrow,\downarrow,\uparrow\rangle}{\sqrt{6}}\right)$$

$$= \left(\frac{2|\downarrow,\downarrow,\uparrow\rangle+(-1)|\downarrow,\uparrow,\downarrow\rangle+(-1)|\uparrow,\downarrow,\downarrow\rangle}{\sqrt{6}/2}\right) = (-2)\mathbf{P}^{\square\square}_{\substack{\boxed{a}\boxed{b}\\c}\,\substack{\boxed{a}\boxed{b}\\c}}|\uparrow,\downarrow,\downarrow\rangle\sqrt{6}$$

$$\mathbf{P}^{\square\square}_{\substack{\boxed{a}\boxed{c}\\b}\,\substack{\boxed{a}\boxed{b}\\c}}|\downarrow,\downarrow,\uparrow\rangle\sqrt{6} = \left(\frac{0|\downarrow,\downarrow,\uparrow\rangle+(+1)|\downarrow,\uparrow,\downarrow\rangle+(-1)|\uparrow,\downarrow,\downarrow\rangle+(+1)|\downarrow,\uparrow,\downarrow\rangle+(-1)|\uparrow,\downarrow,\downarrow\rangle+0|\downarrow,\downarrow,\uparrow\rangle}{\sqrt{2}}\right)$$

$$= \left(\frac{(+1)|\downarrow,\uparrow,\downarrow\rangle+(-1)|\uparrow,\downarrow,\downarrow\rangle}{\sqrt{2}/2}\right) = (-2)\mathbf{P}^{\square\square}_{\substack{\boxed{a}\boxed{c}\\b}\,\substack{\boxed{a}\boxed{b}\\c}}|\uparrow,\downarrow,\downarrow\rangle\sqrt{6}$$

This result is more easily seen by letting *(ac)* work first on the right index-(k) of projector $\mathbf{P}_{[j](k)}$.

$$\mathbf{P}_{\boxed{ab}\,\boxed{ab}}^{\;}(ac)\left|\downarrow,\downarrow,\uparrow\right\rangle=\mathbf{P}_{\boxed{ab}\,\boxed{ab}}^{\;}\left|\downarrow,\downarrow,\uparrow\right\rangle D_{x,x}^E(ac)+\mathbf{P}_{\boxed{ac}\,\boxed{ac}}^{\;}\left|\downarrow,\downarrow,\uparrow\right\rangle D_{y,x}^E(ac)$$

$$\mathbf{P}_{\boxed{ab}\,\boxed{ab}}^{\;}\quad\left|\uparrow,\downarrow,\downarrow\right\rangle=\mathbf{P}_{\boxed{ab}\,\boxed{ab}}^{\;}\left|\downarrow,\downarrow,\uparrow\right\rangle\left(\frac{-1}{2}\right)\quad+\quad[\quad\quad 0\quad\quad]\left(\frac{-\sqrt{3}}{2}\right)$$

(25.3.9a)

Also, projection (25.3.7) might use an anti-symmetric right index-(k) $(_{(k)=y=\frac{\boxed{ac}}{\boxed{b}}})$ on state $\left|\downarrow\uparrow\uparrow\right\rangle=(ac)\left|\uparrow\uparrow\downarrow\right\rangle$.

$$\mathbf{P}_{\boxed{ab}\,\boxed{ac}}^{\;}\left|\downarrow,\uparrow,\uparrow\right\rangle=\mathbf{P}_{\boxed{ab}\,\boxed{ac}}^{\;}(ac)\left|\uparrow,\uparrow,\downarrow\right\rangle$$

$$=\mathbf{P}_{\boxed{ab}\,\boxed{ab}}^{\;}\left|\uparrow,\uparrow,\downarrow\right\rangle D_{x,y}^E(ac)+\mathbf{P}_{\boxed{ac}\,\boxed{ac}}^{\;}\left|\uparrow,\uparrow,\downarrow\right\rangle D_{y,y}^E(ac)\qquad\text{(25.3.9b)}$$

$$=\mathbf{P}_{\boxed{ab}\,\boxed{ab}}^{\;}\left|\uparrow,\uparrow,\downarrow\right\rangle\left(\frac{-\sqrt{3}}{2}\right)\quad+\quad[\quad\quad 0\quad\quad]\left(\frac{1}{2}\right)$$

But, once again the result is the same except for an overall phase and factor $(-2/\sqrt{3})$ to that of (25.3.6). In either of the two preceding alternative projections, the left index-[j] can be symmetric $([j]=x=\frac{\boxed{ab}}{\boxed{c}})$ or antisymmetric $([j]=y=\frac{\boxed{ac}}{\boxed{b}})$ without otherwise altering either equation.

This shows that the right index is governed by the *state-permutaion* -symmetry, that is, whether two spins are equal or not, while the left index is governed by *particle-permutaion*-symmetry, that is, whether two particles are the same or not. We do not consider cases where *a*, *b*, or *c* are repeated, but orbit states 1, 2, or 3 and spin states $\uparrow$ and $\downarrow$ will often be repeated in what follows.

This is used in the labeling of the states (25.3.5) through (25.3.8) by two tableaus. The left tableau has the particle labels *(a,b,c)* while the right tableau has state labels (1,2,3) or $\{\uparrow,\downarrow\}$ replacing *a*, *b*, or *c exactly according to the projector's right index-(k) and location of state labels m = (1,2,3) or $\{\uparrow,\downarrow\}$ on the particles a, b, and c in the state $\left|m,m',m''\right\rangle=\left|m_a,m'_b,m''_c\right\rangle$ being projected*. The following are examples.

$$\left|\frac{\boxed{ab}\,\boxed{-2}\,\boxed{-1}}{\boxed{c}\,\boxed{+3}}\right\rangle=\mathbf{P}_{\boxed{ab}\,\boxed{ab}}^{\;}\left|-2,-1,+3\right\rangle(norm)\quad\text{(25.3.10a)}\qquad\left|\frac{\boxed{ab}\,\boxed{-2}\,\boxed{+3}}{\boxed{c}\,\boxed{-1}}\right\rangle=\mathbf{P}_{\boxed{ab}\,\boxed{ac}}^{\;}\left|-2,-1,+3\right\rangle(norm)\quad\text{(25.3.10b)}$$

Permutation anti-symmetry rules out putting the same state in a column as was shown in (25.3.7).

$$\left|\frac{\boxed{ab}\,\boxed{-2}\,\boxed{-1}}{\boxed{c}\,\boxed{-2}}\right\rangle=0=\mathbf{P}_{\boxed{ab}\,\boxed{ab}}^{\;}\left|-2,-1,-2\right\rangle\quad\text{(25.3.10c)}\qquad\left|\frac{\boxed{ab}\,\boxed{-2}\,\boxed{+3}}{\boxed{c}\,\boxed{-2}}\right\rangle=0=\mathbf{P}_{\boxed{ab}\,\boxed{ac}}^{\;}\left|-2,-2,+3\right\rangle\quad\text{(25.3.10d)}$$

But repeated states in rows are allowed.

$$\left|\frac{\boxed{ab}\,\boxed{-2}\,\boxed{-2}}{\boxed{c}\,\boxed{-1}}\right\rangle=\mathbf{P}_{\boxed{ab}\,\boxed{ac}}^{\;}\left|-2,-1,-2\right\rangle(norm)\quad\text{(25.3.10e)}\qquad\left|\frac{\boxed{ab}\,\boxed{-2}\,\boxed{-2}}{\boxed{c}\,\boxed{+3}}\right\rangle=\mathbf{P}_{\boxed{ab}\,\boxed{ab}}^{\;}\left|-2,-2,+3\right\rangle(norm)\quad\text{(25.3.10f)}$$

Fermi-Dirac-Pauli anti-symmetric states

Orbital-tableau states like the above and (25.3.5e) are combined using S_N-Clebsch-Gordan coefficients (S_NCGC) with spin-tableau states (25.3.6-8) to make Pauli-allowed spin-orbit states. The simplest case is the following for which the (S_3CGC) sum is a single term for each state in the ^{4}S quartet.

$$\left| p^3\, ^4S_{\boxed{\uparrow\uparrow\uparrow}\,\boxed{1}\,M_S=3/2}^{\quad\quad\quad S=3/2} \right\rangle = \left| \boxed{\uparrow\uparrow\uparrow} \right\rangle \left| \boxed{\begin{smallmatrix}1\\2\\3\end{smallmatrix}} \right\rangle,\quad \left| \begin{smallmatrix}3/2\\1/2\end{smallmatrix} \right\rangle = \left| \boxed{\uparrow\uparrow\downarrow} \right\rangle \left| \boxed{\begin{smallmatrix}1\\2\\3\end{smallmatrix}} \right\rangle,\quad \left| \begin{smallmatrix}3/2\\-1/2\end{smallmatrix} \right\rangle = \left| \boxed{\uparrow\downarrow\downarrow} \right\rangle \left| \boxed{\begin{smallmatrix}1\\2\\3\end{smallmatrix}} \right\rangle,\quad \left| \begin{smallmatrix}3/2\\-3/2\end{smallmatrix} \right\rangle = \left| \boxed{\downarrow\downarrow\downarrow} \right\rangle \left| \boxed{\begin{smallmatrix}1\\2\\3\end{smallmatrix}} \right\rangle \quad (25.3.11)$$

The p^3 doublet states ^2L, with L yet to be determined, are each a sum of two terms that use the S_3 coefficients $C_{A\,B\,B}^{E_1 E_1 A_2} = 1/\sqrt{2}$ and $C_{B\,A\,B}^{E_1 E_1 A_2} = -1/\sqrt{2}$ from (24.2.40a) to give Pauli-anti-symmetry (A_2).

$$\left| p^3\, ^2L_{\boxed{\uparrow\uparrow}\boxed{\downarrow}\,\boxed{12}\boxed{3}\,M_S=1/2}^{\quad\quad\quad\quad S=1/2} \right\rangle = C_{A\,B\,B}^{E_1 E_1 A_2} \left| \boxed{\begin{smallmatrix}a&b\\c\end{smallmatrix}} \boxed{\begin{smallmatrix}\uparrow\uparrow\\\downarrow\end{smallmatrix}} \right\rangle \left| \boxed{\begin{smallmatrix}a&c\\b\end{smallmatrix}} \boxed{\begin{smallmatrix}12\\3\end{smallmatrix}} \right\rangle + C_{B\,A\,B}^{E_1 E_1 A_2} \left| \boxed{\begin{smallmatrix}a&c\\b\end{smallmatrix}} \boxed{\begin{smallmatrix}\uparrow\uparrow\\\downarrow\end{smallmatrix}} \right\rangle \left| \boxed{\begin{smallmatrix}a&b\\c\end{smallmatrix}} \boxed{\begin{smallmatrix}12\\3\end{smallmatrix}} \right\rangle \quad (25.3.12a)$$

$$\left| p^3\, ^2L_{\boxed{\uparrow\downarrow}\boxed{\downarrow}\,\boxed{12}\boxed{3}\,M_S=-1/2}^{\quad\quad\quad\quad S=1/2} \right\rangle = C_{A\,B\,B}^{E_1 E_1 A_2} \left| \boxed{\begin{smallmatrix}a&b\\c\end{smallmatrix}} \boxed{\begin{smallmatrix}\uparrow\downarrow\\\downarrow\end{smallmatrix}} \right\rangle \left| \boxed{\begin{smallmatrix}a&c\\b\end{smallmatrix}} \boxed{\begin{smallmatrix}12\\3\end{smallmatrix}} \right\rangle + C_{B\,A\,B}^{E_1 E_1 A_2} \left| \boxed{\begin{smallmatrix}a&c\\b\end{smallmatrix}} \boxed{\begin{smallmatrix}\uparrow\downarrow\\\downarrow\end{smallmatrix}} \right\rangle \left| \boxed{\begin{smallmatrix}a&b\\c\end{smallmatrix}} \boxed{\begin{smallmatrix}12\\3\end{smallmatrix}} \right\rangle \quad (25.3.12b)$$

This is how permutation multiplicity and *(abc)* labels disappear, killed by Pauli! But, spin degeneracy of 4 quartet-states and 2 doublet-states is still here. Also there are *eight* orbital doublet pairs corresponding to an *octet* of tableaus that have a unitary *U(3) multiplicity* of $\ell^{E_1} = 8$ for the Pauli-allowed E_1-orbitals.

$$U(3)\text{ octet tableau basis:} \left\{ \boxed{\begin{smallmatrix}1&1\\2\end{smallmatrix}}\, \boxed{\begin{smallmatrix}1&2\\2\end{smallmatrix}}\, \boxed{\begin{smallmatrix}1&2\\3\end{smallmatrix}}\, \boxed{\begin{smallmatrix}1&3\\2\end{smallmatrix}}\, \boxed{\begin{smallmatrix}1&1\\3\end{smallmatrix}}\, \boxed{\begin{smallmatrix}1&3\\3\end{smallmatrix}}\, \boxed{\begin{smallmatrix}2&2\\3\end{smallmatrix}}\, \boxed{\begin{smallmatrix}2&3\\3\end{smallmatrix}} \right\} \quad (25.3.13)$$

Each of three orbital quantum labels $\{1:(m=-1),\, 2:(m=0),\, 3:(m=+1)\}$ for a *p*-electron orbit ($\ell=1$) may be repeated in tableau rows (but not in columns). Spin $S=1/2$ has the usual *U(2) multiplicity* of $\ell^{E_1} = 2$ above.

b. Three-particle orbital states: Nitrogen (2p)³ Example

Perhaps, the simplest non-trivial example of 3-particle states is the $(2p)^3$ configuration of the lowest levels of Nitrogen. The possible arrangements are diagrammed in figures below as they were in the tableau arrays of the 2D-oscillator in Fig. 21.3.2(b). The symmetrized (A_1) orbitals of 2 and 3 p-particles are repeated in Fig. 25.3.2 and for para-symmetry (E_1) and anti-symmetry (A_2) in Fig. 25.3.3.
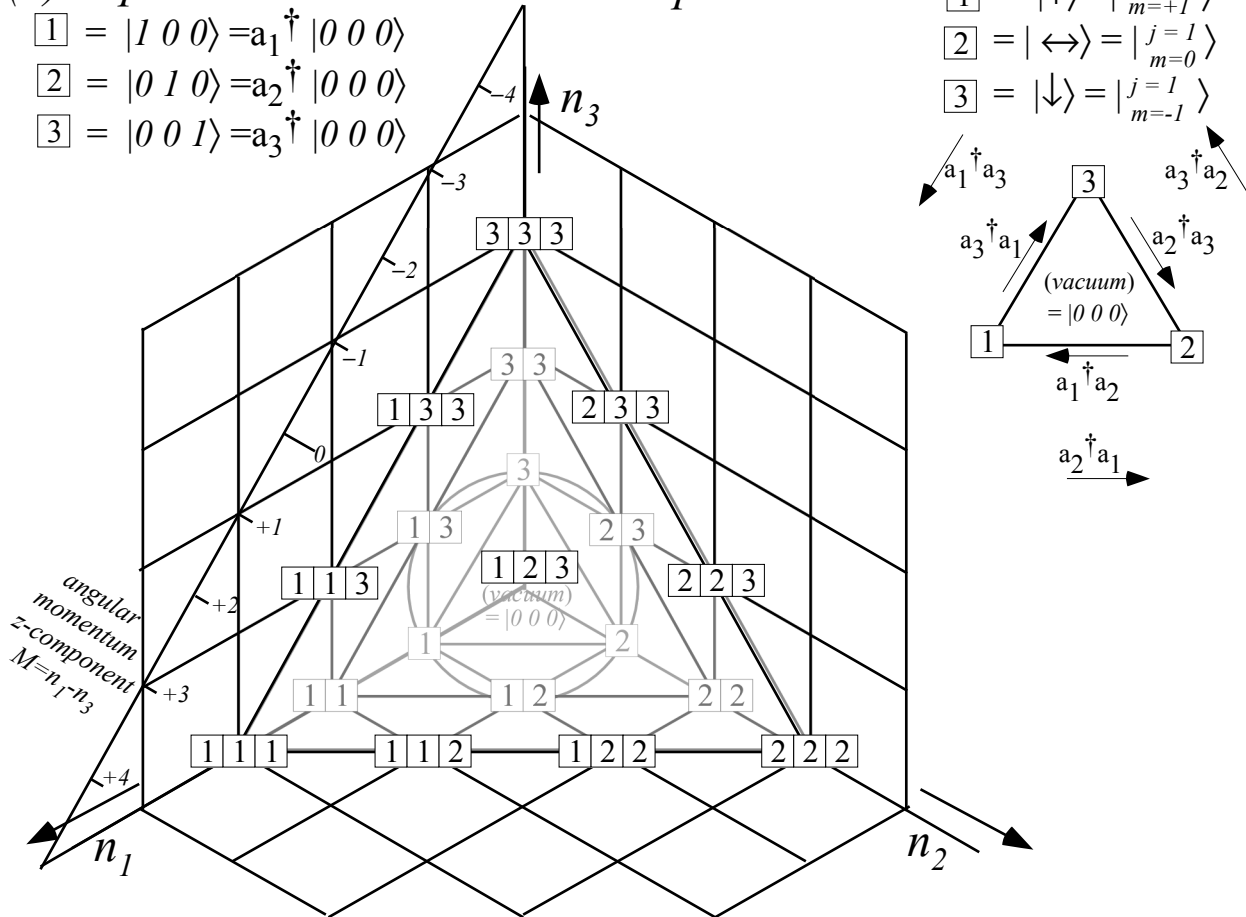
Fig. 25.3.2 U(3) orbital states for p (l=1) for 1-3 particles that are symmetric.

Each tableau has 3D Cartesian integer coordinates (n_1, n_2, n_3) that are the values of number operators $(a_1\bar{a}_1, a_2\bar{a}_2, a_3\bar{a}_3)$ or, in the old fashioned notation of Ch. 21: $(a_1^\dagger a_1, a_2^\dagger a_2, a_3^\dagger a_3)$. All tableaus with the same total number $N = n_1 + n_2 + n_3$ of particles lie in the same plane that is normal to the $(1,1,1)$ direction and a distance $N/\sqrt{3}$ from the vacuum origin. The plane has orthogonal D and Q axes that measure the *dipole-sum D* of z-component momentum and the *quadrupole-sum Q* of squared-z-component momentum.

$$D = \langle L_z \rangle = n_3 - n_1 = M_L \quad (25.3.14a) \qquad Q = \langle L_z^2 \rangle = n_3 + n_1 = N - n_2 \ (25.3.14b)$$

Fig. 25.3.4 shows how a (D,Q) plot finds the orbital quantum L states present in a given tableau manifold.

(b) (U(3) ℓ-1 states)
Para-symmetric
p³-states
Anti-symmetric
p²-states

(b) (U(3) ℓ-1 states)
Anti-symmetric
p³-state $\boxed{\begin{array}{c}1\\2\\3\end{array}}$ *(L=0)*
          M=0

Anti-symmetric
p²-states (L= 1)

$\boxed{\begin{array}{c}2\\3\end{array}}$ *M=+1*

$\boxed{\begin{array}{c}1\\3\end{array}}$ *M= 0*

$\boxed{\begin{array}{c}1\\2\end{array}}$ *M=-1*
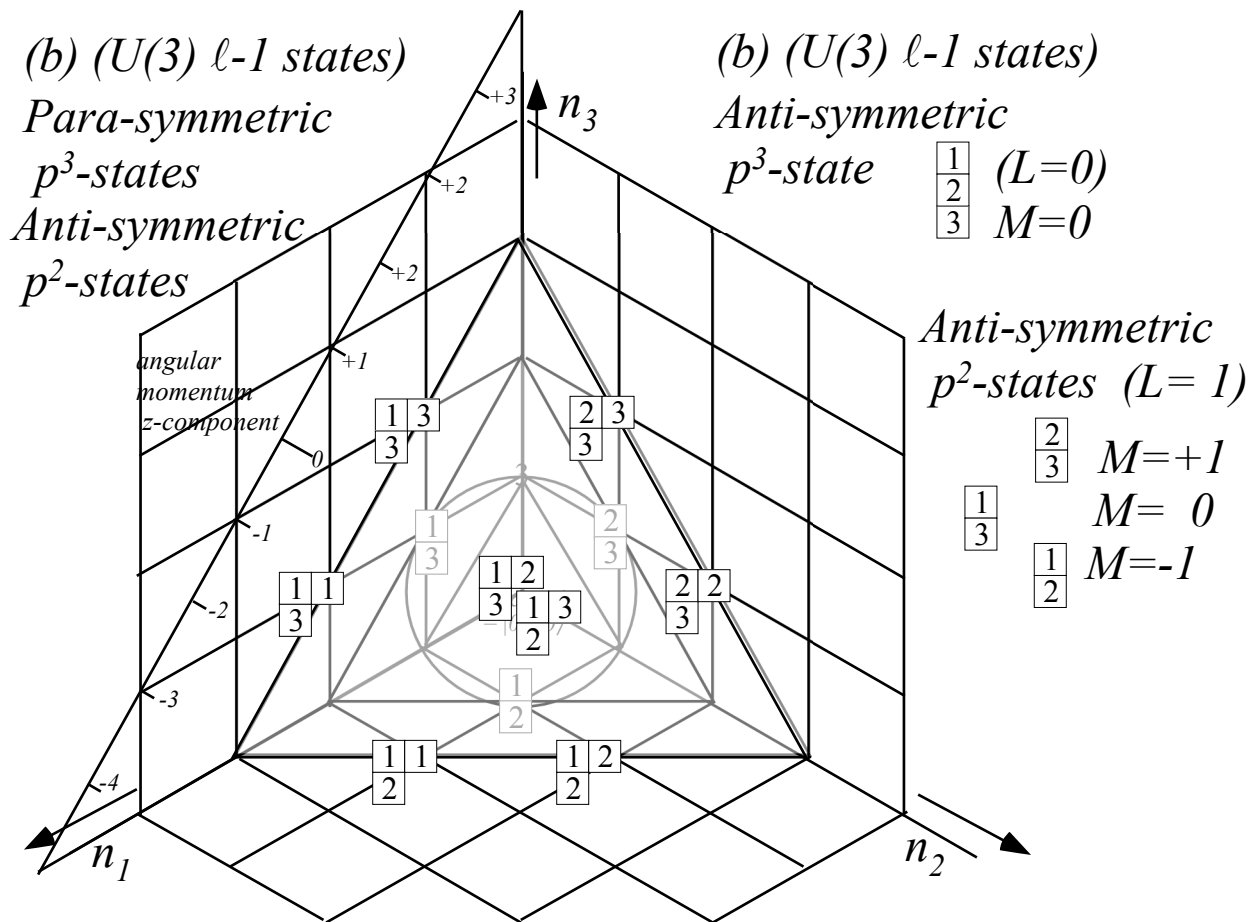
Fig. 25.3.3 U(3) orbital states for p (l=1) for 2-3 particles that are para-or-anti-symmetric.

The fundamental (1-particle) triplet states in Fig. 25.3.4(a) have z-momentum $D = M_L = +1, 0, -1$ consistent with a total momentum quantum number $L=1$. The same is true of the anti-symetric 2-particle triplet in figure (c). (Carbon $(p)^{2}\,^{3}P$ in Fig. 24.1.3 is a triplet in both orbit and, by Pauli exclusion, spin.) Four symmetric 2-particle [20] states in figure (b) have unique values $M_L = +2, +1, -1,$ and -2 so they belong to a D-quintet *(L=2)* orbital, but two have equal $M_L = 0$. There must be an S-singlet *(L=0)* mixed in there.
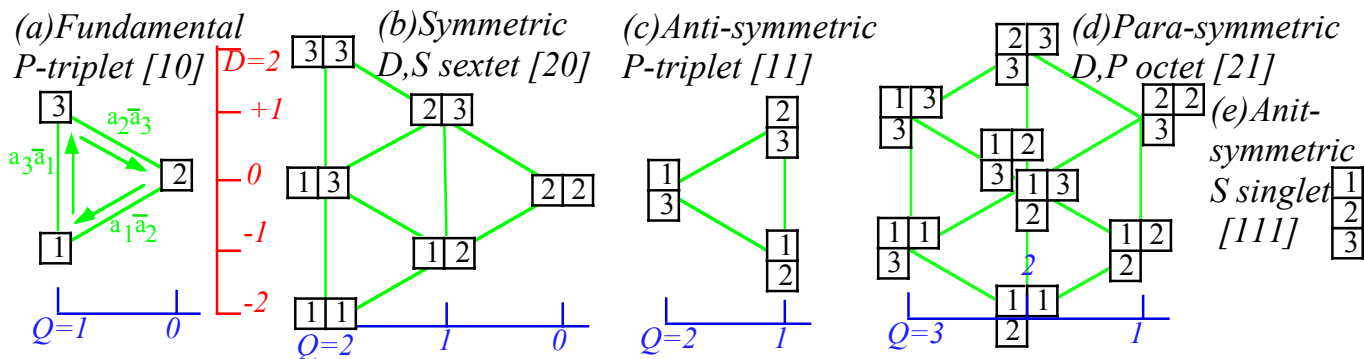
Fig. 25.3.4 (D,Q) Dipole-Quadrupole plots of U(3) orbital states for p (ℓ=1) having 1-3 particles.

Indeed, from Fig. 24.1.3 we recall that the latter is $(p)^2\,^1S$, a singlet in both spin and orbit, and it lies above the other spin singlet level $(p)^2\,^1D$ in this $U(3)$ sextet [20] of Fig. 25.3.4(b). (Recall Hund's rule.) Disentangling the $(p)^2\,^1S$ from the $(p)^2\,^1D$ state in the $U(3)$ tableau basis requires $U(3)$ defined operators.

c. Multi-particle U(3) orbital operators

The primary $U(N)$ operators are the elementary e_{jk} operators introduced in Chapter 2 of Unit 1. They were defined by their fundamental N-by-N representations that are zero-matrices with a single 1 at the (j,k)-position, that is, j^{th} row and k^{th} column. Later in Chapter 21, we generalized these operators to the 2D oscillator by replacing the elementary e_{jk} with the more powerful $\mathbf{a}_j^\dagger\mathbf{a}_k$, which in our new notation is simply $a_j\bar{a}_k$. A special case of elementary operator is the number operator $\mathbf{a}_k^\dagger\mathbf{a}_k = e_{kk} = a_k\bar{a}_k$.

Finally, the present Chapter introduced in Sec. 24.3 the idea of multiple boson operators for particles a, b, c, and so on, making us distinguish between 1-particle e_{jk} and N-particle sums E_{jk}.

$$\mathbf{a}_j^\dagger\mathbf{a}_k = e_{jk} = a_j\bar{a}_k \;(25.3.5a) \qquad\qquad \mathbf{a}_j^\dagger\mathbf{a}_k + \mathbf{b}_j^\dagger\mathbf{b}_k + \ldots = E_{jk} = a_j\bar{a}_k + b_j\bar{b}_k + \ldots (25.3.5b)$$

Nevertheless, each and every elementary (or advanced) operator obeys the same commutation relation.

$$\begin{aligned}\left[e_{jk},e_{pq}\right] &= e_{jk}e_{pq} - e_{pq}e_{jk} \\ &= \delta_{pk}e_{jq} - \delta_{qj}e_{pk}\end{aligned} \;(25.3.5c) \qquad \left[E_{jk},E_{pq}\right] = \delta_{pk}E_{jq} - \delta_{qj}E_{pk} \;(25.3.5d)$$

This is a simple result of fundamental boson commutation relations.

$$\left[\mathbf{a}_j,\mathbf{a}_k^\dagger\right]=\delta_{jk}\mathbf{1}, \;\; \left[\mathbf{a}_j,\mathbf{a}_k\right]=0, \;\; \left[\mathbf{a}_j,\mathbf{b}_k^\dagger\right]=0, \;\; \left[\mathbf{b}_j^\dagger,\mathbf{b}_k^\dagger\right]=0, \;\; \left[\mathbf{b}_j,\mathbf{b}_k^\dagger\right]=\delta_{jk}\mathbf{1}, \;\ldots \qquad (25.3.5e)$$

$$\left[\bar{a}_j,a_k\right]=\delta_{jk}\mathbf{1}, \;\; \left[\bar{a}_j,\bar{a}_k\right]=0, \;\; \left[\bar{a}_j,b_k\right]=0, \;\; \left[b_j,b_k\right]=0, \;\; \left[\bar{b}_j,b_k\right]=\delta_{jk}\mathbf{1}, \;\ldots \qquad (25.3.5f)$$

1-particle e_{jk} relations derived here apply to N-particle E_{jk} since all a's commute with all b's, and so forth.

$$\begin{aligned}\left[e_{jk},e_{pq}\right] = \;&a_j\bar{a}_k a_p\bar{a}_q \;\;\;\; - \;\;\;\; a_p\bar{a}_q a_j\bar{a}_k \\ =\; &a_j\left(\delta_{pk} + a_p\bar{a}_k\right)\bar{a}_q - a_p\left(\delta_{qj} + a_j\bar{a}_q\right)\bar{a}_k \\ =\; &\delta_{pk}a_j\bar{a}_q + a_j a_p\bar{a}_k\bar{a}_q - \delta_{qj}a_p\bar{a}_k - a_p a_j\bar{a}_q\bar{a}_k = \delta_{kp}e_{jq} - \delta_{jq}e_{pk}\end{aligned} \qquad (25.3.5c)$$

From these relations it is possible to construct all representations of multi-particle operators E_{jk} that make up the angular momentum component operators L_x, L_y, and L_z who define orbital states of definite L.

We begin with the p-orbit ($\ell=1$) representation of L_x, L_y, and L_z from (23.1.1) in Chapter 23.

$$D^1_{mn}(L_x) = \frac{1}{\sqrt{2}}\begin{pmatrix} \cdot & 1 & \cdot \\ 1 & \cdot & 1 \\ \cdot & 1 & \cdot \end{pmatrix}, \quad D^1_{mn}(L_y) = \frac{-i}{\sqrt{2}}\begin{pmatrix} \cdot & 1 & \cdot \\ -1 & \cdot & 1 \\ \cdot & -1 & \cdot \end{pmatrix}, \quad D^1_{mn}(L_z) = \begin{pmatrix} 1 & \cdot & \cdot \\ \cdot & 0 & \cdot \\ \cdot & \cdot & -1 \end{pmatrix} (25.3.6a)$$

It's then easy to read off the elementary form of the operators L_x, L_y, and L_z .

$$L_x = \left(E_{12}+E_{23}+E_{21}+E_{32}\right)/\sqrt{2}, \quad L_y = -i\left(E_{12}+E_{23}-E_{21}-E_{32}\right)/\sqrt{2}, \quad L_z = E_{11}-E_{33} \;(25.3.6b)$$

The angular momentum raising operators L_+ and L_- were defined by (23.1.5) in Chapter 23.

$$L_+ = L_x + iL_y = \sqrt{2}\left(E_{12}+E_{23}\right), \quad L_- = L_x - iL_y = \sqrt{2}\left(E_{21}+E_{32}\right) = L_+^\dagger, \quad L_z = [L_+,L_-] \;(25.3.6b)$$

Symmetric p²-orbitals: U(3) sextet

The first non-trivial application of elementary creation-destruction pairs is to the *[2,0]* sextet states $\{|\boxed{1}\boxed{1}\rangle, |\boxed{1}\boxed{2}\rangle, |\boxed{1}\boxed{3}\rangle, |\boxed{2}\boxed{2}\rangle, |\boxed{2}\boxed{3}\rangle, |\boxed{3}\boxed{3}\rangle,\}$. Identical-boson ladder operator formulas (21.1.15) apply directly.

$$E_{12}|n_1,n_2\rangle = a_1\bar{a}_2|n_1,n_2\rangle = a_1\sqrt{n_2}|n_1,n_2-1\rangle = \sqrt{n_1+1}\sqrt{n_2}|n_1+1,n_2-1\rangle$$

$$E_{23}|n_1,n_2,n_3\rangle = a_2\bar{a}_3|n_1,n_2,n_3\rangle = a_2\sqrt{n_3}|n_1,n_2,n_3-1\rangle = \sqrt{n_2+1}\sqrt{n_3}|n_1,n_2+1,n_3-1\rangle$$

Or, one may apply elementary operations e_{jk} to each particle *a*, *b*, *c*, and so forth in turn, as follows.

$$E_{23}|3_a3_b3_c\rangle = |2_a3_b3_c\rangle + |3_a2_b3_c\rangle + |3_a3_b2_c\rangle = \sqrt{3}\frac{|2_a3_b3_c\rangle + |3_a2_b3_c\rangle + |3_a3_b2\rangle}{\sqrt{3}} = \sqrt{3}|\boxed{2}\boxed{3}\boxed{3}\rangle$$

$$a_2\bar{a}_3|n_1=0,n_2=0,n_3=3\rangle = a_1\sqrt{3}|0,0,2\rangle = \sqrt{1}\sqrt{3}|0,1,2\rangle = E_{23}|\boxed{3}\boxed{3}\boxed{3}\rangle = \sqrt{3}|\boxed{2}\boxed{3}\boxed{3}\rangle \qquad (25.3.7)$$

The e_{jk} procedure shows $a=\mathbf{a}^\dagger$ or $\bar{a}=\mathbf{a}$ factors $\sqrt{n_k}$ or $\sqrt{n_k+1}$ arise by adjusting norms as in the following.

$$E_{23}\frac{|2_a3_b3_c3_d\rangle + |3_a2_b3_c3_d\rangle + |3_a3_b2_c3_d\rangle + |3_a3_b3_c2_d\rangle}{2} \qquad = E_{23}|\boxed{2}\boxed{3}\boxed{3}\boxed{3}\rangle$$

$$= \frac{|2_a2_b3_c3_d\rangle + |2_a2_b3_c3_d\rangle + |2_a3_b2_c3_d\rangle + |2_a3_b3_c2_d\rangle}{2} \qquad = \sqrt{6}\left[\frac{|2_a2_b3_c3_d\rangle + |2_a3_b2_c3_d\rangle + |2_a3_b3_c2_d\rangle}{\sqrt{6}}\right.$$

$$+ \frac{|2_a3_b2_c3_d\rangle + |3_a2_b2_c3_d\rangle + |3_a2_b2_c3_d\rangle + |3_a2_b3_c2_d\rangle}{2} \qquad \left. + \frac{|3_a2_b2_c3_d\rangle + |3_a2_b3_c2_d\rangle + |3_a3_b2_c2_d\rangle}{\sqrt{6}}\right]$$

$$+ \frac{|2_a3_b3_c2_d\rangle + |3_a2_b3_c2_d\rangle + |3_a3_b2_c2_d\rangle + |3_a3_b2_c2_d\rangle}{2} \qquad = \sqrt{6}|\boxed{2}\boxed{2}\boxed{3}\boxed{3}\rangle \qquad (25.3.8a)$$

The creation $(a\bar{a})$ operator formulas give the same result but by a more compact notation.

$$E_{23}|\boxed{2}\boxed{3}\boxed{3}\boxed{3}\rangle = a_2\bar{a}_3|n_1=0,n_2=1,n_3=3\rangle = a_2\sqrt{3}|0,1,2\rangle = \sqrt{2}\sqrt{3}|0,2,2\rangle = \sqrt{6}|\boxed{2}\boxed{2}\boxed{3}\boxed{3}\rangle \quad (25.3.8b)$$

The matrix elememts for the *[2,0]* sextet states are one of the following forms.

$$E_{11}|\boxed{1}\boxed{1}\rangle = 2|\boxed{1}\boxed{1}\rangle, \quad E_{21}|\boxed{1}\boxed{1}\rangle = \sqrt{2}|\boxed{1}\boxed{2}\rangle, \quad E_{21}|\boxed{1}\boxed{2}\rangle = \sqrt{2}|\boxed{2}\boxed{2}\rangle, \quad E_{21}|\boxed{1}\boxed{3}\rangle = |\boxed{2}\boxed{3}\rangle, \quad E_{21}|\boxed{2}\boxed{3}\rangle = 0$$

Elementary operator representations are then found as follows.

$E_{12} = E_{21}^\dagger =$

	11	12	22	13	23	33
11	.	$\sqrt{2}$	.	.	.	.
12		.	$\sqrt{2}$	.	.	.
22			.	.	.	.
13				.	1	.
23					.	.
33						.

$E_{23} = E_{32}^\dagger =$

	11	12	22	13	23	33
11	.	.	.	.	.	.
12		.	.	1	.	.
22			.	.	$\sqrt{2}$	.
13				.	.	.
23					.	$\sqrt{2}$
33						.

$E_{13} = E_{31}^\dagger =$

	11	12	22	13	23	33
11	.	.	.	$\sqrt{2}$	.	.
12		.	.	.	1	.
22			.	.	.	.
13				.	.	$\sqrt{2}$
23					.	.
33						.

(25.3.9)

All operators that can relate one sextet state to another, that is 36 "super-elementary" operators, can be made by combining products of E_{12} and E_{23} and their conjugates $E_{21} = E_{12}^\dagger$ and $E_{32} = E_{23}^\dagger$. For example, the third operator is

$E_{13} = [E_{12}, E_{23}]$ according to (25.3.5). (Verify by E_{ab}-commutation and by $(a\bar{a})$ operator algebra.) The first operators we need are the angular momentum L_+, L_-, L_x, and L^2 from (25.3.6b).

$$L_+ = L_x + iL_y = \sqrt{2}\left(E_{12} + E_{23}\right) \qquad L_- = L_+^\dagger = \qquad\qquad L^2 = L_+L_- + L_z(L_z - 1)$$

	11	12	22	13	23	33
11	·	2	·	·	·	·
12	·	·	2	$\sqrt{2}$	·	·
22	·	·	·	·	2	·
13	·	·	·	·	$\sqrt{2}$	·
23	·	·	·	·	·	2
33	·	·	·	·	·	·

	11	12	22	13	23	33
11	·	·	·	·	·	·
12	2	·	·	·	·	·
22	·	2	·	·	·	·
13	·	$\sqrt{2}$	·	·	·	·
23	·	·	2	$\sqrt{2}$	·	·
33	·	·	·	·	2	·

	11	12	22	13	23	33
11	$4+2$	·	·	·	·	·
12	·	6	·	·	·	·
22	·	·	4	$2\sqrt{2}$	·	·
13	·	·	$2\sqrt{2}$	2	·	·
23	·	·	·	·	$4+2$	·
33	·	·	·	·	·	$0+6$

(25.3.10a)

The angular-momentum-squared operator $\langle L^2 \rangle = L(L+1)$ is the one that tells what L-values are present.

$$L_+L_- = \left(L_x + iL_y\right)\left(L_x - iL_y\right) = L_x^2 + L_y^2 - iL_xL_y + iL_yL_x = L_x^2 + L_y^2 + L_z$$
$$L_x^2 + L_y^2 + L_z^2 = L_+L_- + L_z^2 - L_z$$

(25.3.10b)

Commutatuion $[L_x, L_y] = L_xL_y - L_yL_x = iL_z$ helps find L^2 matrices. Of six eigenvalues, five are $L(L+1) = 6$ implying an *(L=2)* or D-orbital. The 6th *L*-value *(L=0)* implies an S-orbital. Both are projected below.

$$P(L = 0) = \frac{\begin{pmatrix} 4 - 2(2+1) & 2\sqrt{2} \\ 2\sqrt{2} & 2 - 2(2+1) \end{pmatrix}}{0(0+1) - 2(2+1)} = \frac{1}{3}\begin{pmatrix} 1 & -\sqrt{2} \\ -\sqrt{2} & 2 \end{pmatrix} \qquad (25.3.11a) \qquad P(L = 2) = \frac{1}{3}\begin{pmatrix} 2 & \sqrt{2} \\ \sqrt{2} & 1 \end{pmatrix} (25.3.11b)$$

This gives the transformation matrix for two tableau sextets $\left|\boxed{2}\boxed{2}\right\rangle$ and $\left|\boxed{1}\boxed{3}\right\rangle$ and *L*-orbitals with *M=0*.

$$\begin{pmatrix} \left\langle \boxed{2}\boxed{2} \Big| {}^{L=0}_{M=0} \right\rangle & \left\langle \boxed{2}\boxed{2} \Big| {}^{L=2}_{M=0} \right\rangle \\ \left\langle \boxed{1}\boxed{3} \Big| {}^{L=0}_{M=0} \right\rangle & \left\langle \boxed{1}\boxed{3} \Big| {}^{L=2}_{M=0} \right\rangle \end{pmatrix} = \begin{pmatrix} \left\langle \boxed{0}\boxed{0} \Big| {}^0_0 \right\rangle & \left\langle \boxed{0}\boxed{0} \Big| {}^2_0 \right\rangle \\ \left\langle \boxed{+1}\boxed{-1} \Big| {}^0_0 \right\rangle & \left\langle \boxed{+1}\boxed{-1} \Big| {}^2_0 \right\rangle \end{pmatrix} = \begin{pmatrix} \sqrt{\frac{1}{3}} & \sqrt{\frac{2}{3}} \\ -\sqrt{\frac{2}{3}} & \sqrt{\frac{1}{3}} \end{pmatrix}$$

(25.3.12a)

Compare this to *(M=0)*-Clebsch-Gordan coefficients under $\left|{}^0_0\right\rangle$ and $\left|{}^2_0\right\rangle$ columns of table (24.1.19b).

$$\left| 1 \otimes 1 {}^{L=0}_{M=0} \right\rangle = \sum C^{1\ 1\ 0}_{mm'0} \left|{}^1_0\right\rangle \left|{}^1_0\right\rangle$$

$$= C^{110}_{000} \left|{}^1_0\right\rangle \left|{}^1_0\right\rangle + C^{1\ 1\ 0}_{+1-1\ 0} \left|{}^1_{+1}\right\rangle \left|{}^1_{-1}\right\rangle + C^{1\ 1\ 0}_{-1+1\ 0} \left|{}^1_{-1}\right\rangle \left|{}^1_{+1}\right\rangle$$

$$= -\sqrt{\frac{1}{3}} \left|{}^1_0\right\rangle \left|{}^1_0\right\rangle + \sqrt{\frac{1}{3}} \left|{}^1_{+1}\right\rangle \left|{}^1_{-1}\right\rangle + \sqrt{\frac{1}{3}} \left|{}^1_{-1}\right\rangle \left|{}^1_{+1}\right\rangle$$

$$= -\sqrt{\frac{1}{3}} \left|\boxed{0}\boxed{0}\right\rangle + \sqrt{\frac{2}{3}} \left|\boxed{+1}\boxed{-1}\right\rangle \qquad (25.3.12b)$$

$$\left| 1 \otimes 1 {}^{L=2}_{M=0} \right\rangle = \sum C^{1\ 1\ 2}_{mm'0} \left|{}^1_0\right\rangle \left|{}^1_0\right\rangle$$

$$= C^{112}_{000} \left|{}^1_0\right\rangle \left|{}^1_0\right\rangle + C^{1\ 1\ 1}_{+1-1\ 0} \left|{}^1_{+1}\right\rangle \left|{}^1_{-1}\right\rangle + C^{1\ 1\ 2}_{-1+1\ 0} \left|{}^1_{-1}\right\rangle \left|{}^1_{+1}\right\rangle$$

$$= \sqrt{\frac{2}{3}} \left|{}^1_0\right\rangle \left|{}^1_0\right\rangle + \sqrt{\frac{1}{6}} \left|{}^1_{+1}\right\rangle \left|{}^1_{-1}\right\rangle + \sqrt{\frac{1}{6}} \left|{}^1_{-1}\right\rangle \left|{}^1_{+1}\right\rangle$$

$$= \sqrt{\frac{2}{3}} \left|\boxed{0}\boxed{0}\right\rangle + \sqrt{\frac{1}{3}} \left|\boxed{+1}\boxed{-1}\right\rangle \qquad (25.3.12c)$$

The tableau results (25.3.12a) agree up to an overall column phase with the CGC results (25.3.12b-c).

Para-symmetric p³-orbitals: U(3) octet

The $U(3)$ octet bases $\left\{ \boxed{\begin{smallmatrix}1&1\\2\end{smallmatrix}}, \boxed{\begin{smallmatrix}1&2\\2\end{smallmatrix}}, \boxed{\begin{smallmatrix}1&2\\3\end{smallmatrix}}, \boxed{\begin{smallmatrix}1&3\\2\end{smallmatrix}}, \boxed{\begin{smallmatrix}1&1\\3\end{smallmatrix}}, \boxed{\begin{smallmatrix}1&3\\3\end{smallmatrix}}, \boxed{\begin{smallmatrix}2&2\\3\end{smallmatrix}}, \boxed{\begin{smallmatrix}2&3\\3\end{smallmatrix}} \right\}$ (25.3.13) plotted in Fig. 25.3.4(d) are para-symmetric combinations due to *[2,1]* tableau projections (25.3.5e) analogous to spin *U(2)* examples (25.3.6-8). For example, an elementary operation on the *(M=1)*-tableau state begins with primitive *(M=1)*-ket relations.

$$E_{23}\left|1_a 3_b 3_c\right\rangle = \left|1_a 2_b 3_c\right\rangle + \left|1_a 3_b 2_c\right\rangle, \quad E_{23}\left|3_a 1_b 3_c\right\rangle = \left|2_a 1_b 3_c\right\rangle + \left|3_a 1_b 2_c\right\rangle, \quad E_{23}\left|3_a 3_b 1_c\right\rangle = \left|2_a 3_b 1_c\right\rangle + \left|3_a 2_b 1_c\right\rangle.$$

Then E_{23} acts on a ($\boxed{\begin{smallmatrix}a&b\\c\end{smallmatrix}}$ $\boxed{\begin{smallmatrix}a&b\\c\end{smallmatrix}}$) projection of $\left|1_a 3_b 3_c\right\rangle$. (Recall 3rd line of (25.3.5e) or 2nd line of (25.3.8a).)

$$E_{23}\left|\boxed{\begin{smallmatrix}1&3\\3\end{smallmatrix}}\right\rangle = E_{23}\frac{\left|1_a 3_b 3_c\right\rangle + \left|3_a 1_b 3_c\right\rangle - 2\left|3_a 3_b 1_c\right\rangle}{\sqrt{6}} = \frac{\left|1_a 2_b 3_c\right\rangle - 2\left|2_a 3_b 1_c\right\rangle + \left|3_a 1_b 2_c\right\rangle + \left|1_a 3_b 2_c\right\rangle - 2\left|3_a 2_b 1_c\right\rangle + \left|2_a 1_b 3_c\right\rangle}{\sqrt{6}}$$

$E_{23}\left|\boxed{\begin{smallmatrix}a&b\\c\end{smallmatrix}}\ \boxed{\begin{smallmatrix}1&2\\3\end{smallmatrix}}\right\rangle$ is a combination of $\left|\boxed{\begin{smallmatrix}a&b\\c\end{smallmatrix}}\ \boxed{\begin{smallmatrix}1&2\\3\end{smallmatrix}}\right\rangle$ and $\left|\boxed{\begin{smallmatrix}a&b\\c\end{smallmatrix}}\ \boxed{\begin{smallmatrix}1&3\\2\end{smallmatrix}}\right\rangle$ states. (Recall 3rd and 5th rows of (24.5.5e).)

$$\left|\boxed{\begin{smallmatrix}1&2\\3\end{smallmatrix}}\right\rangle = \frac{2\left|1_a 2_b 3_c\right\rangle - 1\left|2_a 3_b 1_c\right\rangle - 1\left|3_a 1_b 2_c\right\rangle - 1\left|1_a 3_b 2_c\right\rangle - 1\left|3_a 2_b 1_c\right\rangle + 2\left|2_a 1_b 3_c\right\rangle}{2\sqrt{3}}$$

$$\left|\boxed{\begin{smallmatrix}1&3\\2\end{smallmatrix}}\right\rangle = \frac{0\left|1_a 2_b 3_c\right\rangle - 1\left|2_a 3_b 1_c\right\rangle + 1\left|3_a 1_b 2_c\right\rangle + 1\left|1_a 3_b 2_c\right\rangle - 1\left|3_a 2_b 1_c\right\rangle + 0\left|2_a 1_b 3_c\right\rangle}{2}$$

$$(25.3.13a)$$

The last step is to add up the scalar product or overlap of $E_{23}\left|\boxed{\begin{smallmatrix}a&b\\c\end{smallmatrix}}\ \boxed{\begin{smallmatrix}1&3\\3\end{smallmatrix}}\right\rangle$ with $\left|\boxed{\begin{smallmatrix}a&b\\c\end{smallmatrix}}\ \boxed{\begin{smallmatrix}1&2\\3\end{smallmatrix}}\right\rangle$ or $\left|\boxed{\begin{smallmatrix}a&b\\c\end{smallmatrix}}\ \boxed{\begin{smallmatrix}1&3\\2\end{smallmatrix}}\right\rangle$.

$$\left\langle\boxed{\begin{smallmatrix}1&2\\3\end{smallmatrix}}\left|E_{23}\right|\boxed{\begin{smallmatrix}1&3\\3\end{smallmatrix}}\right\rangle = \frac{1}{2\sqrt{3}}\frac{1}{\sqrt{6}}\left(2+2-1-1+2+2\right) = \sqrt{\frac{1}{2}}$$

$$\left\langle\boxed{\begin{smallmatrix}1&3\\2\end{smallmatrix}}\left|E_{23}\right|\boxed{\begin{smallmatrix}1&3\\3\end{smallmatrix}}\right\rangle = \frac{1}{2}\frac{1}{\sqrt{6}}\left(0+2+1+1+2+0\right) = \sqrt{\frac{3}{2}}$$

$$(25.3.13b) \qquad\qquad\qquad\qquad (25.3.13c)$$

Overlaps are the same for $E_{23}\left|\boxed{\begin{smallmatrix}a&c\\b\end{smallmatrix}}\ \boxed{\begin{smallmatrix}1&3\\3\end{smallmatrix}}\right\rangle$ with $\left|\boxed{\begin{smallmatrix}a&c\\b\end{smallmatrix}}\ \boxed{\begin{smallmatrix}1&2\\3\end{smallmatrix}}\right\rangle$ or $\left|\boxed{\begin{smallmatrix}a&c\\b\end{smallmatrix}}\ \boxed{\begin{smallmatrix}1&3\\2\end{smallmatrix}}\right\rangle$ (Recall 4th or 6th rows of (24.5.5e). State-op E_{23} commutes with particle-ops *(abc)*. E_{23} cares *what* each particle is *doing* but not *who* they *are*!

For 2-column tableaus, simple hooklength formulas shown in Fig. 25.3.5 give matrix elements such as (25.3.13b-c) shown in Fig. 25.3.5(e). Tableau hooks make it easier to derive representations like those of (25.3.9-10) and find what tableau combinations have definite *L*. By Fig. 25.3.4(d), we see *[2.1]*-octet orbits are either *(L=1)* or else *(L=2)*. Detailed derivation of octet orbital states is left as an exercise.

Fig. 25.3.5 U(m)-Tableau hooklength formulas for atomic orbital matrix representations

Many have contributed to angular momentum coupling besides the originators Wigner, Racah, Clebsch and Gordan. Some have gone on to develop similar formulas for higher unitary groups *U(m)*. Pioneers in this area include Schwinger, Baird, Biedenharn, Bincer, Gelfand, Louck, and Moshinsky.

25.4 Rotational Tensor Levels for High J

Rotational or orbital mechanics of atomic electrons in anisotropic potentials is analogous to the quantum mechanics of molecular rotation, and it was first studied in early days of quantum theory. Bethe described the splitting of orbital levels by anisotropic crystalline fields having point symmetries ranging from octahedral (O) to orthorhombic (D_2). This is one of the best known group theory applications

In modern formalism the crystal field orbital eigensolutions are found by first expressing the Hamiltonian H in terms of (Racah-Wigner) tensors T_q^k and then diagonalizing a representation of H in an orbital basis $\left\{ \cdots |n,L,N\rangle \cdots |n',L',M'\rangle \cdots \right\}$. Wigner-Eckart theorem (25.1.20) represents each tensor component in terms of coupling or Clebsch-Gordan coefficients (CGC) $C_{qMM'}^{kLL'}$ and reduced matrix elements.

$$\left\langle n',L',M' \left| T_q^k \right| n,L,M \right\rangle = C_{q\ M\ M}^{k\ L\ L'} \left\langle n'L' \left\| T^k \right\| nL \right\rangle \tag{25.4.1}$$

The remainder of the problem (and most of the numerical labor) involves truncating the basis, summing the operators, and matrix diagonalization of the result.

Molecular rotations in a vacuum may be described analogously using anisotropic Hamiltonians. In the simplest cases the rotational Hamiltonians are conveniently expressed as polynomials of angular momentum operators J_x, J_y, and J_z defined with respect to the molecular frame. Pure rotational Hamiltonians conserve J and cannot couple rotational states $|J,K\rangle$ and $|J',K'\rangle$ having different J values. This makes the rotational analysis simpler than the external crystal field problem since numerical diagonalization is limited to treating individual $(2J + 1)$ dimensional block matrices. Even so, heavy molecules tend to have high J. For example, SF_6 spectra with $J = 150$ and higher can be resolved, and so the numerical problem is still quite formidable.

However, for high-J states it is possible to make approximations. It turns out that for high symmetry the diagonal ($K = K'$) contributions to the tensor matrix elements are dominant, and for high J and K they can be approximated by an asymptotic expression for the Clebsch-Gordan coefficients in terms of a Wigner rotation matrix or a Legendre polynomial. (Here the reduced matrix factor is unity.)

$$\left\langle J,K \left| T_0^k \right| J,K \right\rangle = C_{0\ K\ K}^{k\ J\ J} \cong D_{0,0}^k \left(0,\Theta_{JK},0\right) = P_k \left(\cos\Theta_{JK}\right) \tag{25.4.2a}$$

The polar angle θ_{JK} is that of the angular-momentum cones introduced in Figures 23.1.1, and 23.1.2.

$$\cos\Theta_{JK} = K \Big/ \left[J(J+1)\right]^{1/2}, \quad K = J, J-1, J-2,\dots \tag{25.4.2b}$$

The approximation (25.4.2a) is valid in the limit that J and K are both large compared to the tensorial rank $(K \gg k)$. The angle Θ_{JK} is the apex half-angle of a cone with a slant height of $\sqrt{\left[J(J+1)\right]}$ and altitude of K. The cone is the locus of the quantum angular-momentum vector J subject to the constraints $\langle \mathbf{J} \cdot \mathbf{J} \rangle = \left[J(J+1)\right]$ and $\langle J_z \rangle = K$ imposed by the state $|J,K\rangle$. The cone angle Θ_{JK} is a measure of the quantum uncertainty (ΔJ_x) or (ΔJ_y) of transverse components for that state.

The possible motion of a classical angular-momentum J vector can be displayed using a rotational energy (RE) surface. RE surfaces are radial plots of rotational energy as a function of the direction of the J vector in the body frame for a constant magnitude $|J| = \sqrt{[J(J+1)]}$ of the angular-momentum. The classical J vector, while fixed in a laboratory frame, follows a body-frame trajectorythat conserves both energy E and magnitude $|J|$ of J.

Each classically allowed J trajectory is a topography line on an RE surface, that is the intersection of an RE surface for a given $|J|$ with an energy sphere for a given E. Examples of RE surfaces for D_2 and O shall see the quantum eigenvalues can be related to special "quantizing" J trajectories and that these can be approximated by the intersection of the angular momentum cones with the RE surface.

a. Rigid rotors $(D_\infty \supset D_2 \ \text{symmetry})$

The following starts with a review of the rigid rotor theory introduced in Section 23(c) and extends it to asymmetric rotors using geometry of *Rotational Energy Surfaces (RES)*. Then RES are used for non-rigid rotors and coupled rotors to develop a powerful conceptual and computational theory of their spectra.

Rotational Energy Surfaces (RES)

The Hamiltonian for an, in general, asymmetric rigid rotor or top follows from (23.1.21)

$$H = AJ_x^2 + BJ_y^2 + CJ_z^2 \tag{25.4.3}$$

An RES of H follows if we substitute classical body-frame angular-momentum components

$$J_x = -\langle J \rangle \sin\beta \cos\gamma, \quad J_y = \langle J \rangle \sin\beta \sin\gamma, \quad J_z = \langle J \rangle \cos\beta. \tag{25.4.4a}$$

Here the J magnitude is a constant approximated by binomial theorem to about *1/2*-quantum above J.

$$\langle J \rangle = \sqrt{J(J+1)} \cong J + \tfrac{1}{2} \tag{25.4.4b}$$

The exact quantum magnitude is $\langle J^2 \rangle = J(J+1)$ from (23.1.10). The resulting energy expression

$$E = J(J+1)\left[A\sin^2\beta\cos^2\gamma + B\sin^2\beta\sin^2\gamma + C\cos^2\gamma \right] \tag{25.4.5}$$

is plotted radially in Fig. 25.4.1 to give RES as a function of body-frame polar coordinates of azimuth $(\phi = -\gamma)$ and polar angle $(\theta = \beta)$ for the J vector. These angles are two of the three Euler angles (α, β, γ) introduced in Chapter 10 and Appendix 10A.

Three examples of rigid top RE surfaces are shown in Fig. 25.4.1 for the cases of *(a)* a *prolate symmetric top* $(A = B < C)$, *(b)* an *asymmetric top* $(A < B < C)$, and *(c)* an *oblate symmetric top* $(A < B = C)$. A *(J=10)*-surface has one contour line for each of *(2J+1=21)* quantum energy levels for *J=10*. Quantum J-phase paths are labeled in Fig. 25.4.1(d), an expanded view of Fig. 25.4.1(a), and satisfy the following *Bohr J_z-quantization conditions* found by solving (25.4.5). The $(\pm)$ is due to time reversal symmetry.

$$\frac{1}{\hbar}\int J_z d\gamma = \pm K = \pm(J, J-1, J-2, \ldots 0), \quad \text{where:} \quad J_z = \pm\sqrt{\frac{J(J+1)(C\cos^2\gamma + B\sin^2\gamma) - E}{(C\cos^2\gamma + B\sin^2\gamma) - A}} \quad (25.4.6)$$

Time reversal symmetry requires that for each **J** on a *K*-path there is a –**J** on a –*K*-path of equal *E*.

Tensor operator mechanics

To improve the quantum mechanics it helps to rewrite the Hamiltonian in terms of tensor operators or as a *J*-operator multipole expansion. The *J*-multipole functions,

$$T_q^k = D_{0q}^k(0,\beta,\gamma)^* = \sqrt{\frac{4\pi}{2k+1}}\langle J\rangle^k Y_q^k(\gamma,\beta)) \quad (25.4.7)$$

are analogous to spatial multipole functions defined in (23.3.8). Consider quadrupole J-functions first.

$$T_0^0 = \mathbf{J}\cdot\mathbf{J} = \langle J\rangle^2 \qquad = \quad \left(J_x^2 + J_y^2 + J_y^2\right), \quad (25.4.8a)$$

$$T_0^2 = \tfrac{1}{2}\langle J\rangle^2\left(3\cos^2\beta - 1\right) = \tfrac{1}{2}\left(2J_z^2 - J_x^2 - J_y^2\right), \quad (25.4.8b)$$

$$\left(T_2^2 + T_{-2}^2\right) = \langle J\rangle^2\frac{\sqrt{6}}{2}\sin^2\beta\cos 2\gamma = \quad \frac{\sqrt{6}}{2}\left(J_x^2 - J_y^2\right). \quad (25.4.8c)$$

Solving this for J_x^2, J_y^2, and J_z^2 gives a tensor operator expression for a rigid rotor Hamiltonian (25.4.3).

$$H = \frac{A+B+C}{3}T_0^0 + \frac{2C-A-B}{3}T_0^2 + \frac{A-B}{\sqrt{6}}\left(T_2^2 + T_{-2}^2\right) \quad (25.4.9)$$

Only the first term survives for a *spherical top* (*A = B = C*). *Symmetric tops* (*A = B ≠ C)* have the first two terms. The *asymmetric tops* (*A ≠ B ≠ C*) use all three. The energy is given by (25.4.8) and (25.4.9).

$$E = J(J+1)\left[\frac{A+B+C}{3} + \frac{2C-A-B}{6}\left(3\cos^2\beta - 1\right) + \frac{A+B}{2}\sin^2\beta\cos 2\gamma\right]. \quad (25.4.10)$$

The preceding *multipole expansion* is equal to the polynomial expression (25.4.5) but has some quantum mechanical advantages over it. Tensor multipole operator expressions like (25.4.9) provide matrix elements in terms of CGC and reduced matrix elements of the Wigner-Eckart theorem (25.4.1). Only one reduced matrix $\left\langle J\|T^2\|J\right\rangle$ is needed. The scalar eigenvalue of (25.4.8a) is *J(J+1)* by (23.1.10).

$$\left\langle J\|T^0\|J\right\rangle = J(J+1)$$

Tensor matrices are found by evaluating the easiest component $\left\langle {}_J^J|T_0^2|{}_J^J\right\rangle$ by elementary means.

$$\left\langle {}^J_J \middle| T_0^2 \middle| {}^J_J \right\rangle = \left\langle {}^J_J \middle| \tfrac{1}{2}\left(3J_z^2 - J_x^2 - J_y^2 - J_z^2\right) \middle| {}^J_J \right\rangle = \left\langle {}^J_J \middle| \tfrac{1}{2}\left(3J_z^2 - \mathbf{J}\bullet\mathbf{J}\right) \middle| {}^J_J \right\rangle$$
$$= \tfrac{1}{2}\left(3J^2 - J(J+1)\right) = \tfrac{1}{2}\left(2J^2 - J\right) \tag{25.4.11}$$

Then the Wigner-Eckart theorem (25.4.1) and CGC formulas (23.4.20) give

$$\left\langle {}^J_K \middle| T_0^2 \middle| {}^J_J \right\rangle = C_0^2\,{}^J_J\,{}^J_J \left\langle J \middle\| T^2 \middle\| J \right\rangle = \frac{2\left(2J^2 - J\right)}{\sqrt{(2J+3)(2J+2)\,2J(2J-1)}}. \tag{25.4.12}$$

Solving gives the desired reduce matrix element:

$$\left\langle J \middle\| T^2 \middle\| J \right\rangle = \sqrt{(2J+3)(2J+2)\,2J(2J-1)}\,/\,4. \tag{25.4.13}$$

Still you might wonder why we deal with tensor T-operators when *J*-polynomials seem simpler. The reasons for using tensor operators become clearer when comparing the work involved with higher-degree polynomials and corresponding high-rank tensors. Manipulating and computing matrix elements for fourth- or sixth-degree polynomials can be extremely laborious while fourth- or sixth-rank tensors use the same Wigner-Eckart analysis as the T^2 example above.

 Symmetric top energy levels (J = 10 Example)
The trajectories on the RE surface for $A = B = 0.2$ and $C = 0.6$ [see Figures 25.4.1(a and d)] are precisely the ones that correspond to exact quantum energy levels for $J = 10$. If the cone-angle cosine formula (25.4.2b) is substituted into the tensor RE surface energy expression (25.4.10) for $A = B$ one obtains

$$E = J(J+1)\left[\frac{2B+C}{3} + \frac{C-B}{3}\left(3\frac{K^2 J(J+1)}{J(J+1)} - 1\right)\right], \tag{25.4.14}$$

$$E = BJ(J+1) + (C-B)K^2. \tag{25.4.15}$$

This is the exact symmetric top quantum energy level equation. Recall (23.1.21). Here the cone-angle tensor matrix element approximation (25.4.2) gives an exact result. The angular-momentum cones exactly define the quantizing *J* trajectories shown in Fig. 25.4.1a. The same applies to the oblate symmetric top surface shown in Fig. 25.4.1c. However, *J*-trajectories for the asymmetric top in Fig. 25.4.1(b) are not flat circles like symmetric top paths. Then cone intersections are approximate averages of $\langle J_z \rangle = K$ -values.
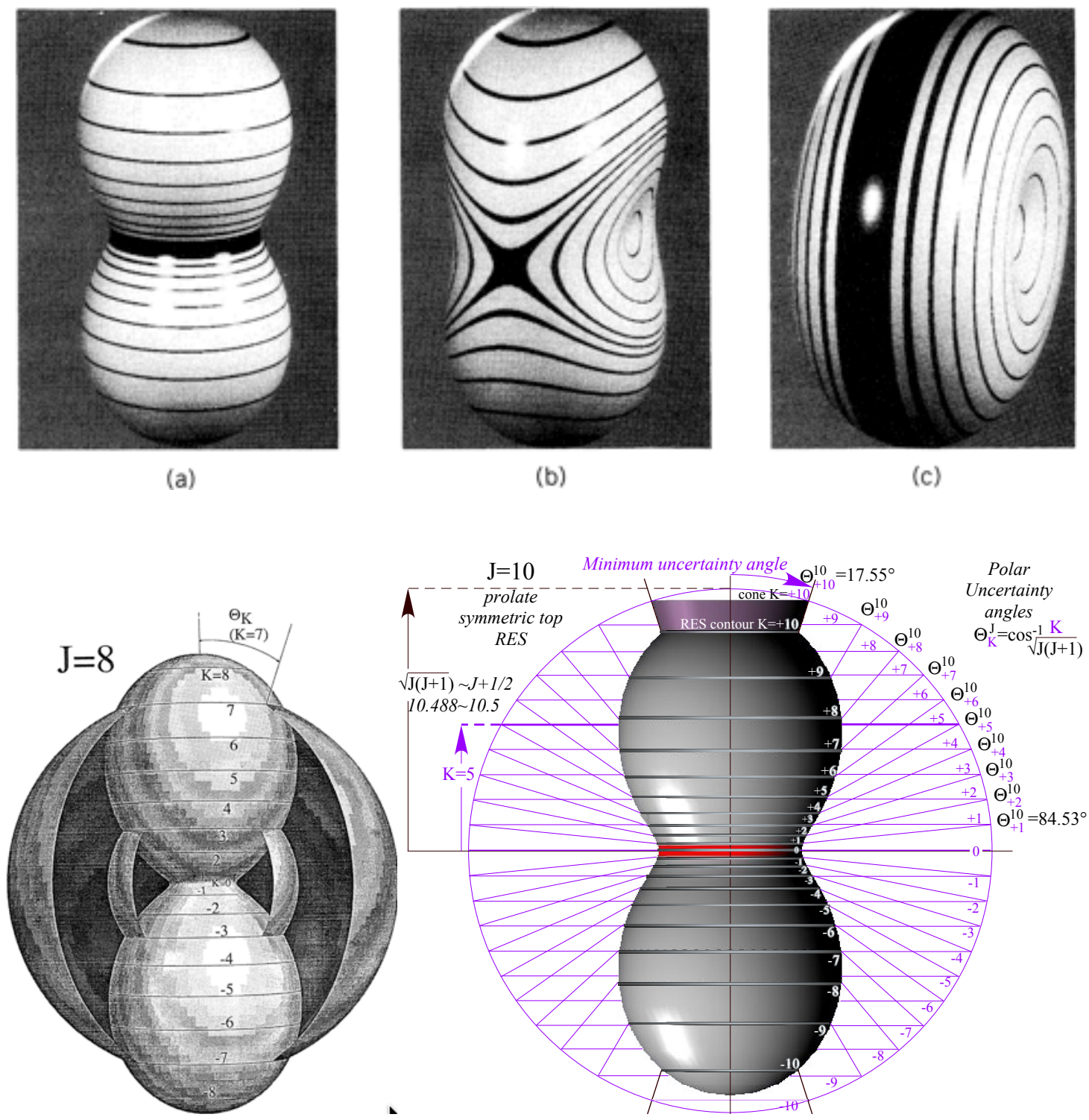
Fig. 25.4.1 *Rotational energy (RE) surfaces for rigid rotors. (a) Prolate symmetric top (A = 0.2, B = 0.2, C = 0.6). (b) Rigid asymmetric top (A = 0.2, B = 0.4, C = 0.6). (c) Oblate symmetric top (A = 0.2, B = 0.6, C – 0.6). (d) Prolate symmetric top with J = 10 quantum energy levels.*

Asymmetric top energy levels (J = 10 Example)

This *J*-inversion symmetry and the D_2 rotational symmetry of top Hamiltonian (25.4.3) or (25.4.9) combine to give (at least) a D_{2h} symmetry to the RE surface regardless of the symmetry of the rotor which it models. The simplest rigid molecule having the surface shown in Fig. 25.4.1(b) would be a bent XY_2 structure like the water molecule.

It is evident that every path on the asymmetric surface in Fig. 25.4.1b belongs to a mirror image pair of *(±K)*-paths with exception of the *(K=0)* path. The exceptional path is the x-shaped *separatrix* curve that crosses the saddle points on the ±*y* axes. The separatrix divides the surface into regions containing two different kinds of trajectory pairs. One kind of trajectory pair encircles the high-energy regions centered on the ±*z*-axes or *C* axis. These paths are distorted versions of the paths for the prolate top shown in Fig. 25.4.1a. The other pairs encircle the low-energy valley regions around the ±*x* axes or *A* axis, and they are distorted versions of the oblate symmetric top paths in Fig. 25.4.1(c).

The separation of regions is manifested in the quantum level spectrum that is shown in the lower center portion of Fig. 25.4.2. Here the lower energy quasi-oblate pairs of trajectories are each identified with quasi-degenerate or *clustered* pairs of energy levels below the separatrix level at *44 cm^{-1}*. Similarly, the quasi-prolate pairs are indicated in the high-energy region on the right-hand side of Fig. 25.4.2. The levels belonging to each pair are indicated inside magnifying circles that give D_2 symmetry labels for each level and the magnitude of the splitting between each pair.

The *rotational fine structure* splitting is the intercluster frequency splitting such as the 150 GHz splitting between the lowest two pairs. This is approximately the frequency of classical precession or the wobbling frequency for the *J* vector to go once around the lowest energy path. The intracluster splitting such as the 26 kHz splitting of the A_1B_1 pair in the lowest circle is called *superfine structure*. This corresponds to the frequency of a purely quantum mechanical tunneling process between equivalent pairs of semiclassical paths. If the molecule was set initially into a localized nonstationary state with *J*-wobbling around the lowest (*K* = 10) path near the +*x* axis, then it would gradually evolve into a similar motion around the equivalent (*K* = -10) path near the –*x* axis after which it would return and (more or less) repeat the whole process at a rate of 26 kHz.

The cluster doublets are the angular momentum analogs or inversion doublet levels of a two-well oscillator potential discussed in Chapter 2. (Recall Fig. 2.12.7.)   The stationary A_1 or B_1, eigenstates are, respectively, symmetric or antisymmetric combinations of two separate but equivalent wave functions localized on separate but equivalent paths or *K*-states : $|z\rangle$ (or positive K_z) and $|\bar{z}\rangle$ (or negative K_z).

VISUALIZING THE J = 10
LEVELS OF AN
ASYMMETRIC TOP
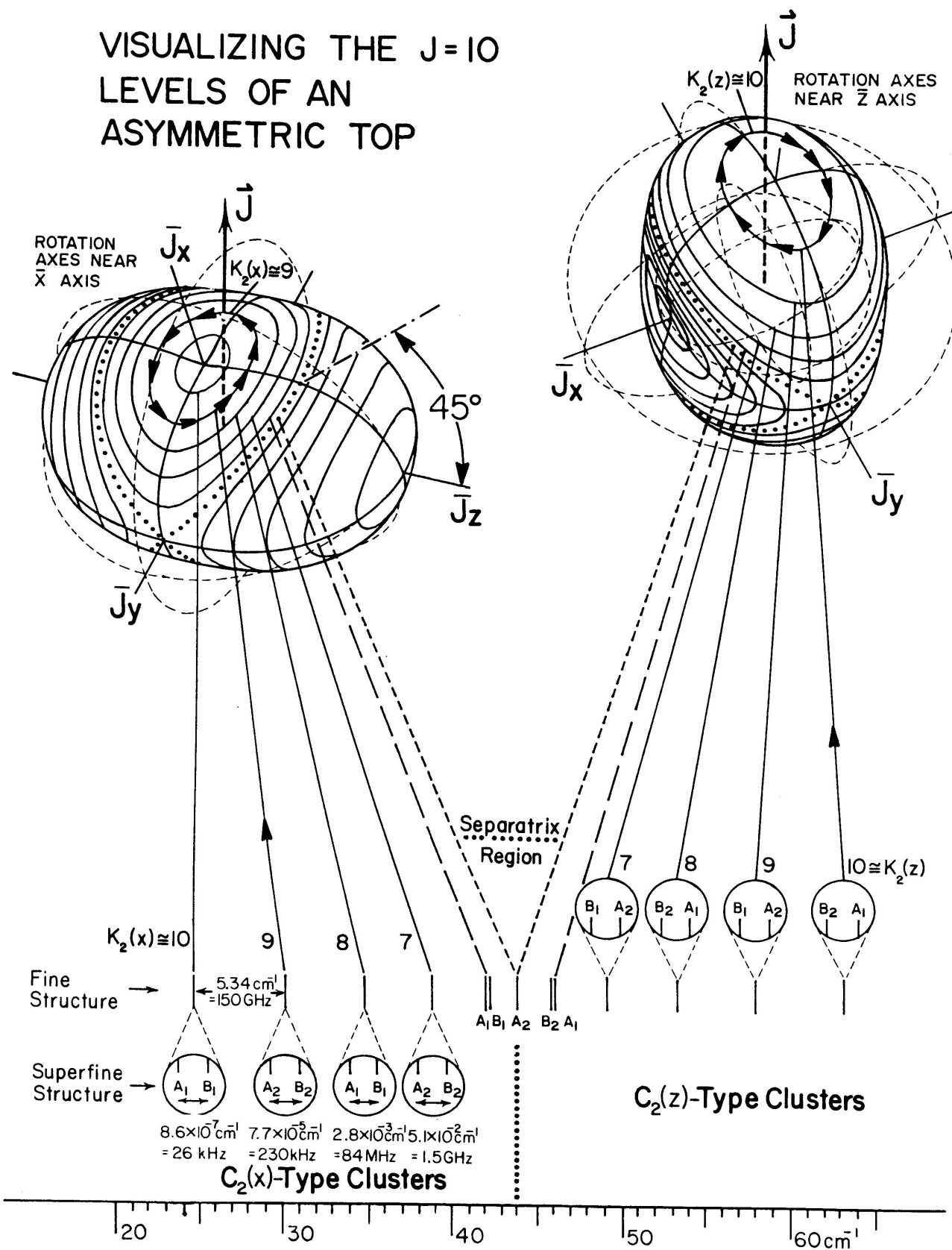
Fig. 25.4.2   *J = 10 asymmetric top energy levels and related RE surface paths (A = 0.2, B = 0.4, C = 0.6). Clustered pairs of levels are indicated in magnifying circles that show superfine splittings.*

Eigenvectors	$|z\rangle$	$|\bar{z}\rangle$	Eigenvalues
$|A\rangle$	$1/\sqrt{2}$	$1/\sqrt{2}$	$E^A(K) = E_K + 2S_K$
$|B\rangle$	$1/\sqrt{2}$	$-1/\sqrt{2}$	$E^B(K) = E_K - 2S_K$

where: $\quad S_K = v_K e^{-P_K}$

and: $\quad P_K = i \int\limits_{\gamma-}^{\gamma+} d\gamma \sqrt{\dfrac{J(J+1)(C\cos^2\gamma + B\sin^2\gamma) - E_K}{(C\cos^2\gamma + B\sin^2\gamma) - A}}$

$$(25.4.16a)$$

The degree of separation or localization is given by the tunneling rate S_K and *superfine level splitting* $4S_K$.

This rate S_K varies exponentially with the magnitude of a path integral between the points $\gamma\pm$ of closest approach

of the separate K-paths and proportional to classical precession rate v_K. For the highest-K-paths that have the

greatest separation, the precession rate v_K is more than a million times faster than tunneling S_K. However, near the

separatrix the tunneling rate or superfine splitting increases enormously while the classical precession rate v_K and

fine structure splitting $(hv_K \approx E_K - E_{K-1})$ reduces near saddles and J-body orientation is fuzzy as is the distinction

between semi-classical (fine) and quantum (superfine) motion.

    A classical rotor is always located on just one K-path at once. A quantum rotor eigenstate of the following

tunneling Hamiltonian submatrix is a ±combination (25.4.16) of two or more K-paths.

$$\langle H \rangle_K = \begin{pmatrix} E_K & 2S_K \\ 2S_K & E_K \end{pmatrix}_{in\ |z\rangle\ and\ |\bar{z}\rangle\ basis}$$

This is necessary for the state to belong to a single irreducible representation such as A_1 or B_1 of the global

symmetry group D_2, which contains the local subgroup C_2 symmetries of x-and-z-axes of the RES.

D_2	1	R_x	R_y	R_z
A_1	1	1	1	1
A_2	1	-1	1	-1
B_1	1	1	-1	-1
B_2	1	-1	-1	1

Table 25.4.1

C_2	1	R
A	1	1
B	1	−1

Table 25.4.2

    A state localized on one K_x -path is a sum (or difference) A_1 and B_1 states. Both $K_x = \pm 10$ states have *0-mod*

2 $(0_2)_x$ symmetry with respect to local symmetry subgroup $C_2(x)$ of x-axis rotation. (Both $K_x = 10$ and $K_x = -10$ are

even numbers.) The combination states are a basis of the induced representation $0_2(\text{of } C_2(x)) \uparrow D_2$ of the global D_2

symmetry induced by the even representation 0_2 of the local symmetry $C_2(x)$. The even induced representation is

indicated by the first column of the $D_2 \supset C_2(x)$ correlation table in the left-hand side of Fig. 25.4.3. The table

gives the D_2 species in the even *(0₂)ₓ* and odd *(1₂)ₓ* induced representations using the Frobenius reciprocity theorem:

$$0_2\left(\text{of } C_2(x)\right)\uparrow D_{2-} = A_1 \oplus B_1 \quad, \qquad\qquad\qquad 1_2\left(\text{of } C_2(x)\right)\uparrow D_{2-} = A_2 \oplus B_2 .$$

An even (odd) induced representation labels even- K_x (odd- K_x) clusters that lie below the separatrix in Fig. 25.4.2. Clusters above the separatrix have local symmetry $C_2(z)$, and clusters corresponding to this region are labeled according to the columns of the $D_2 \supset C_2(z)$ correlation table shown in the right-hand part of Fig. 25.4.3.
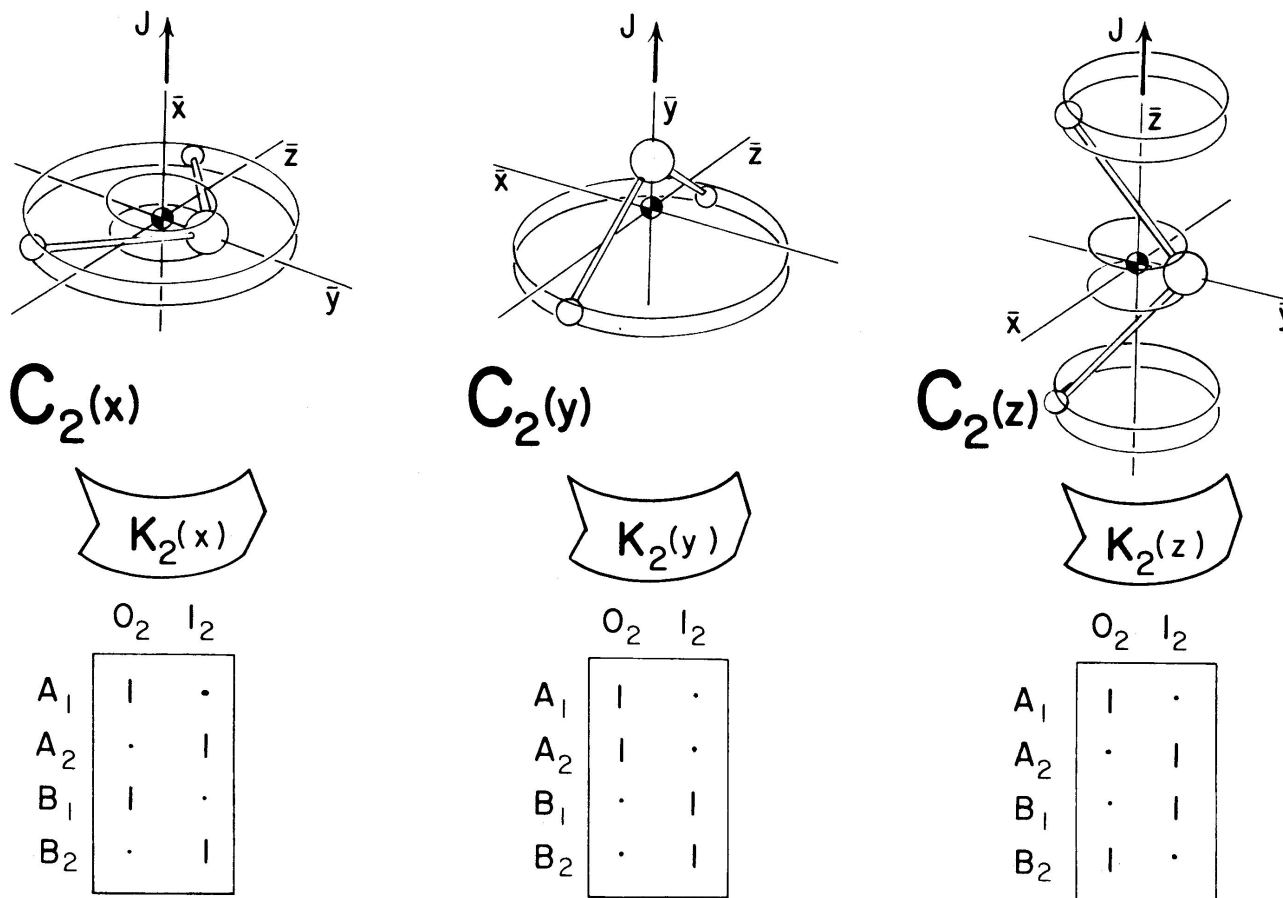
Fig. 25.4.3 *Correlations between the asymmetric top symmetry D₂ and subgroups C₂(x), C₂(y), and C₂(z).*

Sketches of the classical motion correspond to the locally C_2 symmetric trajectories. The $C_2(x)$ motion corresponds to an XY_2 rotating on its side like a boomerang, while $C_2(z)$ motion is like a spinning crankshaft. The $C_2(y)$ motion is around the classically unstable saddle point, and hence no $C_2(y)$ level clusters appear in the spectrum. One should note that the phase portraits describe the precession or "rotation of rotation" rather than rotation itself. Precession-free rotation of a rigid body would occur only if the *J* vector were precisely localized on one of the principal axes, not quite possible for a quantum rotor.

Quantum uncertainty prohibits pure rotation without precession because the transverse components cannot be exactly zero. The transverse components are minimum for the $K = J$ states which have the least cone angle-$\Theta_{J,J}$. This corresponds to minimum angular-momentum uncertainty or angular zero-point motion. States with lower z-component quanta $K=J–1, J–2, …$ have higher uncertainty angles $\Theta_{J,K}$ according to (25.4.2b). The states $|J,K\rangle$ are eigenstates of the symmetric top $(A=B)$-Hamiltonian, and each angular-momentum cone exactly intersects the corresponding semiclassical path on the symmetric top RE surface in Fig. 25.4.1(a).

For the asymmetric top in Fig. 25.4.1(b) the $\Theta_{j,j}$ cones only approximate their corresponding semiclassical trajectories. Asymmetric top trajectories are distorted or "squeezed" so that the projection of J on the local axis of quantization oscillates around the K value that labels each path. The classical precession becomes more and more nonuniform as K decreases and the separatrix is approached. This corresponds to the mixing of more of the states $|J,K\pm2\rangle, |J,K\pm4\rangle$, and so on into the dominant $|J,K\rangle$ component of the eigenstate. The global and local symmetries for the symmetric top are continuous groups O_2 or $D_{\infty h} \supset R_2$ while the asymmetric top has only a discrete set of symmetries $D_2 \supset C_2$. So the K value is not strictly conserved nor is the $\pm K$ degeneracy perfectly maintained in the latter.

However, the extent of breakdown of R_2 symmetry or K conservation is not necessarily related to the splitting of the cluster doublets. K conservation and cluster splitting are separate phenomena associated with different regions of the RE phase space; the former depends upon the shape of the phase paths, and the latter depends upon the height of the pass or saddle region between the equivalent paths. Furthermore, the symmetry properties of the clusters should be associated with a C_2 induced representation and not an R_2 irreducible representation. This point will be amplified by examples involving the higher octahedral symmetry in the following section.

Another point which arises in the study of higher symmetries concerns the ordering of clusters and the symmetry species inside them. The species ordering in Fig. 25.4.2 consists of a repetition of the sequence $A_1B_1A_2B_2$ through the entire spectrum. This remarkably uniform ordering can be related to the number of wave function nodes occurring along and between the semiclassical paths. This sort of ordering was observed in the C_n energy band level structure $A_1E_1 \cdots B_1B_2 \cdots E_1A_2$ in Chapter 9.
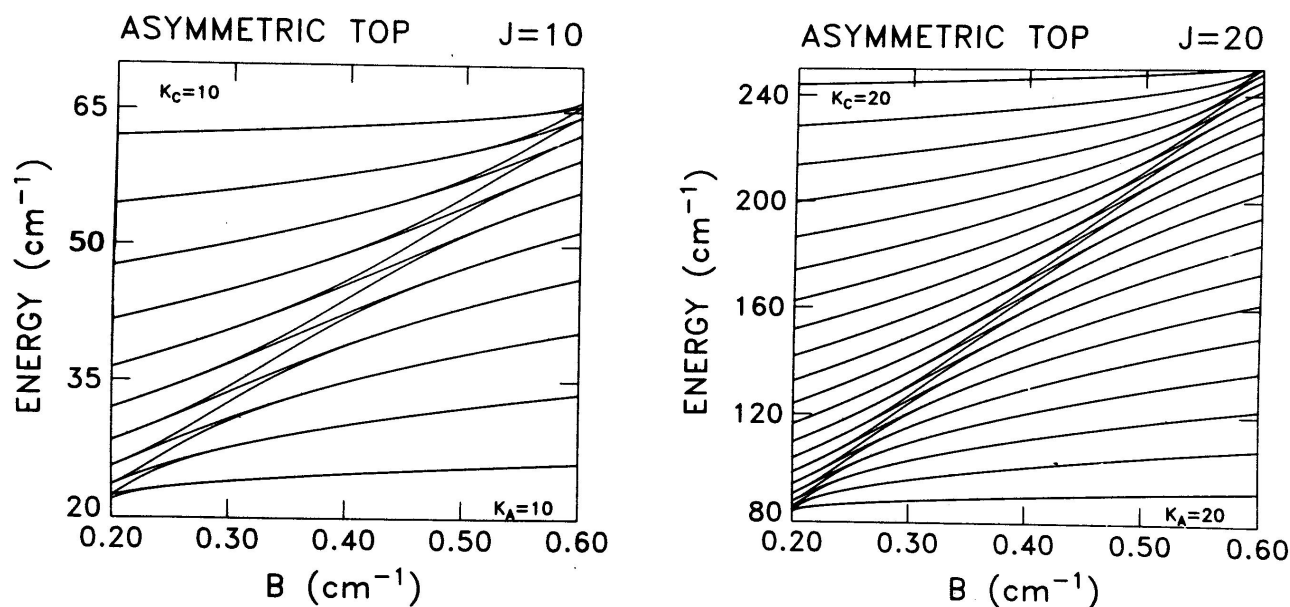
Fig. 25.4.4 *Rigid rotor energy levels correlations for angular momentum J = 10 and J = 20.*

Level correlation between C₂(x) and C₂(z) symmetry

The coefficients A, B, and C determine the symmetry of the rotor Hamiltonian (25.4.3) and its RE surface. The surface represents a rotor that is prolate-symmetric ($A = B < C$) in (a) of Fig. 25.4.1, asymmetric ($A < B < C$) in (b), and oblate-symmetric ($A < B = C$) in (c). The two extreme symmetric rotor cases have levels labeled by different $R_3 \supset R_2$ subgroup chains. The prolate case is labeled by $R_2(z)$ and the oblate case by $R_2(x)$. The intermediate asymmetric case is labeled using finite subgroup chains $R_3 \supset D_2 \supset C_2$. Furthermore, different subgroups are appropriate for different levels; the levels below the separatrix belong to $C_2(x)$ and those above belong to $C_2(z)$.

      In Fig. 25.4.4 the *J=10* and *J=20* levels are plotted as a function of parameter B which ranges between the prolate ($B = 0.2$ cm⁻¹) and oblate ($B = 0.6$ cm⁻¹) cases. Coefficients $A = 0.2$ cm⁻¹ and $C = 0.6$ cm⁻¹ are fixed. One can see that most *J=10* symmetric top doublets tend to stick together for most values of B and even more so for *J=20*. The *J=10* levels in Fig. 25.4.2 lie above the point $B = 0.4$ in the *J=10* plot of Fig. 25.4.4. The separatrix region of the levels in the center of Fig. 25.4.2 is the transition region where doublets split and trade levels in Fig. 25.4.4. The separatrix or transition region appears to be a small fraction of the *J=10* spectrum and even smaller part for *J=20*.

      The doublets in the upper left-hand part of Fig. 25.4.4 above the transition region belong to $C_2(z) \uparrow D_2$ induced representations. Those in the lower right-hand part belong to $C_2(x) \uparrow D_2$ doublets. This correlation plot

should be compared to the lattice level correlation diagrams in Fig. 14.2.11. The latter involves a correlation between bands of doublets of levels belonging to $C_n(z) \uparrow D_n$ induced representations and n-fold degenerate clusters or bands of levels belonging to $C_2(x) \uparrow D_n$ representations. For $n = 2$ the plot in Fig. 16.1.2 is more closely analogous to the one in Fig. 25.4.4. Then the A_1, A_2, B_1 and B_2 levels (which are the band boundaries plotted in Fig. 14.2.11) are the only levels allowed; the E-type levels do not exist for $n = 2$. The transition region occurs at the tops of the potential barriers.

By analogy the asymmetric top spectral transition region occurs at the top (or bottom) of the saddles on the RE surface. The saddle points are on the $\pm$ axes and rise linearly with the coefficient B of J_y^2. Certain of the transition levels are seen to rise rapidly and quasi-linearly in Fig. 25.4.4, while their doublet partners are seen to sail right through the transition region. Wave symmetry determines which of the D_2 species are most sensitive to the y-axis saddle. The correlation table in Fig. 25.4.3 for the $C_2(y)$ symmetry shows that only A_1 and A_2 are symmetric (0_2). Therefore only they have wave antinodes and substantial amplitudes on the saddles, and it is therefore A_1 and A_2 levels that "divorce" their partners in the transition region.

Outside the transition region the pairs of levels mostly stick together to form quasi-degenerate tunneling doublets. One exception is the $K = \pm 1$ double near the lower left-hand side of Fig. 25.4.4. It splits immediately, that is to first order. This is analogous to the first order splitting observed in Fig. 16.1.2. Symmetry allows nonzero matrix elements between this pair of states. In this case it is matrix element $\langle K = 1 | T_2^2 | K = -1 \rangle$ and its conjugate that cause the $K = \pm 1$ doublet to split.

b. Semirigid spherical tops *[Octahedral (O) Symmetry]*

We now consider the high-J eigenvalues of octahedrally symmetric tensor Hamiltonians. The fourth-rank tensor term in the Hamiltonian,

$$H = BT_0^0 + 4t_{044}\left[T_0^4 + \sqrt{\frac{5}{14}}\left(T_4^4 + T_{-4}^4 \right) \right] \tag{25.4.17}$$

is the same, apart from its overall scale factor, as the one introduced in (25.1.25). Its polynomial form

$$H = BJ^2 + 10t_{044}\left(J_x^4 + J_y^4 + J_z^4 - \tfrac{3}{5}J^4 \right) \tag{25.4.18}$$

was also introduced in (25.1.25). It is known as the *Hecht Hamiltonian* after K. T. Hecht who first applied it to the analysis of methane (CH_4) spectra taken by E. Plyler in 1960. The Hamiltonian describes rotation-vibrational distortion of molecules having tetrahedral (T_d) as well as octahedral (O_h) symmetry. Changing the sense of rotation $(J \rightarrow -J)$ should give a rotor state with the same energy so all rotors must have only pure rotational energy operators of even rank. The third-rank tetrahedral invariant $J_x J_y J_z$ is forbidden by time-reversal symmetry to appear alone.

(a)   (b)
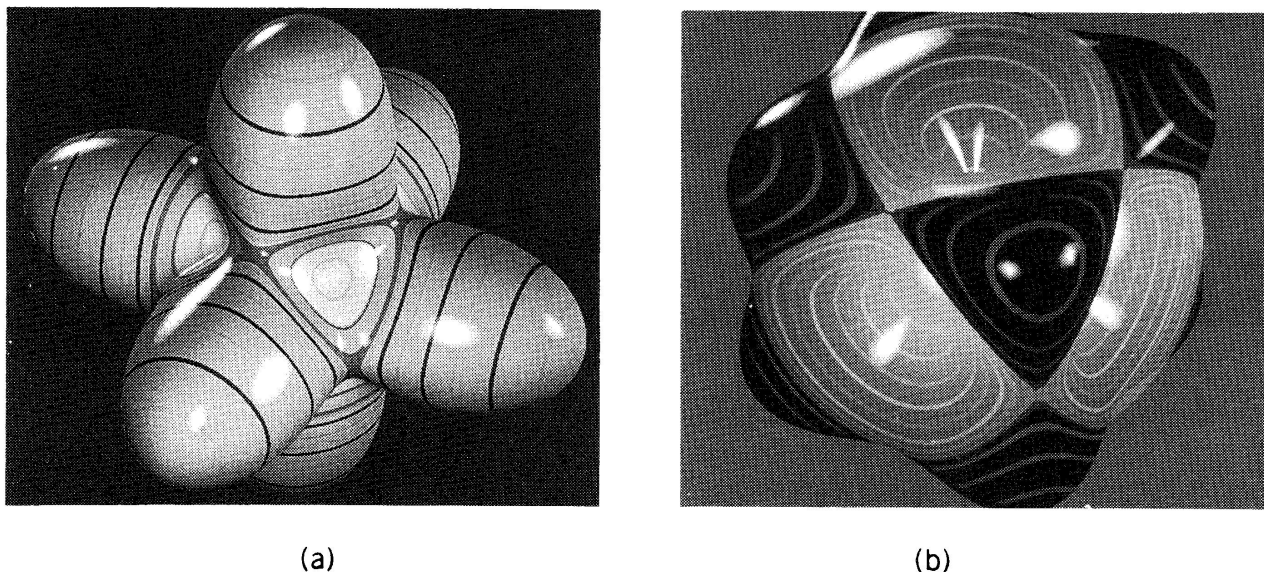
Fig. 25.4.5 *Semirigid rotor RE surfaces with O_h symmetry.* (a) $t_{044} > 0$. (b) $t_{044} < 0$.

O_h Rotational energy surfaces

We now express the Hecht Hamiltonian (25.4.17) in terms of body polar angles as was done in the preceding section for the asymmetric rotor. The polynomial

$$E = B\langle J^2 \rangle + t_{044} \langle J^4 \rangle \left(35 \cos^4 \beta - 30 \cos^2 \beta + 3 + 5 \sin^4 \beta \cos 4\gamma \right) / 2 \qquad (25.4.19)$$

has the form of the harmonic polynomial functions in Eq. (5.6.29). The resulting RE surface is shown in Fig. 25.4.5a for positive centrifugal distortion constant t_{044}. This constant is around 5 Hz for SF_6 and is positive for most octahedral XY_6 molecules. It is greatly exaggerated for the figure so that the hill and valleys are clearly visible.

   In an octahedral XY_6 molecule rotation about the four-fold XY radial bond axes generally has the highest energy for a given J value since these bonds are stretched relatively little by a longitudinal centrifugal force. However, transverse forces which arise during rotation about the three-fold symmetric axes in between the bonds

can bend the molecule relatively easily. Hence, the three-fold symmetry axes lie in RE surface valleys in Fig. 25.4.5a while the four-fold (x, y, z) axes are on peaks. For tetrahedral XY_4 or cubic molecules the sign of t_{044} is negative as it is for the surface in Fig. 25.4.5(b).

Spherical top energy levels (J = 30 Example)

The RE topography lines correspond to quantizing J trajectories and to level clusters in the energy spectrum as shown by the diagram of the $J = 30$ levels of SF_6 in Fig. 25.4.6. The levels consist mainly of clusters of levels belonging to the octahedral symmetry species A_1, A_2, E, T_1, or T_2. The characters of these species are the following Table 25.4.3. (The tetrahedral T_d group has a similar table where T_1 and T_2 are often labeled F_1 and F_2). Local subgroups C_4 and C_3 have characters (from Fig. 7.3.3) listed, too.

O	0°	120°	180°	90°	180°
A_1	1	1	1	1	1
A_2	1	1	1	-1	-1
E	2	-1	2	0	0
T_1	3	0	-1	1	-1
T_2	3	0	-1	-1	1

C_4	0°	90°	180°	270°
0_4	1	1	1	1
1_4	1	i	-1	$-i$
2_4	1	-1	1	-1
3_4	1	$-i$	-1	i

C_3	0°	120°	240°
0_3	1	1	1
1_3	1	$e^{2\pi i/3}$	$e^{-2\pi i/3}$
2_3	1	$e^{-2\pi i/3}$	$e^{2\pi i/3}$

         Table 25.4.3   Table 25.4.4   Table 25.4.5

This spectrum contains clusters of six and eight rotational levels that are analogous to the rigid rotor doublet clusters in Fig. 25.4.2. Above the separatrix region there are repeating sextets (T_1, T_2), (A_2T_2E), (T_1, T_2), or (A_1T_1E) composed of clustered singlet (A_1 or A_2), double (E), or triplet (T_1 or T_2) octahedral symmetry species. Below the separatrix there are two octets $(A_1T_1T_2A_2)$ and (T_2ET_1). Each set of six or eight clustered levels can be related to the same number of semiclassical J trajectories on the RE surface in Fig. 25.4.5 or 25.4.6.

Each set of six rotational levels belongs to one of the C_4 induced representations $0_4 \uparrow O, 1_4 \uparrow O, 2_4 \uparrow O$, or $3_4 \uparrow O$ depending upon whether the effective K value is 0, 1, 2, or 3 modulo 4 for the corresponding set of fourfold symmetric semiclassical trajectories. The correlation tables in the lower right-hand part of Fig. 25.4.7 tell which O species belong to each K_4 cluster and to each set of trajectories. For example, the minimum uncertainty trajectory has $J = K = 30$ and corresponds to the highest energy $2_4 \uparrow O$ or (A_2T_2E) cluster in Fig. 25.4.6.
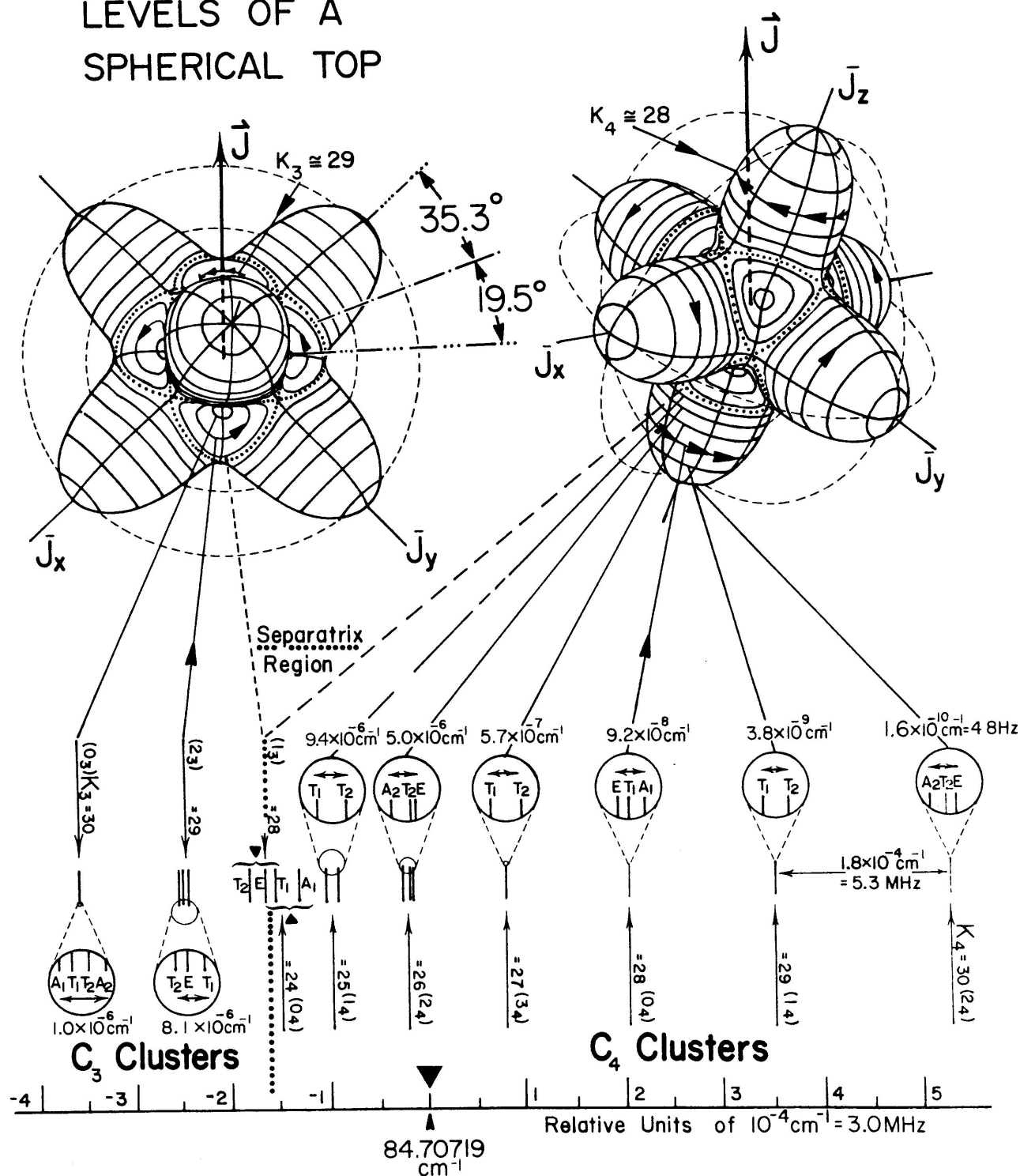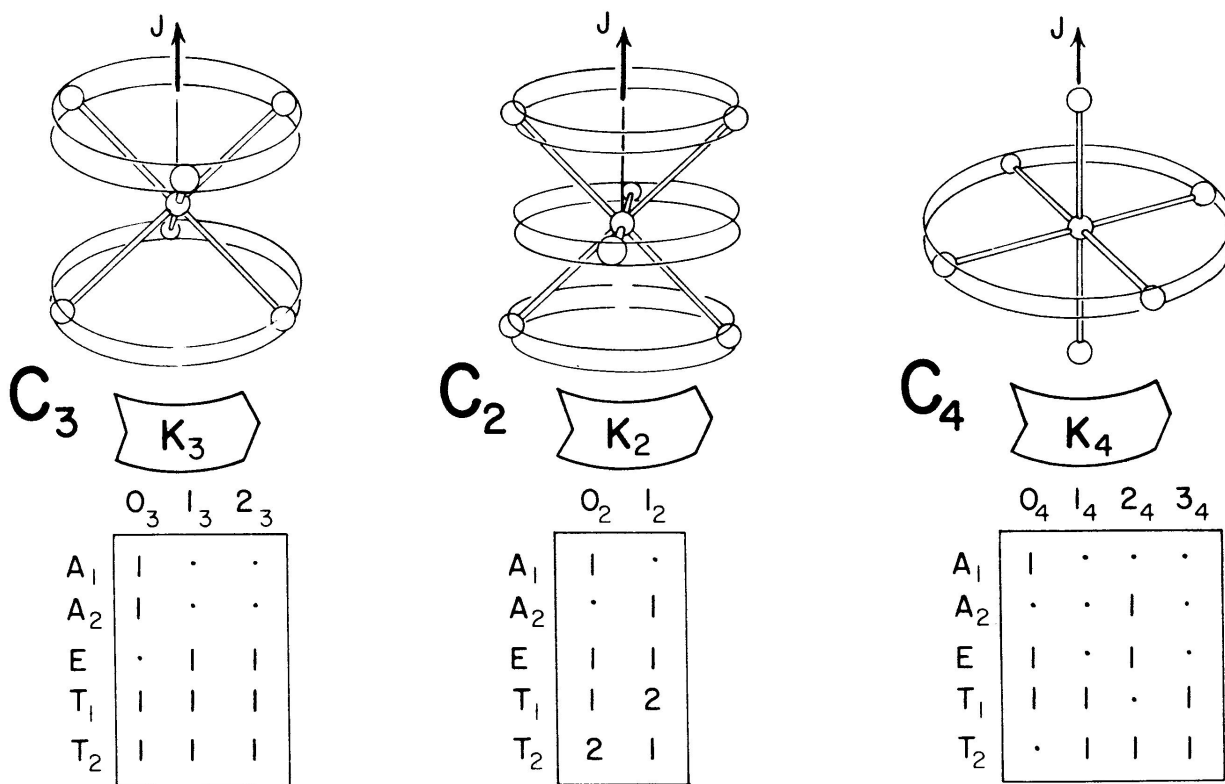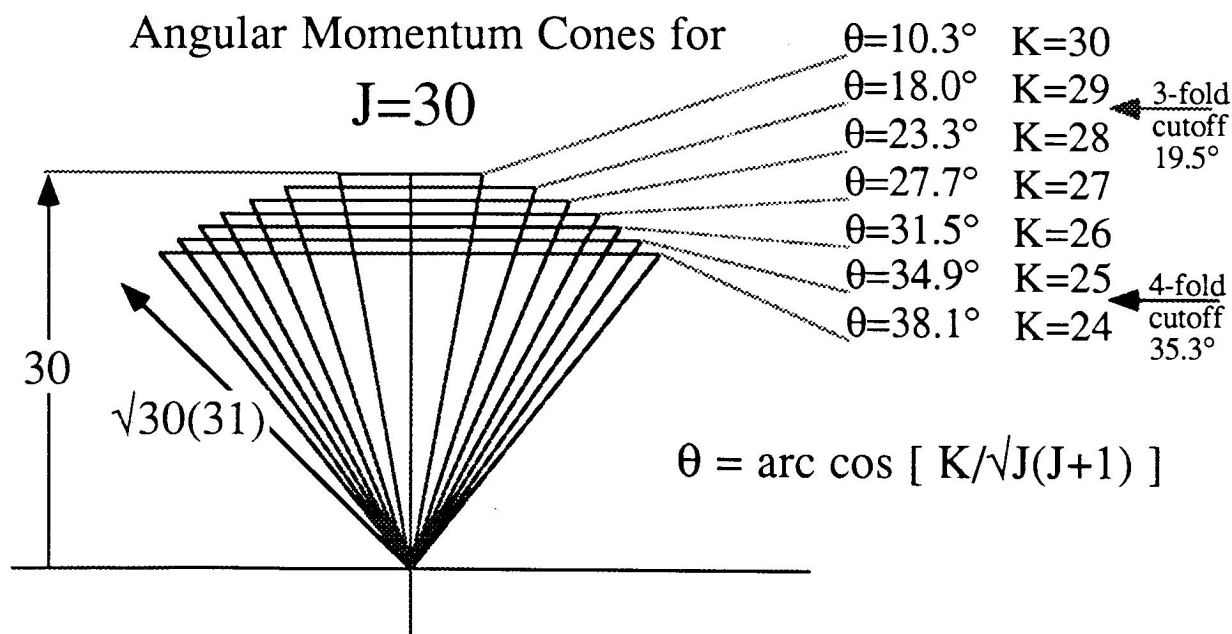
VISUALIZING THE J = 30
LEVELS OF A
SPHERICAL TOP

Fig. 25.4.6 *J = 30 octahedral rotor levels and related RE surface paths.*

C_3, K_3	0_3	1_3	2_3
A_1	I	·	·
A_2	I	·	·
E	·	I	I
T_1	I	I	I
T_2	I	I	I

C_2, K_2	0_2	1_2
A_1	I	·
A_2	·	I
E	I	I
T_1	I	2
T_2	2	I

C_4, K_4	0_4	1_4	2_4	3_4
A_1	I	·	·	·
A_2	·	·	I	·
E	I	·	I	·
T_1	I	I	·	I
T_2	·	I	I	I

Fig. 25.4.7 *Different choices of rotation axes for octahedral rotor corresponding to local symmetry C_3, C_2, and C_4. Tables correlate global octahedral symmetry species with the local ones.*

The highest energy semiclassical trajectories are very close to the intersection of the RE surface with the $K = 30$ angular momentum cone which has half-angle $\Theta_{30\,30} = \cos^{-1}\left(30/\sqrt{(30)(31)}\right) = 10.3°$. A series of $J = 30$ angular momentum cones are drawn for $K = 30$ down to $K = 24$ in Fig. 25.4.8. The next highest $1_4 \uparrow O$ or $(T_1 T_2)$ cluster corresponds to six trajectories which are localized to within about $\Theta_{30\,29} = 18°$ of their respective four-fold symmetry axes. This sequence of clusters ends when $\Theta_{30\,K}$ approaches the angle $35.3°$ between the separatrix and the four-fold axes. The $J = 30$ cutoff value is $K_4 = \sqrt{(30)(31)}\cos 35.3° = 24.9$ or about 25 as shown in Fig. 25.4.8. This corresponds to a weak (T_1, T_2) cluster just above the separatrix in Fig. 25.4.6.

Since the eight three-fold symmetric valley regions of the RE surface are smaller, there are fewer clusters associated with the C_3 induced representations. There is only a $19.5°$ angle between the separatrix and the three-fold axes. Hence, the $J = 30$ cut-off value is $K_3 = \sqrt{(30)(31)}\cos 19.5° = 28.7$ or about 29 as indicated in Fig. 25.4.8. So two $J = 30$ clusters on the three-fold symmetry side of Fig. 25.4.6 belonging to the induced representations $0_3 \uparrow O = (A_1 T_1 T_2 A_2)$ for $K = 30$ and $2_3 \uparrow O = (T_2 E T_1)$ for $K = 29$.

Angular Momentum Cones for

$J=30$

$\theta=10.3°$	$K=30$
$\theta=18.0°$	$K=29$ 3-fold
$\theta=23.3°$	$K=28$ cutoff 19.5°
$\theta=27.7°$	$K=27$
$\theta=31.5°$	$K=26$
$\theta=34.9°$	$K=25$ 4-fold
$\theta=38.1°$	$K=24$ cutoff 35.3°

30

$\sqrt{30(31)}$

$$\theta = \arccos [\ K/\sqrt{J(J+1)}\ ]$$

Fig. 25.4.8 *Quantum (J,K)-cone angles for angular momentum states of total J=30.*

Two C_3 clusters and five or six C_4 clusters are visible in the infrared spectra of tetrafluorosilane (SiF_4) and cubane (C_8H_8) which is shown in Fig. 25.4.9. The spectra are actually due to transitions between level clusters on lower and upper RE surfaces corresponding to ground and vibrationally excited states, respectively. However, the spectra are simply scaled copies of the pure rotational level patterns since the upper and lower RE surfaces have almost the same shape apart from a scale factor. Note that fine structure spectra outside of the separatrix region is relatively insensitve to the J value in that $P(30)$, and $P(31)$, and $P(32)$ are quite similar. Note the similarity of $J = 30$ fine structure patterns for quite different molecules having tetrahedral, cubic, and octahedral shapes.

However, the superfine structure of intracluster splitting depends only on the shape of the RE surface in the neighborhood of the saddle points through a tunneling factor S that can be approximated by an exponential of a phase integral across the saddle region. (Note the rapid decrease of the superfine splitting from about one Megahertz down to just 4.8 Hz as K_4 goes from 25 up to 30 in Fig. 25.4.6.)
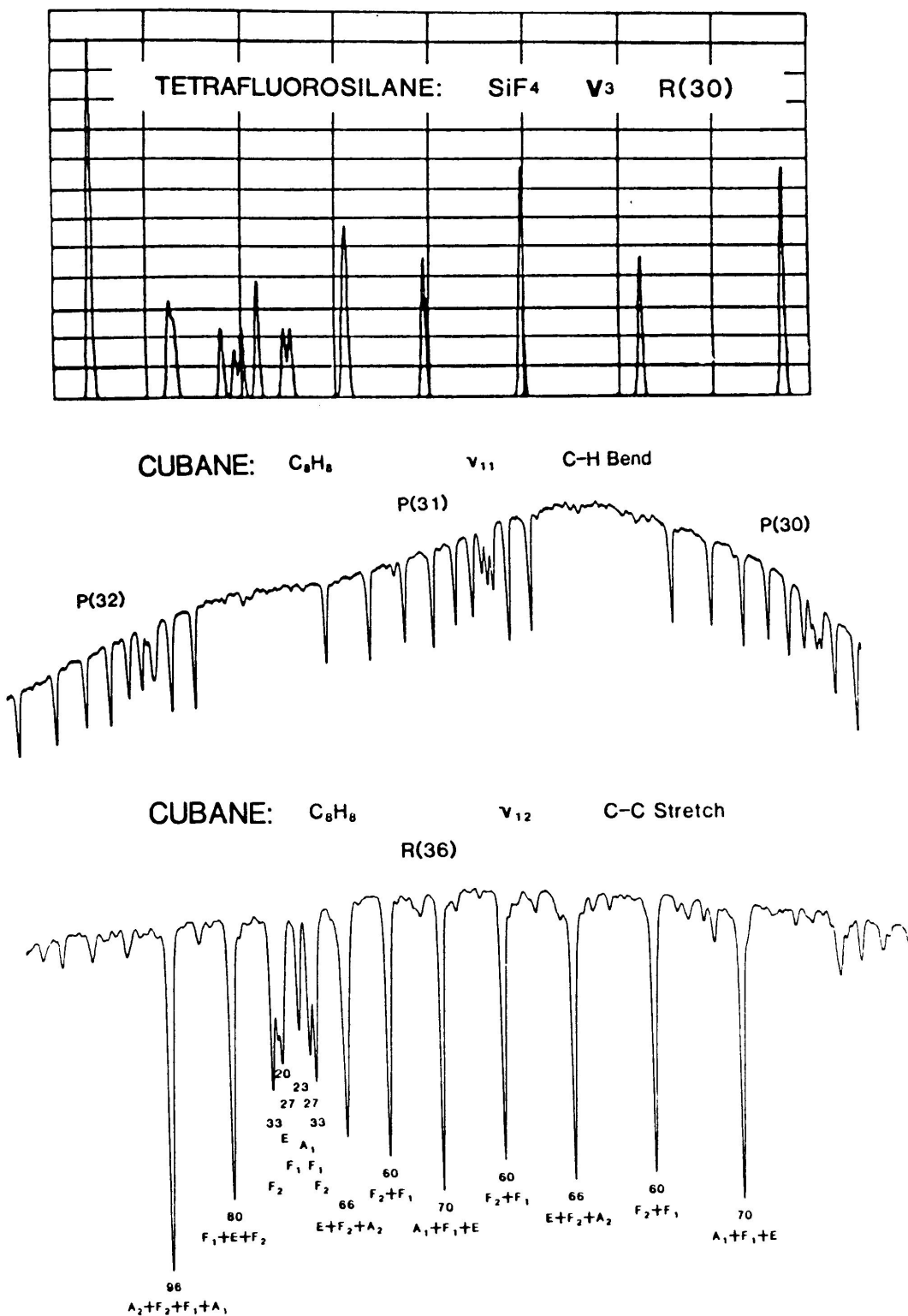
Fig. 25.4.9 *Infrared spectra showing fine structure clusters. Tetrafluorosilane (SiF₄) spectrum from a v₃ R(30)* *transition ____. [After C. W. Patterson, R. S. McDowell, N. G. Nereson, B. J. Krohn, J. S. Wells, and F. R.* *Peterson, J. Mol. Spectrosc. **91**, 416 (1982).[Cubane (C₈H₈) spectrum from v₁₁ P(30), P(31), and P(32),* *transitions; cubane (C₈H₈) spectrum from v₁₂ R(36), transition. [After A. S. Pine, A. G. Maki, A. G. Robiette, B. J.* *Krohn, J. K. G. Watson, and Th Urbanek, J. Am. Chem. Soc., **106**, 891 (1984).]*

Superfine tunneling analysis

The magnitude of superfine splitting may vary by many orders, the splitting patterns have the following invariant form. The first of these is derived from a tunneling matrix between (25.4.20) involving the six *(K₄=28)*-path bases $\{|x\rangle, |\bar{x}\rangle, |y\rangle, |\bar{y}\rangle, |z\rangle, |\bar{z}\rangle,\}$ paths around six octahedral ±x, ±y, and ±z-axes.

$$
\langle H \rangle_{K_4=28} =
\begin{array}{c}
|x\rangle \; |\bar{x}\rangle \; |y\rangle \; |\bar{y}\rangle \; |z\rangle \; |\bar{z}\rangle \\
\begin{pmatrix}
H & 0 & S & S & S & S \\
0 & H & S & S & S & S \\
S & S & H & 0 & S & S \\
S & S & 0 & H & S & S \\
S & S & S & S & H & 0 \\
S & S & S & S & 0 & H
\end{pmatrix}
\end{array}
$$

Eigenvector	$|x\rangle$	$|\bar{x}\rangle$	$|y\rangle$	$|\bar{y}\rangle$	$|z\rangle$	$|\bar{z}\rangle$	Eigenvalue
$\sqrt{6}\,|A_1\rangle =$	1	1	1	1	1	1	$E^{A_1} = H + 4S$
$\sqrt{12}\,|E,1\rangle =$	2	2	−1	−1	−1	−1	$E^E = H - 2S$
$2\,|E,2\rangle =$	0	0	1	1	−1	−1	
$\sqrt{2}\,|T_1,1\rangle =$	1	−1	0	0	0	0	$E^{T_1} = H$
$\sqrt{2}\,|T_1,2\rangle =$	0	0	1	−1	0	0	
$\sqrt{2}\,|T_1,3\rangle =$	0	0	0	0	1	−1	

(25.4.20)   Table 25.4.6

The eigenvectors and eigenvalues for this matrix are given in the Table 25.4.6. The resulting superfine splitting predictions are listed (25.4.21a) along with other similarly derived values for other cluster types.

$$0_4 \uparrow O: \quad 1_4 \text{ or } 3_4 \uparrow O \quad\quad 2_4 \uparrow O$$
$$\Delta E(A_1) = 4S, \quad \Delta E(T_2) = 2S, \quad \Delta E(E) = 2S,$$
$$\Delta E(T_1) = 0, \quad \Delta E(T_2) = 2S, \quad \Delta E(T_2) = 0,$$
$$\Delta E(E) = -2S \quad\quad\quad\quad\quad\quad \Delta E(A_2) = -4S.$$

(25.4.21a)

$$0_3 \uparrow O: \quad 1_3 \text{ or } 2_3 \uparrow O$$
$$\Delta E(A_2) = 3S, \quad \Delta E(T_1) = 2S,$$
$$\Delta E(T_2) = S, \quad \Delta E(E) = 0,$$
$$\Delta E(T_1) = -S \quad \Delta E(T_2) = -2S.$$
$$\Delta E(A_1) = -3S$$

(25.4.21b)

Splitting ratios and ordering of levels hold if tunneling occurs only between nearest neighboring trajectories. The patterns (25.4.20) and (25.4.21) are seen magnified in Fig. 25.4.6.

Just as the asymmetric top maintains $(A_1 A_2 B_1 B_2)$ ordering throughout Fig. 25.4.2 we also note the following overall ordering is maintained throughout the fine structure spectrum of Fig. 25.4.6.

$$0_1 \uparrow O = (A_1 T_1 T_2 A_2 T_2 E T_1 T_2 E T_1)$$

(25.4.22)

Taken together, this would be the largest possible cubic cluster. It contains just the *O* regular representation. Giant clusters like (25.4.22) or the C_2 clusters half this size are possible, too, if stable semi-classical orbits are localized

around low symmetry points. This occurs for octahedral tensor combination of sixth, eighth, and higher ranks. Some examples are described in the next section.

(c) Level Correlation between C_3 and C_4 Symmetry   So far we have considered only the lowest order rotational tensors which exhibit the symmetries D_2 of the rigid rotor and O_h of the semirigid cubic or octahedral rotor. We consider now the effect of the sixth-rank normalized octahedral tensor operator introduced in Eq. (7.3.35),

$$T^{[6]} = \left(1/\sqrt{8}\right)\left[T_0^6 - \left(\sqrt{7}/\sqrt{2}\right)\left(T_4^6 + T_{-4}^6\right)\right], \tag{25.4.23}$$

This will be added in varying amounts to the normalized fourth-rank tensor,

$$T^{[4]} = \left(\sqrt{7}/\sqrt{12}\right)\left[T_0^4 - \left(\sqrt{5}/\sqrt{14}\right)\left(T_4^4 + T_{-4}^4\right)\right], \tag{25.4.24}$$

Introduced in Eqs. (7.3.25) and (25.4.17). A sixth-rank centrifugal distortion may be necessary in the presence of anharmonic and other higher order effects. The magnitude of the $T^{[6]}$ contribution would vary according to a higher power of J than that of $T^{[4]}$ and might be significant at higher J values. Here the magnitudes of their respective contributions are varied artificially through an angle parameter v in a combination which maintains the overall normalization.

$$T^{4,6}(v) = T^{[4]}\cos v + T^{[6]}\sin v. \tag{25.4.25}$$

The exact quantum ($J = 30$)-eigenvalues for this mixed [4,6]-rank tensor operator are plotted as a function of the mixing angle v in Fig. 25.4.10. The plot begins on the left-hand side ($v = 0$) with a scaled copy of the $T^{[4]}$ level spectrum in Fig. 25.4.6 and ends on the right-hand side ($v = \pi$) with the same spectrum inverted. Between these limits the level clusters become completely reorganized.

Certain values of the v parameter in Fig. 25.4.10 are marked (b), (c), (d), and (e). At these values the RE surface of the combination tensor (25.4.25) is drawn in Fig. 25.4.11. The RE surface function used for $T^{[4]}$ is as follows. [Recall (25.4.19)]

$$E^{[4]}(\beta,\gamma) = \left(7/12\right)^{1/2}\left(9/4\pi\right)^{1/2}\left(35\cos^4\beta - 30\cos^2\beta + 3 + 5\sin^4\beta\cos 4\gamma\right)\big/8 \tag{25.4.26}$$

For $T^{[6]}$ the RE function is as follows,

$$E^{[6]}(\beta,\gamma) = (1/8)^{1/2} (13/4\pi)^{1/2} \left(231 \cos^6 \beta - 315 \cos^4 \beta + 105 \cos^2 \beta - 5 \right.$$

$$\left. - 21 \sin^4 \beta \left(11 \cos^2 \beta - 1\right) \cos 4\gamma\right)/16.$$

(25.4.27)
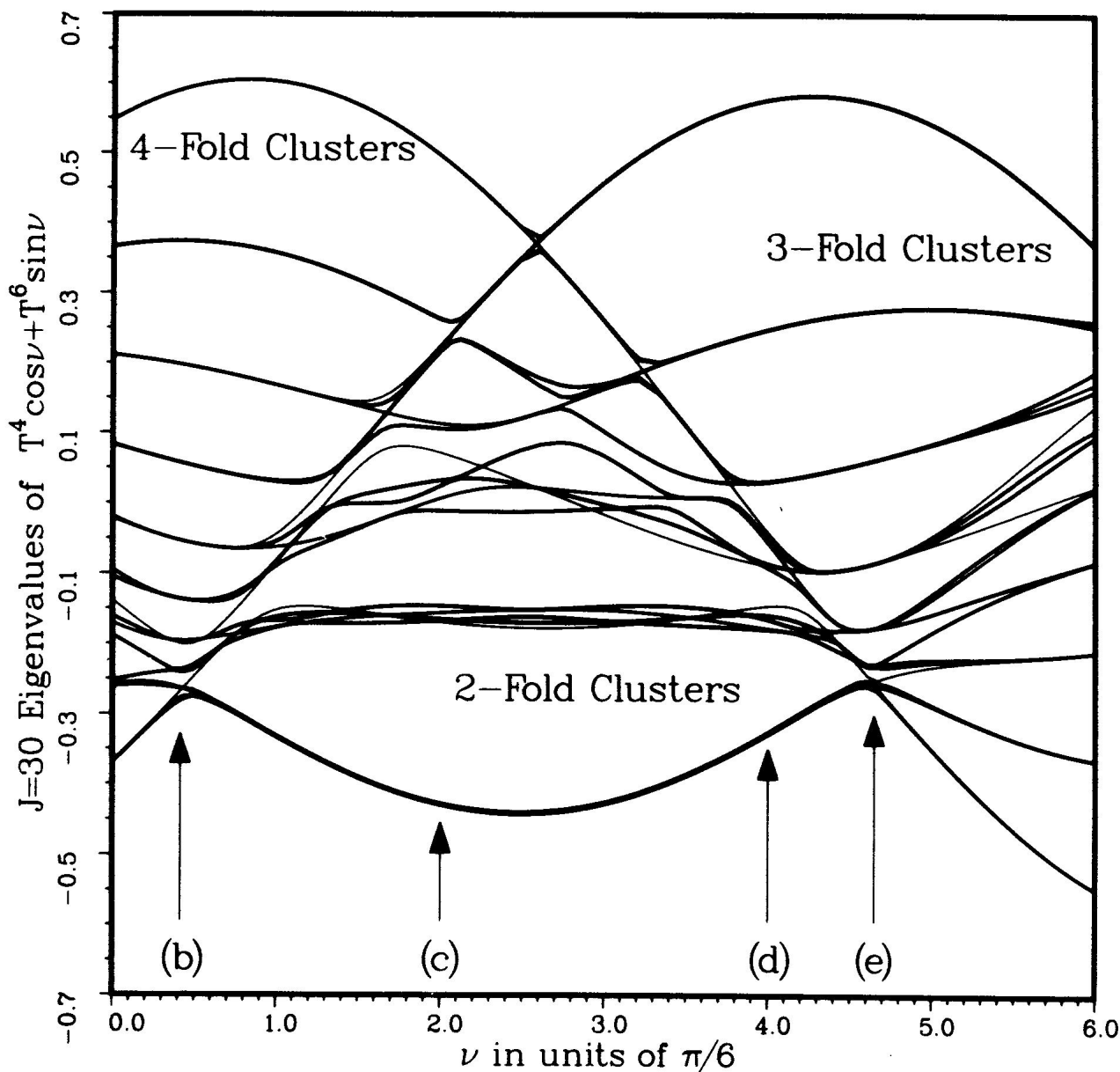
Fig. 25.4.10 *Eigenvalues of $T^{[4,6]}(v)$ tensor in (25.4.25) versus v values (See RES in Fig. 25.4.11.)*

(a) v = 0.0, (b) v = 0.4π/6, (c) v = 2π/6, (d) v = 4π/6 (e) v = 4.6 π/6, (f) v = 5 π/6..

The tensors $T^{[r]}$ and RE functions $E^{[r]}$ have a spherical harmonic normalization factor $\left([2r+1]/4\pi\right)^{1/2}$ that was not

included in the previous definition (25.4.19). This factor is used here to slightly enhance the effect of the sixth-

rank tensor for this particular example. Also, the $|J|^r$ factors are depleted in (25.4.26) and (25.4.27) so that the higher rank tensor effects are not J dependent.

The eigenlevels marked by (b) in Fig. 25.4.10 correspond to the RE surface drawn in Fig. 25.4.11(b). The latter shows that the separatrix has taken over the regions that formerly held C_3 symmetric trajectories, and only C_4 trajectories remain. (Note that these are equally spaced contours and are not quantized paths.) The result is the destruction of C_3 clusters in the spectrum which is composed almost entirely of C_4 clusters above the (b) point in Fig. 25.4.10.

Beyond this point a remarkable new type of cluster is formed. Just above the points marked (c) and (d) in Fig. 25.4.10 lie two clusters that contain twelve levels each. These correspond to trajectories which encircle 12 equivalent valleys which lie on the C_2 symmetry axes in Figures 25.4.11(c) and 25.4.11(d). The symmetry species within each of these clusters are exactly the ones contained in the C_2 correlation table in the center of Fig. 25.4.7. The lowest cluster in Fig. 25.4.10 would correspond to $K = 30$ and hence to the even local symmetry or 0_2 column of the $C2$ table which contains species A_1E, T_1, and $2T_2$. The next cluster has $K = 29$ and contains the five species A_2, E, $2T_1$, and T_2 listed in the odd column 1_2. The superfine splittings between these five levels are actually visible in the scale of Figures 25.4.10. As v changes the levels as seem to change order within this cluster. This is the result of competition between tunneling mechanisms.

Between the (b) and (d) points in Fig. 25.4.10 there is another phenomenon which occurs in the upper energy levels. There are a number of crossings or Fermi-like resonances between accidentally coinciding C_3 and C_4 clusters. This is because there are two kinds of mountains on the RE surfaces in Figures 25.4.11(c) and 25.4.11 (d): the C_4 mountains which are shrinking and C_3 mountains which are growing with v. For certain values of v, quantizing paths on one type of mountain are bound to be in resonance with different kinds of paths on the other. The result is an extraordinary kind of tunneling in which eigenfunctions are delocalized over both kinds of paths at once and a peculiar hybrid superfine eigenlevel structure occurs.

The spectral region containing the unusual fine structure is bounded on the right-hand side by the (e) point in Fig. 25.4.10 which corresponds to the RE surface in Fig. 25.4.11(e). At this point the eight C_3 mountains dominate the surface geometry entirely and the eigenlevels are composed entirely of very strong C_3 clusters of eight levels each. The final 25.4.11(f) shows the situation at $v = 5.0(\pi/6)$ where the C_4 trajectories begin to return. Now they are occupying the valleys.
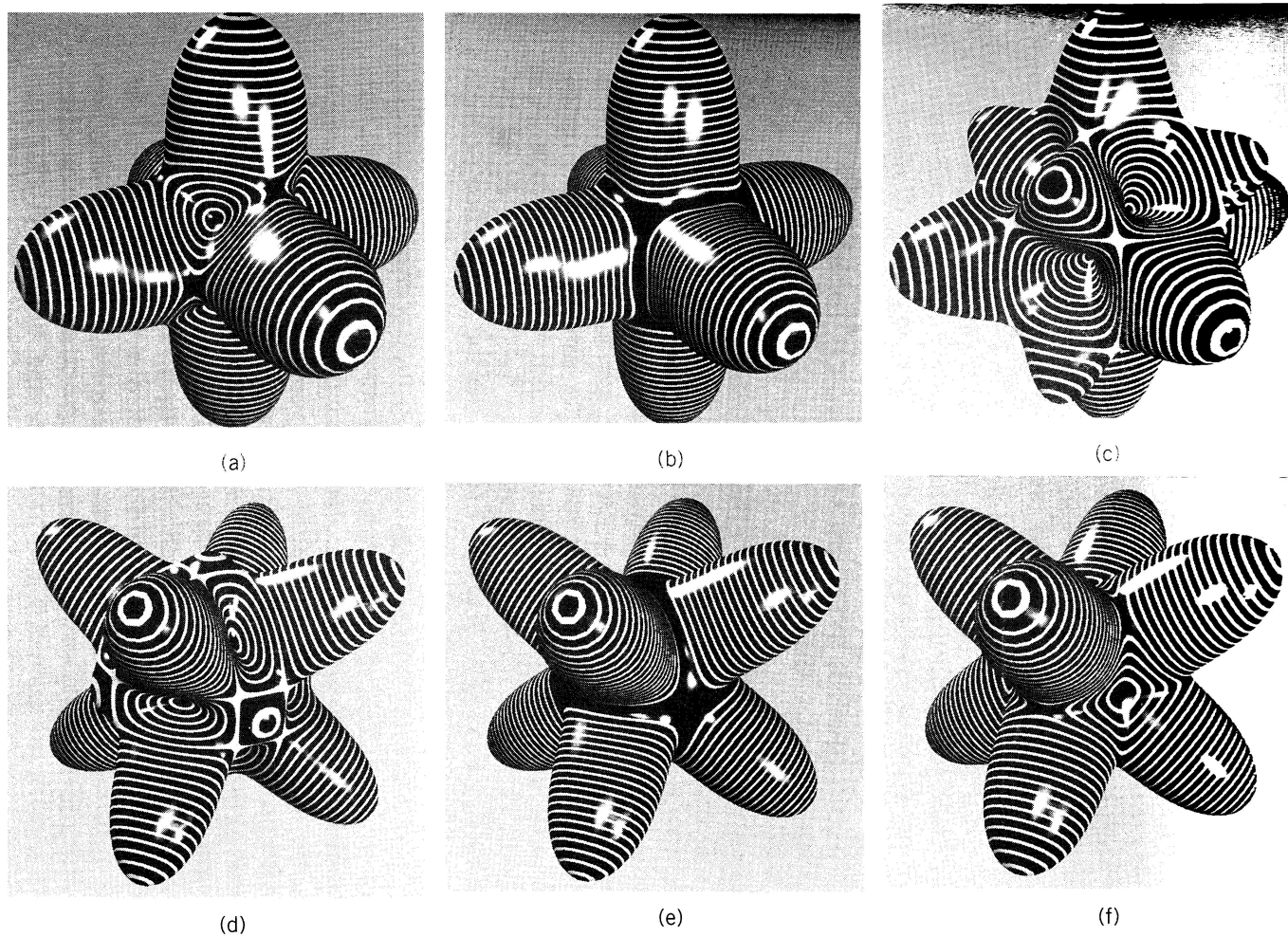
Fig. 25.4.11 *RE surfaces corresponding to selected v values in Fig. 25.4.10.*

(a) v = 0.0, (b) v = 0.4π/6, (c) v = 2π/6, (d) v = 4π/6 (e) v = 4.6 π/6, (f) v = 5 π/6.

25.5 Composite rotors and multiple rotational energy surfaces MRES

Sec. 25.4 introduces Hamiltonians and RE surfaces involving functions of even mulipolarity, that is, constant *(k=0)*, quadratic or quadrupole *(k=2)*, quartic or hexadecapole *(k=4)*, leaving out functions that are linear-dipole *(k=1)*, or octupole *(k=3)* for reasons of time-reversal symmetry. In composite "rotor-rotors" any mulitpolarity is possible and the dipole is of primary utility.

a. Gyro-Rotors

A composite rotor is one composed of two or more objects with more or less independent angular momenta. This could be a molecule with attached methyl (CH_3) "gyro" or "pinwheel" sub-rotors, a system of considerable biological interest. It could be a molecule with a vibration or "phonon" excitation that couples strongly to rotation. Also, any nuclear or electronic spin with significant coupling may be regarded as an elementary sub-rotor. The classical analogy is a spacecraft with gyro(s) on board.

A rotor-rotor Hamiltonian has the following general interaction form.

$$H_{rotor\ R+S} = H_{rotor_R} + H_{rotor_S} + V_{RS} \qquad\qquad (25.5.1)$$

A useful approximation assumes the $rotor_S$ "gyro" is fastened to the frame of $rotor_R$ so the interaction V_{RS} becomes a constraint, does no work, and is thus assumed zero. An asymmetric top with body-fixed spin is the following modified version of (31.1).

$$H_{R+S(Body-fixed)} = AR_x^2 + BR_y^2 + CR_z^2 + H_{rotor_S} + (\sim 0) \qquad\qquad (31.\ 19a)$$

The system total angular momentum is a conserved vector **J=R+S** in the lab-frame and a conserved magnitude |**J**| in the rotor-R body frame. So we use **R=J-S** in place of **R**.

$$\begin{aligned}H_{R,S(fixed)} &= A\left(J_x - S_x\right)^2 + B\left(J_y - S_y\right)^2 + C\left(J_z - S_z\right)^2 + H_{rotor_S}\\ &= AJ_x^2 + BJ_y^2 + CJ_z^2 - 2AJ_xS_x - 2BJ_yS_y - 2CJ_zS_z + H'_{rotor_S}\end{aligned} \qquad (25.5.2b)$$

Gyro-spin components S_a are treated at first as constant classical parameters S_a.

$$\begin{aligned}H_{R,S(fixed)} &= const.\mathbf{1} - 2AS_xJ_x - 2BS_yJ_y - 2CS_zJ_z + AJ_x^2 + BJ_y^2 + CJ_z^2\\ &= M_0\mathbf{T}_0^0 \quad + \quad \textstyle\sum_d D_d\mathbf{T}_d^1 \quad + \quad \textstyle\sum_q Q_q\mathbf{T}_q^2\end{aligned} \qquad (25.5.2c)$$

This is a simple Hamiltonian *multipole tensor operator expansion* having here just a monopole $\mathbf{T}_0^0$ term, three dipole $\mathbf{T}_a^1$ terms, and two quadrupole $\mathbf{T}_q^2$ terms shown in Fig. 25.5.1. Each is a radial plot of a spherical harmonic function $Y_q^k\left(\varphi,\vartheta\right)$ representing a tensor operator $\mathbf{T}_q^k$.
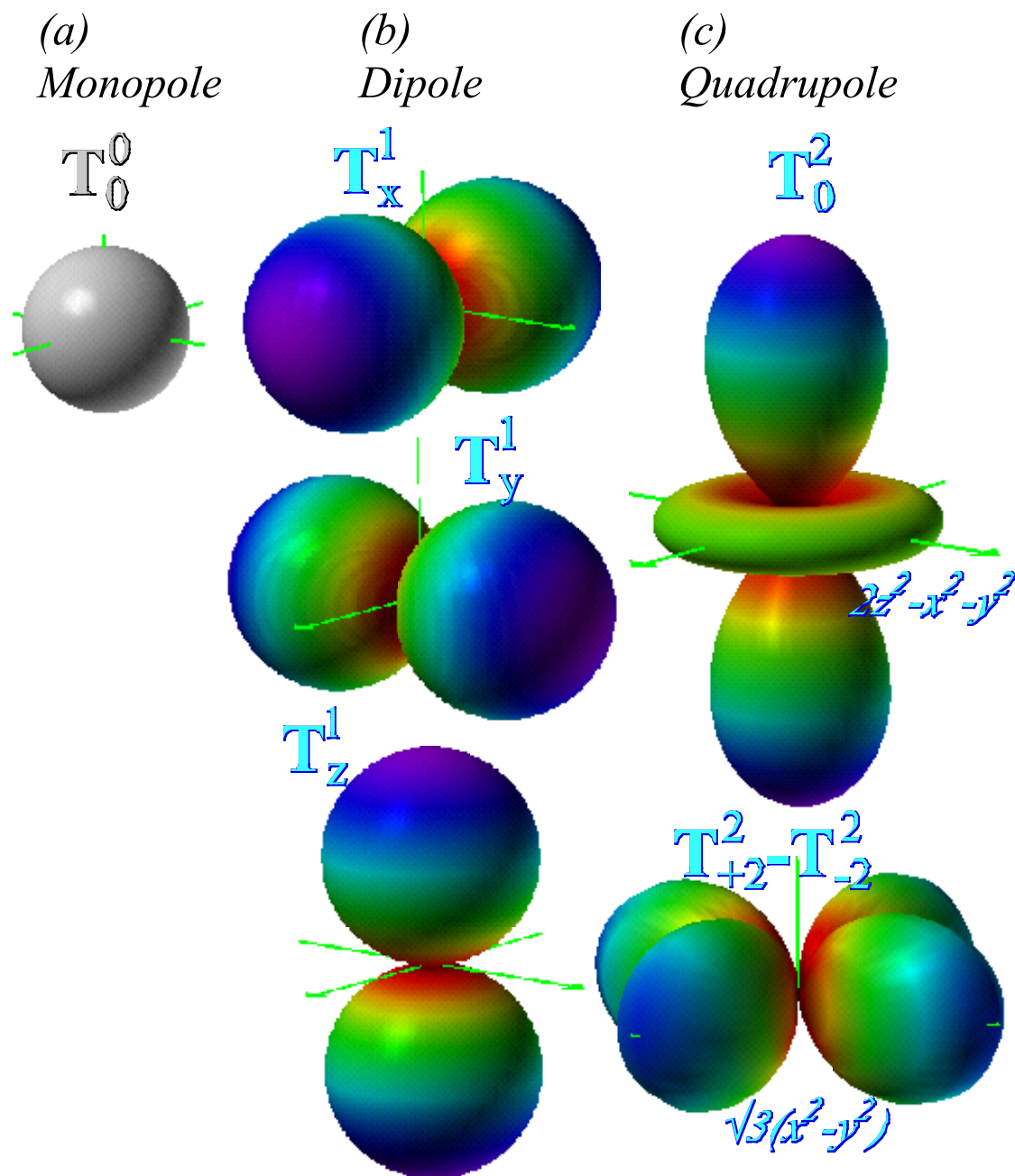
Fig. 25.5.1 The six lowest order RES components needed to describe rigid gyro-rotors.

$$\mathbf{T}^0_0 = \frac{\mathbf{J}^2_x + \mathbf{J}^2_y + \mathbf{J}^2_z}{3} \quad (25.5.3a)$$

$$\mathbf{T}^1_x = \mathbf{J}_x = \frac{\mathbf{T}^1_{+1} + \mathbf{T}^1_{-1}}{\sqrt{2}}$$

$$\mathbf{T}^1_y = \mathbf{J}_y = \frac{\mathbf{T}^1_{+1} - \mathbf{T}^1_{-1}}{i\sqrt{2}} \quad (25.5.3b)$$

$$\mathbf{T}^1_z = \mathbf{J}_z = \mathbf{T}^1_0$$

$$\mathbf{T}^2_{zz} = \frac{2\mathbf{J}^2_z - \mathbf{J}^2_x - \mathbf{J}^2_y}{2} = \mathbf{T}^2_0$$

$$\mathbf{T}^2_{x^2-y^2} = \mathbf{J}^2_x - \mathbf{J}^2_y = \frac{2\left(\mathbf{T}^2_2 - \mathbf{T}^2_{-2}\right)}{\sqrt{6}} \quad (25.5.3c)$$

The constant coefficients or *moments* indicate strength of each multipole symmetry.

$$M_0 = A + B + C + 3H'_{rotor_S} \quad \text{(25.5.4a)}$$

$$\begin{aligned} D_x &= -2AS_x, \\ D_y &= -2BS_y, \quad \text{(25.5.4b)} \\ D_z &= -2CS_z \end{aligned}$$

$$\begin{aligned} Q_{zz} &= \left(2C - A - B\right)/6 \\ Q_{x^2-y^2} &= \left(A - B\right)/2 \end{aligned} \quad \text{(25.5.4c)}$$

The scalar monopole RES (a) is a sphere, while vector dipole RES (b) are bi-spheres pointing along Cartesian axes, and the RES (c) resemble quadrupole antenna patterns. Also, Fig. 25.5.1(a-c) plot the six *s*, *p*, and *d* Bohr-Schrodinger orbitals that are analogs for the six octahedral J-tunneling states listed in Table 24.5.6.

The asymmetric and symmetric rotor Hamiltonians (31.1) and (31.2) are combinations of a monopole (25.5.3a) that, by itself makes a spherical rotor, and varying amounts of the two quadrupole terms (25.5.3c) to give the rigid rotor RES pictured previously in Fig. 31.1 and Fig. 31.2. Both *Q*-coefficients (25.5.4c) are zero for a spherical top *(A=B=C)* but only one is zero for a symmetric top *(A=B)*.

Combining monopole (25.5.3a) with dipole terms (25.5.3b) gives a gyro-rotor Hamiltonian (25.5.2b) for a spherical rotor *(A=B=C)* that has the following form.

$$H = const + BJ^2 - g\mu\mathbf{S}\cdot\mathbf{J} \quad \text{(where: } -g\mu = 2A = 2B = 2C\text{)} \quad \text{(25.5.5)}$$

H resembles a dipole potential **-m·B** for a magnetic moment **m**=*g***J** that precesses clockwise around a lab-fixed magnetic field **B**=μ**S**. (The PE is least for **J** along **S**.)

Here, the Hamiltonian (25.5.5) is a simple example of *Coriolis* rotational energy. It is least for **J** along **S** where |**R**|=|**J-S**| is least and rotor kinetic energy BR^2 is least. (Magnitudes |J| and |S| are constant here.) The spherical rotor-gyro RES in Fig. 25.5.2 is minimum along body axis +**S** and maximum along –**S** where BR^2 is greatest.

As is the case for rigid solid rotors in Fig. 31.1 and Fig. 31.2, the RES energy topography lines determine the precession **J**-paths in the body frame wherein gyro-**S** is fixed in Fig. 25.5.2. The left hand rule gives **J**-precession sense in the body **S**-frame, that is, all **J** precess *anti*-clockwise relative to the "low" on the +**S**-axis or clockwise relative to the "high" on the –**S**-axis. In the lab, **S** precess clockwise around a fixed **J**.

Gyro-RES differ from solid rotor RES that have two opposite "highs" and/or two opposite "lows" separated by saddle fixed points where the precessional flow direction reverses as seen in Fig. 31.2. The gyro-RES in Fig. 25.5.2 has no saddle fixed points and only one "high" and one direction of flow with the same harmonic precession frequency for all **J**-vectors between the high +**S** and low –**S**-axes. This is because the spectrum of the gyro-rotor Hamiltonian (25.A.22) is *harmonic* or *linear* in the *K*.

$$\left\langle {J \atop K} \middle| H \middle| {J \atop K} \right\rangle = const. + BJ(J+1) - 2BK \quad \text{(25.5.6)}$$

In contrast, even the symmetric rigid rotor spectrum (31.4) is *quadratic* in K. Other rotors shown in Fig. 31.2 and Fig. 31.4 have levels that are quite non-linear.
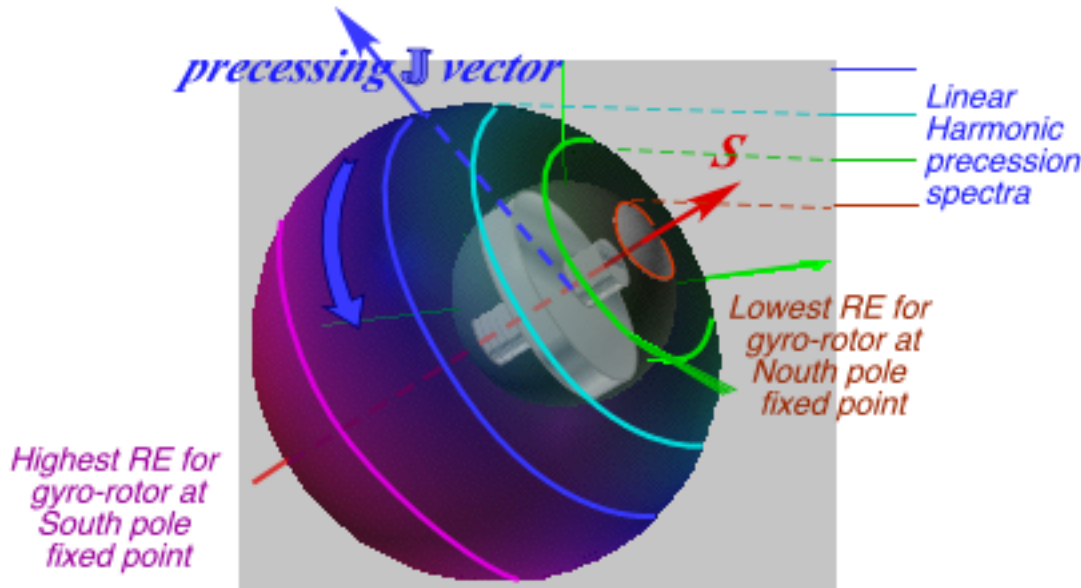

*Fig. 25.5.2 The spherical gyro-rotor RES is a cadioid of revolution around gyro spin **S***

b. 3D-Rotor and 2D-Oscillator Analogy

One associates linear levels with harmonic *oscillators* not rotors, but the gyro-rotor's linear spectrum lighlights a 150-year-old analogy between motions of 3D rotors and 2D vibrations. Stokes [] described 2D electric vibration or *optical polarization*, by a 3D vector later known as Stokes vector and labeled appropriately by the letter **S**. (Now we say **S** labels "spin.") Stokes' spin uses Hamilton *quaternions*, redone 80 years later as Pauli *spinor* σ_μ components of a general 2D Hermitian operator H.

$$H = \begin{pmatrix} A & B-iC \\ B+iC & D \end{pmatrix} = \frac{A+D}{2}\sigma_0 + \frac{A-D}{2}\sigma_A \quad + B\sigma_B \quad + C\sigma_C,$$

$$\text{where: } \sigma_0 = \begin{pmatrix} 1 & 0 \\ 0 & 1 \end{pmatrix}, \ \sigma_A = \begin{pmatrix} 1 & 0 \\ 0 & -1 \end{pmatrix}, \ \sigma_B = \begin{pmatrix} 0 & 1 \\ 1 & 0 \end{pmatrix}, \ \sigma_C = \begin{pmatrix} 0 & -i \\ i & 0 \end{pmatrix}.$$

(25.5.7)

Labels: *A("Asymmetric-diagonal"), B("Bilateral-balanced"), and C("Circular-Coriolis")* are alternatives to Pauli's dry z, x, and y, respectively. The 2D Hamiltonian has a **S·J** form of Coriolis coupling (25.5.5).

$$H = \quad S_0\mathbf{1} \quad + S_A J_A \quad + S_B J_B \quad + S_C J_C \quad = S_0 J_0 + \vec{S} \bullet \mathbf{J},$$

$$\text{where: } \quad J_0 = \mathbf{1}, \quad J_A = \frac{\sigma_A}{2}, \quad J_B = \frac{\sigma_B}{2}, \ J_C = \frac{\sigma_C}{2},$$

$$\text{and: } S_0 = (A+D)/2, \ S_A = (A-D), \ S_B = 2B, \quad S_C = 2C.$$

(25.5.8)

The 2D-3D analogy is helped by using elementary oscillator ladder $a^\dagger a$ operators.

$$\mathbf{J}_0=\mathbf{N}=a_1^\dagger a_1 + a_2^\dagger a_2, \ \mathbf{J}_A=\frac{1}{2}\left(a_1^\dagger a_1 - a_2^\dagger a_2\right), \ \mathbf{J}_B=\frac{1}{2}\left(a_1^\dagger a_2 + a_2^\dagger a_1\right), \ \mathbf{J}_C=\frac{-i}{2}\left(a_1^\dagger a_2 - a_2^\dagger a_1\right).$$

$$\text{where: } a_1^\dagger a_1 = \begin{pmatrix} 1 & 0 \\ 0 & 0 \end{pmatrix}, \ a_1^\dagger a_2 = \begin{pmatrix} 0 & 1 \\ 0 & 0 \end{pmatrix}, \ a_2^\dagger a_1 = \begin{pmatrix} 0 & 0 \\ 1 & 0 \end{pmatrix}, \ a_2^\dagger a_2 = \begin{pmatrix} 0 & 0 \\ 0 & 1 \end{pmatrix}.$$

(25.5.9)

This easily gives Schwinger's 3D angular momentum raising-lowering operators $\mathbf{J}_+ = \mathbf{J}_B + i\mathbf{J}_C = a_1^\dagger a_2$ and $\mathbf{J}_- = \mathbf{J}_B - i\mathbf{J}_C = a_2^\dagger a_1$, where 2D dimensions *1* and *2* are *spin-up (+ℏ/2)* and *spin-down (-ℏ/2)* instead of *x*-and *y*-polarized states envisioned by Stokes.

Angular 3D ladder operation is replaced by far simpler 2D oscillator operations.

$$\mathbf{J}_+ \left| n_1 n_2 \right\rangle = a_1^\dagger a_2 \left| n_1 n_2 \right\rangle = \sqrt{n_1 + 1}\sqrt{n_2} \left| n_1 + 1, n_2 - 1 \right\rangle$$
$$\mathbf{J}_- \left| n_1 n_2 \right\rangle = a_2^\dagger a_1 \left| n_1 n_2 \right\rangle = \sqrt{n_1}\sqrt{n_2 + 1} \left| n_1 - 1, n_2 + 1 \right\rangle$$

(25.5.10)

2D oscillator states are labeled by *total* number $N=(n_1+n_2)$ of quanta and the *net* quantum population $\Delta N=(n_1-n_2)$. 3D angular momentum states $\left| {}^J_K \right\rangle$ are labeled by total momentum $J=N/2=(n_1+n_2)/2$ and *z*-component $K=N/2=(n_1+n_2)/2$, just half (or *ℏ/2*) of N and ΔN.

$$\left| n_1, n_2 \right\rangle = \frac{\left(a_1^\dagger\right)^{n_1}\left(a_2^\dagger\right)^{n_2}}{\sqrt{n_1! n_2!}}\left| 0,0 \right\rangle = \left| {}^J_K \right\rangle = \frac{\left(a_1^\dagger\right)^{J+K}\left(a_2^\dagger\right)^{J-K}}{\sqrt{(J+K)!(J-K)!}}\left| 0,0 \right\rangle, \ \text{where:} \begin{cases} n_1 = J + K \\ n_2 = J - K \end{cases}$$ (25.5.11)

From this point, Schwinger's derivation of quantum angular momentum matrices $D^J_{MK}\left(\alpha\beta\gamma\right)$ in (31.5) and (31.6), becomes relatively straightforward. Also, it gives Clebsch-Gordan Wigner-Eckart relations upon which RE matrix calcualtions depend, as well as the asymptotic values for RE surface approximations such as (31.10).

$$\left\langle {}^{J'}_{K'} \left| T^k_q \right| {}^J_K \right\rangle = C^{k\,J\,J'}_{q\,K\,K'}\left\langle J' \|k\| J \right\rangle \sim C^{k\,J\,J}_{0\,K\,K}\left\langle J \|k\| J \right\rangle \sim D^J_{JK}\left(\Theta^J_K\right).$$

c. Gyro-Rotors and 2D-Local Mode Analogy

In molecular rotation theory, the $\mathbf{T}_0^2$ term along with $\mathbf{T}_0^0$ make the initial unperturbed Hamiltonian (31.3) of a symmetric top, and gyro terms $\mathbf{T}_q^1$ are viewed as perturbations. For vibration theory, the latter make up a normal mode Hamiltonian and the former $\mathbf{T}_0^2$ term is viewed as an anharmonic perturbation.

The effect of $\mathbf{T}_0^2$, seen in Fig. 25.5.3(c), is to replace the stable fixed point $+B$ (representing the (+)-normal mode) by a saddle point as B bifurcates (splits) into a pair of fixed points that head toward the $\pm A$-axes. So one normal mode dies and begats two stable local modes whereby one mass may hold its energy and not have to give it all up to the other in the usual beating process. (The A-modes are anharmonically *detuned*.)

Pairs of classical modes, each localized on different sides of an RES in Fig. 25.5.3, are analogous to asymmetric top $\pm K$-precession pairs in Fig. 25.4.2 and are degenerate in a classical RES picture. Quantum-tunneling Hamiltonians (31.15) split each trajectory pair to a superfine doublet with ($\pm$)-eigenstates on *both* RES paths in Table 31.1), and so also will quantum gyro-spin doublets have **J** both up *and* down the A-axis in Fig. 25.5.3c.
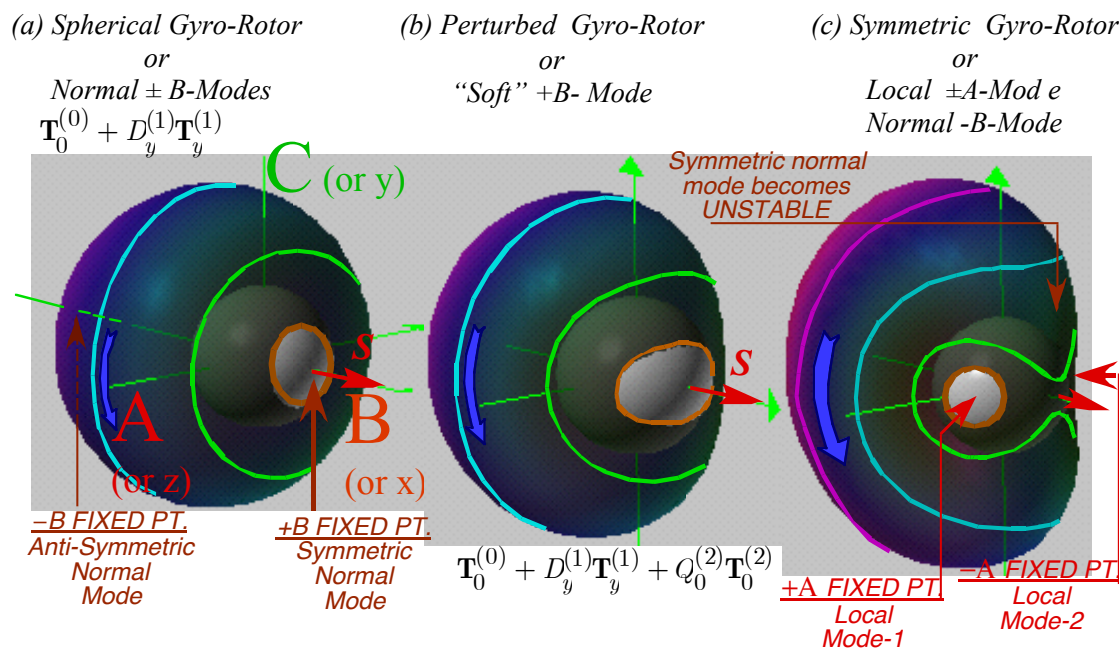

Fig. 25.5.3 A spherical gyro-rotor becomes a symmetricgyro-rotro by adding $\mathbf{T}_0^2$.

d. Multiple Gyro-Rotor RES and Eigen-surfaces

While simple quantum rotors have **J** on multiple RES paths, a gyro-rotor **J** may on multiple paths *and surfaces*. For quantum spin **S** the Gyro-rotor the distribution may occupy over multiple RES.

The simplest semi-classical theory of **S** considers just +**S** and -**S**. The RES for each is plotted one on top of other as in Fig. 25.5.4 (a) while component RES are shown in Fig. 25.5.4(b) for +**S** and in Fig. 25.5.4(c) for -**S**. An energy sphere is shown intersecting an RES pair for an asymmetric gyro-rotor. If the spin **S** is set to zero, the pair of RES collapse to a rigid asymmetric top RES shown in Fig. 31.2 having angular inversion (time-reversal **J**→-**J**) and reflection symmetry. The composite RES in Fig. 25.5.4(a) has inversion symmetry but lacks reflection symmetry. Its parts in Fig. 25.5.4 (b) and in Fig. 25.5.4 (c) have neither reflection nor inversion symmetry due to their gyro-spins ±**S**.
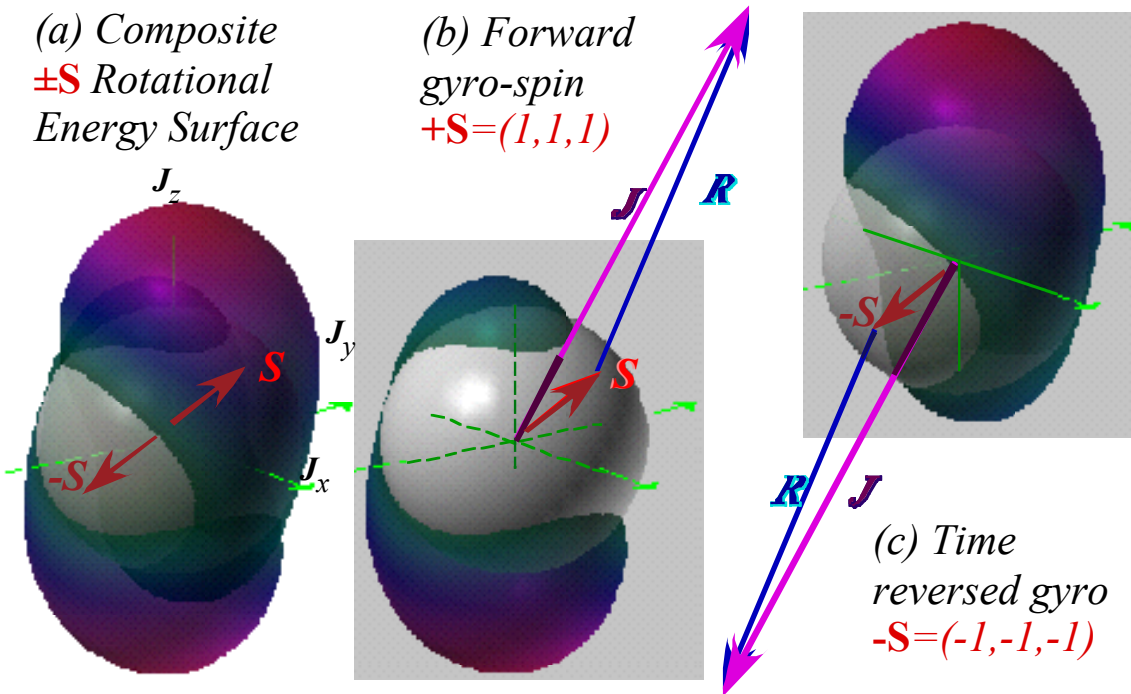

Fig. 25.5.4 Asymmetric gyro-rotor RES. (a) Composite ±S. (b) Forward spin +S. (c) Reversed spin – S.

A quantum theory of multiple RES involves a tunneling or mixing between its base states. The simplest quantum gyro-spin is a two-state spin-1/2 having a 2-by-2 Hamiltonian matrix. Semi-classical gyro-rotor dynamics are approximated by a pair of RES obtained from eigensolutions of the following 2-by-2 matrix for each classical orientation (β,γ) of the **J**-vector in the body frame.

$$H_{R,S(quantized)} = A\mathbf{J}_x^2 + B\mathbf{J}_y^2 + C\mathbf{J}_z^2 - A\mathbf{J}_x\boldsymbol{\sigma}_x - B\mathbf{J}_y\boldsymbol{\sigma}_y - C\mathbf{J}_z\boldsymbol{\sigma}_z + const.$$

$$= \begin{pmatrix} \text{RE}_{atop} - JC\cos\beta & -AJ\cos\gamma\sin\beta - iBJ\sin\gamma\sin\beta \\ -AJ\cos\gamma\sin\beta + iBJ\sin\gamma\sin\beta & \text{RE}_{atop} + JC\cos\beta \end{pmatrix} \quad (25.5.12)$$

where: $\text{RE}_{atop} = J^2(A\cos^2\gamma\sin^2\beta + B\sin^2\gamma\sin^2\beta + C\cos^2\beta)$

Fig. 25.5.5 compares of views of both the classical RES of Fig. 25.5.4 (top half of Fig. 25.5.5) and the semi-classical RES (bottom half of Fig. 25.5.5) resulting from inserting quantum spin $S=\sigma/2$ matrices in (25.5.2) to give (25.5.12) then diagonalizing and plotting the resulting eigenvalues. Each *sc*-RES surface is an asymmetric RES perturbed around where the *c*-RES cross. The inner surface is particularly affected by a bifurcation into an unstable saddle point and a pair of loops around fixed points.
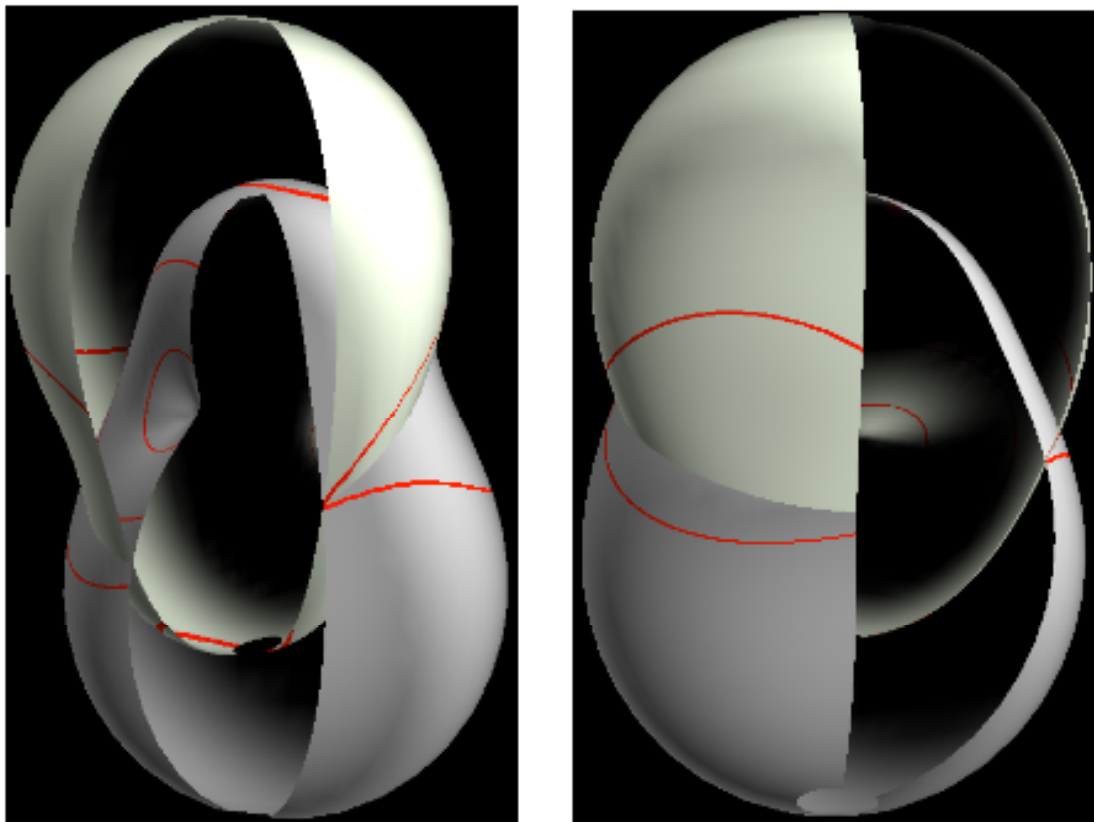

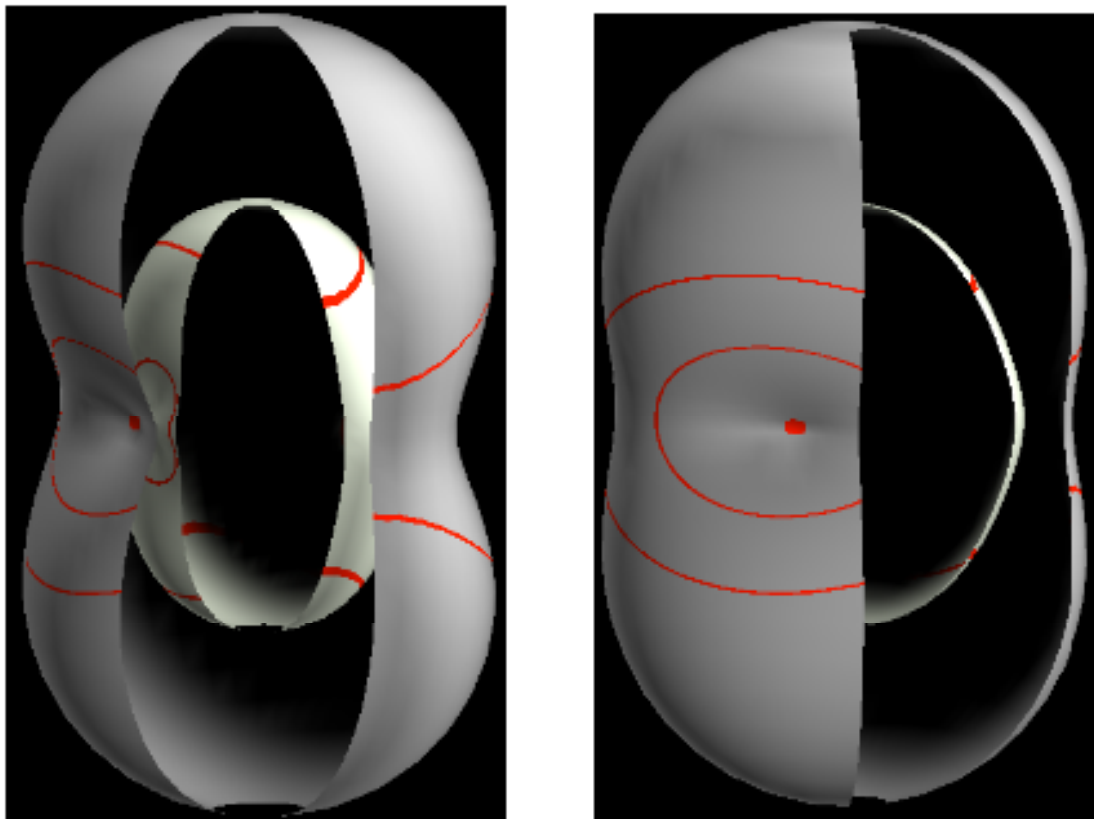*Fig. 25.5.5 (a) Views of classical gyro-rotor c-RES in Fig. 25.5.4 (a) based on (25.5.2).*

Fig. 25.5.5 (b) Views of semi-classical gyro-rotor sc-RES based on eigenvalues of (25.5.12) with **S**=σ/2.